Stanford MEDICINE

Stanford University School of Medicine
Department of Surgery
presents

THE 23rd ANNUAL EMILE F. HOLMAN LECTURE In Surgery

and

13th Annual Resident Research Day

Friday, May 13, 2022

Stanford Center for Academic Medicine
Stanford University

The 23rd Annual
Emile F. Holman Lecture In Surgery
and
13th Annual Resident Research Day

Friday, May 13, 2022

Stanford Center for Academic Medicine
Stanford University

10:30 AM – 12: 00 PM	Poster Presentations *Center for Academic Medicine Courtyard*
12:00 PM – 1:00 PM	Lunch *Center for Academic Medicine Courtyard*
1:00 PM – 5:00 PM	Abstracts *Ground Rounds*
5:00 PM – 6:15 PM	Holman Lecture *Ground Rounds*
6:15 PM – 6:30 PM	Awards Ceremony - Best in Category *Ground Rounds*
6:30 PM	Holman Reception *Center for Academic Medicine Courtyard*

Stanford MEDICINE | Department of Surgery

Emile Frederic Holman, MD

August 12, 1890 to March 19, 1977
Founding Chair – Department of Surgery
Stanford University

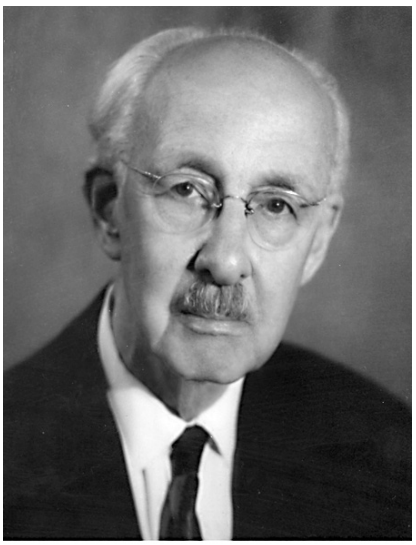

Emile Holman

Emile Frederic Holman, the son of a Methodist minister, was born in Missouri and then moved with his family as a teenager to southern California. He entered Stanford University as a math major in 1907; he dropped out for a semester to learn shorthand and typing in order to support himself. Upon his return, he performed stenographic work for Stanford's founding President, David Starr Jordan. After graduation, Holman stayed on as Secretary to President Jordan until 1914 when Holman went to Oxford as a Rhodes Scholar. Thereafter, began a key period of education at Johns Hopkins University.

Of some note, Sir William Osler wrote a letter recommending Holman for admission to The Johns Hopkins School of Medicine; Holman received his M.D. degree from Hopkins in 1918. He then became Assistant in Surgery in the Surgical Hunterian Laboratory, the research lab of the noted surgeon, William Stewart Halsted. He continued in Halsted's residency program until 1923, serving as the last resident surgeon at the time of Halsted's death in 1922. His loyalty to Professor Halsted was legendary; it was Holman who first brought the principles of the Halstedian residency to the west. In 1925 he returned to Stanford as Associate Professor of Surgery and in 1926 he was named head of the Department, a position he held for 29 years until his retirement from the faculty in 1955.

"... as a scholar, innovator, teacher and clinical surgeon, he pioneered a truly academic surgical program at a time when there were few others west of the Mississippi." — William P. Longmire, Jr

Dr. Holman is perhaps best known for his pioneering work in vascular surgery and, in particular, the physiology of arteriovenous fistulas. This research won him the coveted Samuel D. Gross prize from the Philadelphia Academy of Surgery in 1930 and the Rudolph Matas Medal in Vascular Surgery from Tulane in 1954. He was elected a member of The Johns Hopkins Society of Scholars in 1970. His co-authors over the years are a literal compendium of the substantial physicians and surgeons of the 20th century. Less well known were his fundamental ideas and observations on skin grafting. In 1924 he published a paper of his early work in the identification and characterization of the phenomenon of rejection of transplanted skin (from a parent to a child), particularly the accelerated rejection of second transplants from the same donor. These observations were not pursued, though many believe formed the basis for Medawar's work a quarter of a century later. His astute observations were recognized at the International Congress of The Transplantation Society in 1972 nearly 50 years after his paper was published.

Perhaps most importantly, Dr. Holman was a humanist as well as a scientist, devoted to the service of his fellow man. During World II his patriotism and selflessness were obvious during his volunteer time in the Pacific, though 51 at the time. His experiences in both World Wars made him a fervent critic of war; he did not hesitate to speak out against national policy or social injustice.

In all, he was perhaps the most Halsted-like graduate of any of the Halstedian residents.

"He was a man not easily forgotten. Yet it was not by bombast or power that he attracted attention. It was by his sharp and incisive mind, by his thoughtful and gentle demeanor and by his perpetual search for truth and excellence in science that we remember him." — James B.D. Mark, M.D

In his in memoriam tribute in the Journal of Thoracic and Cardiovascular Surgery, Frank Gerbode, in describing Dr. Holman's life and accomplishments, chose to quote William Shakespeare in King Lear: "We have seen the best of our time. We that are younger shall never see so much nor live so long." ■

Mary T. Hawn, MD, FACS

Professor and Chair
Emile Holman Professor in Surgery

The 2022 Emile F. Holman Lectureship and the Stanford Surgery Research Symposium had an unprecedented number and high caliber abstracts submitted this year. We're thrilled to continue the long tradition of showcasing the outstanding research by our trainees. This year we are honored to welcome Dr. Daniella Ladner from Northwestern University back to the as our Holman Visiting Professor. Dr. Ladner completed both her resident and transplant surgery training at Stanford University.

I'm grateful to Dr. Arden Morris, Vice Chair for Clinical Research, Dr. Olivia Martinez, Vice Chair for Translational Reserch and the surgical research council for their stewardship of this program and selection of the top abstracts for presentation.

Emile F. Holman was the first of the classically trained surgeons to move west, and for 29 years served as the founding Executive Head of the Department of Surgery at Stanford University. He established the tradition of an integrated research program, permeating every aspect of the surgical department, which continues to this day. We honor his legacy today.

A critical component of research within the department is the active participation of our residents under the mentorship of surgeons and scientists across our university. The residents devote themselves to a project designed, first and foremost, to advance the field, but also to advance their own professional development and further forge their path in academic surgery. Basic science laboratories throughout the Department, the University and beyond are but one option, clinical research outcomes, education, device design and many others are options; advanced degrees are also possible.

I'm grateful to all of our faculty mentors and investigators for their commitment to this endless and exhilarating cycle of training the next generation of surgeon leaders. We're showcasing the abstracts that represent an enormous amount of work and preparation. We are proud of all their accomplishments! ■

Arden M. Morris, MD, MPH

Professor and Vice Chair for
Research Department of Surgery
Director, S-SPIRE Center
Stanford University School of Medicine

Olivia M. Martinez, PhD

Johnson and Johnson Distinguished Professor
Vice Chair for Basic & Translational Research
Department of Surgery
Stanford University School of Medicine

Welcome to the 23th Annual Emile F. Holman Lectureship and 13th Resident Research Day in Surgery!

We are delighted to return to a fully in-person meeting at a fantastic venue- the Stanford Center for Academic Medicine.

This year, we are honored to host former Stanford resident and fellow Dr. Daniela Ladner as our Visiting Professor.

The Stanford Department of Surgery residents, post-docs, fellows and students once again have been extremely productive. In a record high, 66 individuals submitted 88 abstracts!

The best abstracts from each Department of Surgery trainee scientist are captured in this booklet. We invite you to read them all and hope you will share our appreciation of the diverse interests and disciplines represented within our department, from basic science to translational, clinical, bioinformatics, education, and health services research. We will continue the tradition of poster and podium presentations from our top-scoring trainee scientists. For the remaining abstracts, an online poster session is available at the Holman Day website surgery.stanford.edu/holman/2022.html.

We encourage each of you to actively engage with questions and discussion for those who describe work that particularly piques your interest.

Many thanks to Dr. Hawn and our spectacular Holman Day staff committee, Rachel Baker, Joseph Martinez, and Julia Miranda for planning this meeting! We would also like to recognize the heroic work of the Department of Surgery's Research Oversight Committee for abstract review and creation of the 2022 program—many thanks to each of you.

Clinical and Health Services Research Reviewers:
James R. . Korndorffer, Jr., MD, MHPE
Marc Melcher, MD, PhD
Arden M. Morris, MD, MPH
Rejoice F. Ngongoni, MD
George R. Poultsides, MD,MS
Todd Wagner, PhD
Sherry Wren, MD

Basic and Translational Research Reviewers:
James Dunn, MD, PhD
Sheri Krams, PhD
Nicholas Leeper, MD
Olivia Martinez, PhD
Sakti Srivastava, MBBS, MS
Daniel J. Stoltz, MD
Derrick Wan, MD

Please join us in congratulating our trainees and colleagues in the Department of Surgery for the curiosity, passion, and systematic inquiry that they continue to apply to their scholarly work!

Sincerely,

Arden M. Morris, MD, MPH and Olivia M. Martinez, PhD ■

Daniela P. Ladner, MD, MPH, FACS

Professor of Surgery (Organ Transplantation) and Medical Social Sciences, Director of the Northwestern University Transplant Research Collaborative called NUTORC, the Associate Surgical Director for liver transplant and hepatobiliary.

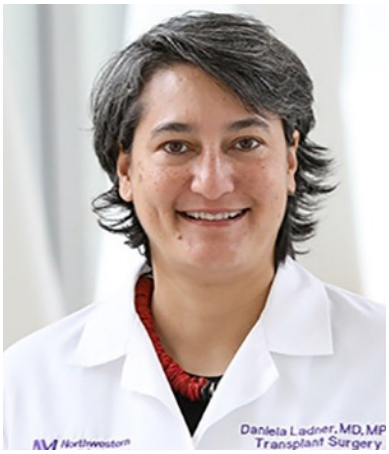

Dr. Daniela Ladner is a clinician-scientist with over 140 peer-reviewed publications (H-Factor 27) and is one of the most highly NIH funded surgeons with >$4.5M per year.

As a transplant surgeon she performs liver and kidney transplants, donor hepatectomies and nephrectomies, hepatobiliary surgery, laparoscopic removals of polycystic kidneys and general surgeries in transplant patients.

She directs NUTORC - a large transdisciplinary network of clinical and scientific collaborators which has led to over >700 transdisciplinary manuscripts and > $50M+ in federal funding since 2009.

Her own R01 funded research focuses on cirrhosis epidemiology and risk prediction (R01 x 2, U24) and process improvement in kidney transplantation (R01).

Dr. Ladner directors 3 training programs: (i) The postdoctoral T32 (Transplant Surgery Scientist Program) for future transplant clinician-scientists, (ii) the T35 Northwestern Summer Program for Medical Students, focused on guiding underrepresented minorities towards a clinician-scientist pathway, and (iii) the Summer Student Immersion Program for give 20-25 high school, college, and medical students an immersive research experience.

Dr. Ladner takes particular pride in mentoring clinicians across disciplines, many of which have progressed to being faculty at R01 universities with independent funding of their own. ■

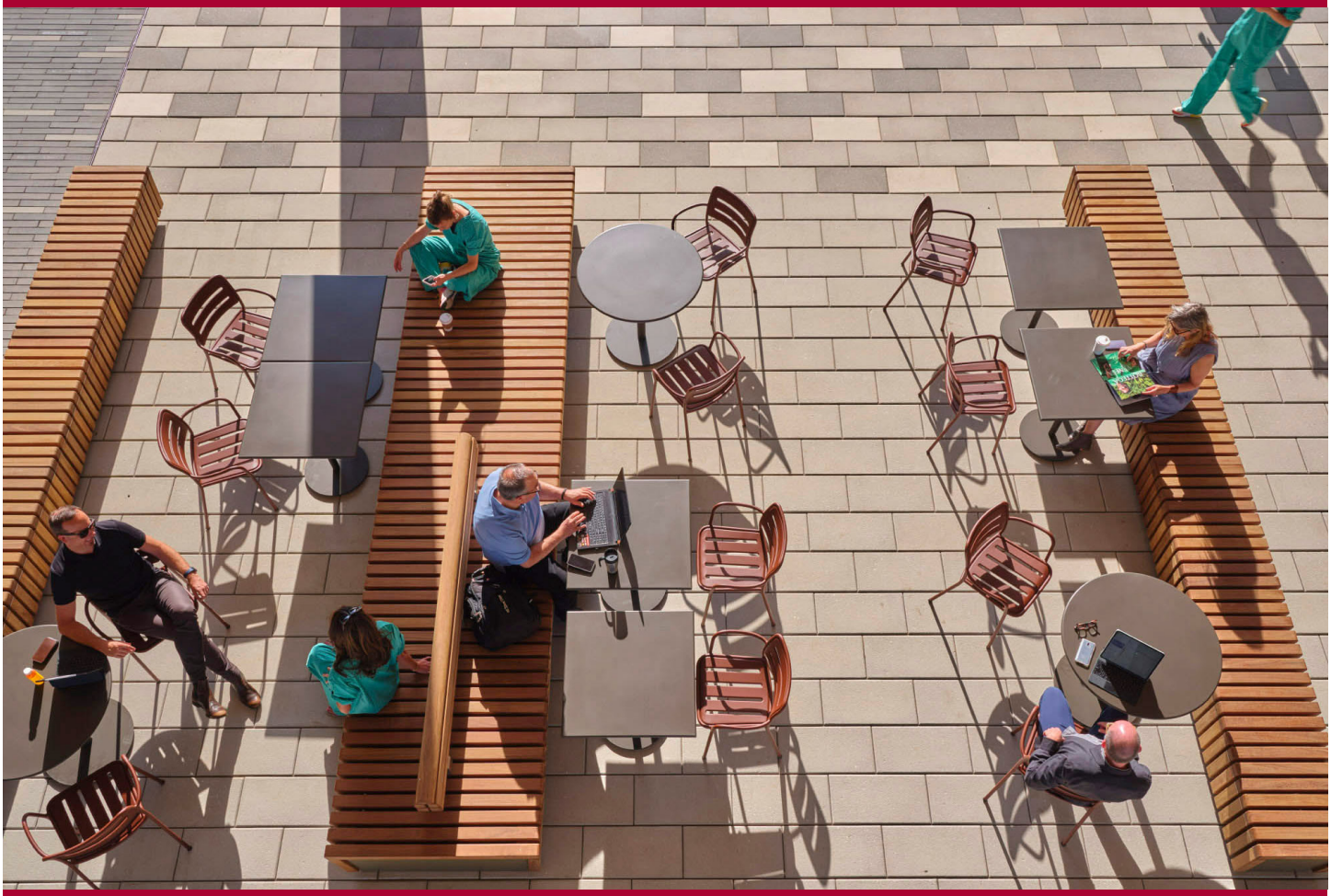

PROGRAM

Resident Research Day

Poster Presentations – Clinical

Center for Academic Medicine Courtyard

10:30 AM – 12:00 PM

Title of Presentation	Presenter
Effect of an online home-based prehabilitation program on outcomes after colorectal surgery	Cintia Kimura, MD, PhD
The Impact of Care Fragmentation on Pancreatic Cancer Care: More Complex Than it Seems	Amy Li, MD
Comparing Outcomes of Laparoscopic Transgastric Necrosectomy to Endoscopic Cystgastrostomy: Single Institution Cohort Study	Rejoice Ngongoni. MD, MHS
Outcome-Specific Injury Scores (OSIS): Prognostication Tools Based on Fall-Related Injury Patterns in Older Adults	Taylor Anderson, MD
The Cost-Effectiveness of Prepectoral Versus Subpectoral Breast Reconstruction: A Markov Analysis	Pooja Yesantharao, MD, MS
Development of a Portable Device to Quantify Hepatic Steatosis in Donated Livers using an AI Algorithm	Mac Klinkachorn, MS
See One Online, Do One, Teach One: YouTube as a Learning Resource for Surgeons	Jonathan DeLong, MD
Foot Burns in Persons with Diabetes	David Perrault, MD

Poster Presentations – Basic

Title of Presentation	Presenter
Fibroblast sub-populations are modified with fat grafting to treat radiation-induced fibrosis	Darren Abbas, MD
Multi-Modal Analysis of Cell Populations and Architectural States Mediating the Progression and Resolution of Pulmonary Fibrosis	Jason Guo, PhD
Predicting Abnormal Left Ventricular Ejection Fraction Using Echocardiograms	Vy Ho, MD
EBV+ PTLD tumor microRNAs Detected in Circulating Extracellular Vesicles are Decreased in Pediatric Transplant Recipients with EBV+PTLD	Jeanna M Enriquez
Identification of Engrailed-1 Positive Fibroblasts within Fibrotic Capsule During Foreign Body Response	Jennifer Parker
Adipocyte progenitor cells embedded in collagen gels accelerate bone formation in a murine calvarial critical defect model	Asha Cotterell, MS
Transdermal Deferoxamine Improves Acute Wound Healing In Chronic Irradiated Skin In A Mouse Model	Hendrik Lintel
Quantitative Analysis of the Collagen Matrix Ultrastructure in Mouse Hearts after Myocardial Infarction	John Lu, MPhil, MSc

Resident Research Day

Abstracts – Clinical

Grand Rounds
1:00 PM – 2:45 PM
Four minutes are allotted following each presentation for Q&A

Moderators:
Elsie Ross, MD
Cliff Sheckter, MD

	Title of Presentation	Presenter
1:05 - 1:13	Tackling the Bedside Artificial Intelligence Barrier: Natural Language Processing to Extract Injury ICD10 Diagnosis Codes Real-Time from Electronic Medical Records	Jeff Choi, MD, MSc
1:18 - 1:26	Predictive Value of Clinical Complete Response After Chemoradiation for Rectal Cancer	Charles Liu, MD, MS
1:31 - 1:39	Out-of-Pocket Spending and Work Loss After Common Surgical Procedures Among Working-age Adults	Kathryn Taylor, MD
1:44 - 1:52	Despite increasing costs, perfusion machines expand the donor pool of livers and could save lives	Thomas Handley, MD
1:57 - 2:05	Technical Variant Liver Grafts Show Equal Graft Survival to Whole Liver Grafts in Pediatric Liver Transplantation at High Volume Transplant Centers	Dan Stoltz, MD
2:10 - 2:15	Remote Access to Electronic Medical Record Reduces Overall EMR Time for Vascular Surgery Residents - poster presentation???	Vy Ho, MD
2:23 -2:31	Machine Learning Can Predict Recurrence Patterns after Liver Transplantation in Hepatocellular Carcinoma Patients: Analysis from the US Multicenter HCC Transplant Consortium	Raja Narayan, MD MPH
2:36 - 2:44	Health Equity Ratings US of Burn Centers—Does For-Profit Status Matter?	Nada Rizk, MS
2:50 - 3:00	BREAK	

Resident Research Day

Abstracts – Basic

Center for Academic Medicine Courtyard
3:00 PM – 4:45 PM
Four minutes are allotted following each presentation for Q&A

Moderators:
Dan DeLitto, MD, PhD
Varvara Kirchner, MD

	Title of Presentation	Presenter
3:00 - 3:08	Development of a dynamic map of peripheral myeloid cells associated with acute rejection of vascularized composite tissue allograft	James Harden
3:13 - 3:21	Inhibiting Yes-associated protein prevents scarring and promotes regeneration in a large animal model of wound repair	Heather Talbott
3:26 - 3:34	Single-cell CyTOF profiling of pediatric immune responses to organ transplantation demonstrates that allograft type determines post-transplant immune makeup	Mahil Rao, MD, PhD
3:39 -3:47	Adipocytes the forgotten cell in skin fibrosis; exploring the mechanism of fat driven skin fibrosis	Michelle Griffin, MD, PhD
3:52 - 4:00	Appendiceal mucinous neoplasms and pseudomyxoma peritonei tumors are defined by distinct cellular states and a goblet cell identity.	Carlos Ayala, MD, PhD
4:05 - 4:13	Neoadjuvant Intratumoral Immunotherapy with TLR9 Activation and Anti-OX40 Antibody Eradicates Metastatic Cancer	Wan Xing Hong, MS, MD
4:18 - 4:26	Decoding and modulation of spiking activity of the sciatic nerve in an awake and moving rodent	Katharina Fischer, MD
4:31 - 4:39	Treating lymphedema with a propeller lymphatic tissue flap combined with nanofibrillar collagen scaffolds	Peter Deptula, MD
4:45 - 5:00	BREAK	

5:00 PM
The 23rd Annual Emile F. Holman Lecture in Surgery

Daniela P. Ladner, MD, MPH, FACS

“Collaborative science and the quest to solve the mysteries of cirrhosis”

POSTER PRESENTATIONS

Effect of an online home-based prehabilitation program on outcomes after colorectal surgery

Kimura CMS, Bidwell S, Gurland B, Morris AM, Shelton A, Kin C

Introduction: Prehabilitation may optimize surgical outcomes. We evaluated the effect of an online home-based prehabilitation program on 30-day postoperative complication rates and length-of stay among patients undergoing abdominal colorectal surgery.

Methods: Patients were invited to enroll in a prehabilitation program delivered through a mobile application. Through the app, patients received information about the Mediterranean diet and set goals for strength exercises and step count. Adherence was measured by the average of self-reported percentage of days they walked 5,000 steps, completed all strength exercises, and followed the diet. Prehab-users were compared to non-users, and to a previous cohort of colorectal patients who used another version of the app, which only delivered information about ERAS (ERAS-only group, n=127).

Results: Of the 212 patients enrolled, 96 (45%) used the program at least once. Among those, median adherence was 56.9% (IQR 33.3%; 74.9%). No significant differences were observed between users and non-users.

Adjusting for age, ASA classification, surgical approach, concurrent procedures, and presence of anastomosis, Prehab-users had lower complication rate (OR: 0.44, 95%CI: 0.22; 0.90, p=0.024), lower CCI score (coefficient: -4.17, 95%CI -7.31; -1.01, p=0.010), and shorter LOS (coefficient: -1.01, 95%CI -1.94; -0.08, p=0.034) when compared with non-users. Adjusting for the same covariates and comparing with the ERAS-only group, Prehab usage did not significantly affect the complication rate and CCI score (p= 0.202 and 0.177, respectively), but was associated with shorter LOS (coefficient: -0.83, 95%CI -1.66; -0.01, p=0.049).

Conclusion: Web-based prehabilitation may improve outcomes in colorectal surgery, but strategies to improve adherence are critical.

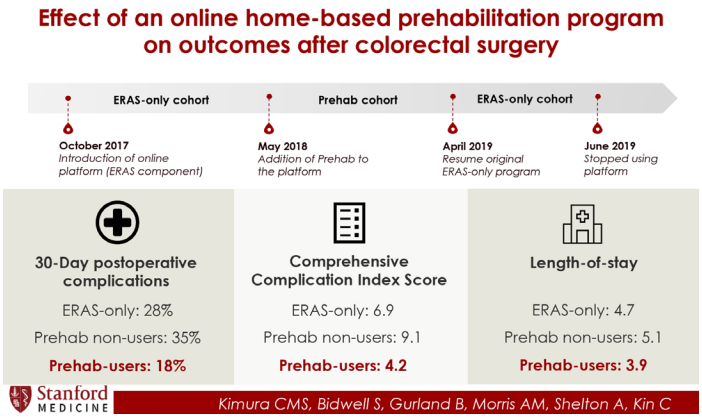

The Impact of Care Fragmentation on Pancreatic Cancer Care: More Complex Than it Seems

Amy Y Li, Rejoice F Ngongoni, John R Bergquist, Jonathan C DeLong, Nicolas B Barreto, Esther M John, Brendan C Visser

Introduction: Fragmentation of care (FC)—care at >1 facility—has been associated with increased cost, delayed treatment, and worse survival for gastrointestinal cancers. We assessed the impact of FC on pancreatic cancer care in California.

Methods: Using the California Cancer Registry, linked with ambulatory surgery, emergency visits and discharge records from the Office of Statewide Health Planning Database, patients diagnosed with non-metastatic pancreatic ductal adenocarcinoma (PDAC) from 2007-2017 were identified. FC was determined by the number of unique facilities where patients received cancer care over the initial 12 months. We evaluated the association between FC and all-cause mortality using multivariable-adjusted Cox regression.

Results: Among 9,464 PDAC patients, 4,545 patients received care at 1 facility (48.0%), 3,571 (37.7%) at 2, and 1,348 (14.2%) at >3. After adjusting for patient, tumor and hospital characteristics, female sex (HR=0.93 [0.89-0.97], p=0.001), high socioeconomic status (highest vs lowest quintile: HR=0.75 [0.70-0.82], p=<0.001) and cancer-hospital designations (all HR<1, p<0.001; see table) were associated with lower mortality. Mortality was lower for patients treated at 2 facilities compared to those treated at 1 facility (HR=0.95 [0.90-0.99], p=0.02), but was similar for patients treated at >3 vs 1 facility (HR=1.01 [0.94-1.07], p=0.87).

Conclusion: Although prior data suggested that FC at >1 facility compromised cancer outcomes, in this large population-based cohort, PDAC patients treated at 2 facilities had better survival. FC is more complex than previously hypothesized. Our ongoing research is directed at better understanding "positive fragmentation" (e.g., seeking higher level of care) versus disjointed care (previously ascribed to fragmentation).

Table: Multivariable Cox Regression of Patient, Tumor and Hospital Variables Associated with All-Cause Mortality of Patients Diagnosed with Pancreatic Adenocarcinoma

Variable	Hazard Ratio	Confidence Interval (95%)	p-value
Patient Factors			
Age, yrs (mean±sd)	1.03	0.97-1.02	0.78
Sex			
Male	1.0 (Reference)		
Female	0.93	0.89-0.97	0.001
Race/Ethnicity			
Non-Hispanic White	1.0 (Reference)		
Non-Hispanic Black	1.07	0.98-1.16	0.15
Hispanic	1.03	0.97-1.09	0.39
Asian/Pacific Islander	1.00	0.93-1.07	0.99
American Indian	1.18	0.89-1.57	0.25
Yang Socioeconomic Status (SES, in quintiles)			
Lowest SES	1.0 (Reference)		
Lower-Middle SES	1.00	0.93-1.08	0.93
Middle SES	0.89	0.83-0.96	0.003
Upper-Middle SES	0.82	0.76-0.88	<0.001
Highest SES	0.75	0.70-0.82	<0.001
Tumor Factors			
Tumor Grade			
Well (I)	1.0 (Reference)		
Moderate (II)	1.14	1.02-1.26	0.02
Poor (III)	1.51	1.36-1.68	<0.001
Undifferentiated (IV)	1.53	1.12-2.09	0.007
Unknown	1.88	1.70-2.07	<0.001
Primary Tumor (T)			
T0/T1	1.0 (Reference)		
T2	3.89	1.62-9.39	0.003
T3	3.43	1.42-8.28	0.006
T4	3.85	1.59-9.32	0.003
TX	4.28	1.77-10.36	0.001
Regional Lymph Nodes (N)			
N0	1.0 (Reference)		
N1	1.00	0.95-1.05	0.99
NX	1.28	1.17-1.41	<0.001
Distant Metastases (M)			
M0	1.0 (Reference)		
M1	1.43	1.13-1.82	0.003
MX	1.21	1.04-1.41	0.01
Hospital Factors			
NCCN-designation*	0.86	0.78-0.94	0.001
NCI-designation*	0.88	0.83-0.94	<0.001
COC accredited*	0.91	0.86-0.96	<0.001
Hospital Size, beds ≥400*	0.95	0.91-1.00	0.06

*These variables are compared to institutions without the corresponding designations.

Abbreviations: yrs, years; sd, standard deviation; SES, socioeconomic status; NCCN, National Comprehensive Cancer Network; NCI, National Cancer Institute; COC, Commission on Cancer.

Comparing Outcomes of Laparoscopic Transgastric Necrosectomy to Endoscopic Cystgastrostomy: Single Institution Cohort Study

Rejoice F Ngongoni MD, Amy Y Li MD, Beatrice J Sun MD, John R Bergquist MD, Jonathan C DeLong MD, Joo Ha Hwang MD PhD, Shai Friedland MD, Samer S Eldika MD, Robert Huang MD, George Poultsides MD, Monica M Dua MD, Brendan C Visser MD

Introduction: Laparoscopic transgastric necrosectomy (LTGN) and endoscopic cystgastrostomy (EC) with lumen-apposing metal stents (LAMS) are alternative approaches for debridement of retrogastric walled-off pancreatic necrosis (WOPN) when the necrosum abuts the gastric wall. However, comparative data is sparse. We present a comparative analysis of outcomes for these two procedures at our institution.

Methods: This is a retrospective study which included patients who underwent LTGN or EC for WOPN between 2011 and 2021. Outcomes included number of debridement procedures, time to symptom resolution, morbidity, and mortality. Logistic regression analysis was performed to predict outcomes.

Results: Among 98 patients, 43 (43.9%) underwent EC and 55 (56.1%) had LTGN. The two groups were similar except as noted in Table 1. Six (14.0%) patients in the EC group had had a recent laparotomy that precluded laparoscopy. EC required a mean of 3.7 debridements (range 2-8). Seven (15.9%) of the EC patients required additional surgical debridement. Among the LTGN patients, 45% underwent concurrent cholecystectomy. Five (8.8%) of the LTGN patients underwent additional endoscopic debridement after LTGN. LTGN provided single-step debridement for 89% of patients (no additional operative, percutaneous or endoscopic drainage) and had shorter time to symptom resolution (7.1 vs 2.2 months, see Table 1).

Conclusion: LTGN and EC are complementary approaches with similar safety profiles. LTGN offers single-stage debridement, may be combined with cholecystectomy and appears to result in faster symptom resolution. EC is a multi-stage debridement with low upfront morbidity and is particularly suitable for patients in whom surgery is contraindicated.

Table 1. Bivariate analysis of outcome predictors for patients undergoing laparoscopic transgastric necrosectomy (LTGN) and endoscopic cystgastrostomy (EC).

Variable	Endo, n (%)	LTGN, n (%)	P-value
	N=43	N=55	
Demographic			
¶Age (mean, SD), yr	54.3 (15.0)	54.0 (15)	ns
¶BMI (mean, SD), kg/m^2	27.7 (5.9)	28.2 (6.2)	ns
Sex			
Male	25 (58.1)	36 (65.5)	ns
Female	18 (41.9)	19 (34.6)	
Perioperative			
¶CCI (mean, SD)	2.1 (1.6)	2.1 (2.0)	ns
¶Size of necrosum (mean, SD), cm	13.6 (5.2)	15.5 (5.6)	0.078
Infected necrosum	25 (58.1)	29 (52.7)	ns
Splanchnic thrombosis	18 (41.9)	10 (18.2)	0.01
Pre-operative ICU	12 (29.9)	16 (29.1)	ns
Concurrent cholecystectomy	0 (0)	25 (45.5)	<0.001
¶Procedure duration (mean, SD), min	69.0 (38.0)	151.3 (45.5)	<0.001
Outcome			
¥Number of procedures (mean, SD)	3.7 (1.7)	1.1 (0.4)	<0.001
¥Number of procedures (median, IQR)	3 (3)	1 (0)	<0.001
¥Hospital LOS (mean, SD), days	13.9 (17.4)	8.1 (10.9)	ns
¥Hospital LOS (median, IQR), days	7 (12)	5(5)	ns
Post-operative ICU	8 (18.6)	15 (27.3)	ns
Post-procedure IR drainage	5 (11.6)	1 (1.8)	0.044
Any complication	26 (60.5)	39 (70.9)	ns
Clavien-Dindo ≥3a complications	18 (41.9)	15 (27.3)	ns
Hemorrhage	5 (11.6)	5 (9.1)	ns
Discharge to home	34 (79.1)	50 (90.9)	ns
Readmission	16 (37.2)	17 (30.9)	ns
Mortality, 30 days	1 (2.3)	2 (3.6)	ns
Mortality, 90 days	1 (2.3)	2 (3.6)	ns
¥Time to symptom res (mean SD), mo	7.1 (9.0)	2.2 (3.1)	<0.001
¥Time to symptom res (median IQR), mo	5 (1)	1 (3)	<0.001
TPN at discharge	4 (9.3)	0 (0)	0.021
Pancreatic insufficiency	13 (30.2)	14 (25.5)	ns
New onset diabetes mellitus	6 (14.0)	14 (25.5)	ns

*SD, standard deviation; ns, not significant; ICU, intensive care unit; CCI, Charlson Comorbidity Index; IQR, interquartile range; LOS, length of stay; IR, interventional radiology; res, resolution; TPN, total parenteral nutrition; ¶ t-test; ¥Mann-Whitney U test

Outcome-Specific Injury Scores (OSIS): Prognostication Tools Based on Fall-Related Injury Patterns in Older Adults

Taylor N. Anderson MD, Jeff Choi MD MSc, Lakshika Tennakoon MD MPhil, David A. Spain MD, Kristan L. Staudenmayer MD MSc

Introduction: Existing injury severity metrics are insufficient for predicting outcomes in older adults (age ≥65). We sought to develop and validate Outcome-Specific Injury Scores (OSIS); a new, practical prognostication tool for assessing risk of adverse outcomes for older adults after traumatic falls.

Methods: We used National Inpatient Sample 2016 to identify older adults admitted after falls who were randomly assigned to either training (30%) or validation (70%) cohort. Five adverse outcomes were selected (Table). Ridge regression, with penalty for multicollinearity, identified strongest injury pattern predictors. Distinct sets of predictors were aggregated into five OSIS using ridge coefficient weights; Jenks optimization was used to categorize severity. Outcome prediction was assessed with adjustment for baseline frailty, age, and sex.

Results: We identified 871,374 fall hospitalization encounters among elderly adults. Distinct injury patterns predicted risk of specific adverse outcomes. For example, the three strongest predictors of mortality were traumatic brain injuries, C2 fractures, and rib fractures, while strongest predictors of disposition to a facility were hip, lower femur, and femoral shaft fractures. Injuries carried different weights within each outcome. Increasing OSIS were associated with increased adjusted odds for all adverse outcomes.OSIS offers distinct advantages over traditional injury severity metrics. These intuitive, outcome-specific scores can be readily calculated at bedside. OSIS represents a valuable new tool for prognosticating risk of specific adverse outcomes after fall-related injury in older adults.

Table. Association between five Outcome-Specific Injury Scores (OSIS) and corresponding adverse outcomes
**adjusted for baseline frailty (≥3 validated markers of frailty), age (65-74, 75-84, ≥85 years), and sex*

	Inpatient mortality		DVT/PE		Respiratory failure		Disposition to Facility		Prolonged hospitalization	
Population with outcome, N (%)	27,274 (3.1)		15,249(1.6)		67,967(7.8)		608,219(69.8)		382,533 (43.9)	
Relevant predictors, N	17		14		11		25		22	
Three strongest predictors	Traumatic brain injuries, C2 fractures, multiple rib fractures		Fractures of lower femur; femoral shaft; upper tibia		Single rib fracture, multiple rib fractures, C2 fractures		Fractures of hip; lower femur; femoral shaft		Fractures of lower, shaft of, and subtrochanteric femur	
OSIS category	score	adjusted* OR [95%CI]	score	adjusted* OR [95%CI]	score	adjusted* OR [95%CI]	score	adjusted* OR [95%CI]	score	adjusted* OR [95%CI]
Very low	0-2	reference	0-1	reference	0-3	reference	0-3	reference	0-2	reference
Low	2-11	1.5 [1.3-1.8]	1-6	1.1 [0.9-1.3]	3-11	1.3 [1.1-1.5]	3-8	1.9 [1.8-2.1]	2-6	1.3 [1.3-1.4]
Moderate	11-28	3.0 [2.6-3.5]	6-15	1.4 [1.1-1.8]	11-19	1.8 [1.7-2.0]	8-14	4.8 [4.6-5.1]	6-12	1.8 [1.7-1.8]
High	≥28.0	7.3 [5.8-9.1]	≥15	1.7 [1.1-2.3]	≥19	2.8 [2.4-3.3]	≥14	6.5 [5.1-8.3]	≥12	2.4 [2.1-2.6]

The Cost-Effectiveness of Prepectoral Versus Subpectoral Breast Reconstruction: A Markov Analysis

Pooja S Yesantharao MD, MS; Gina Eggert BS; Kometh Thawanyarat BS; Gordon K Lee MD, MBA; Rahim S Nazerali MD, MHS

Introduction: Prepectoral implant-based breast reconstruction is thought to confer multiple advantages over subpectoral placement. However, by virtue of less soft tissue coverage, prepectoral implants are also thought to have higher rates of contour irregularities that may require revision. While studies have compared prepectoral versus subpectoral placement, none have systematically reviewed this data against patient satisfaction and overall costs of care, including any downstream revisions. Such an analysis would elucidate the longitudinal cost-effectiveness of each technique. This investigation was a Markov analysis of prepectoral versus subpectoral breast reconstruction.

Methods: This was a Markov analysis using hybrid Monte Carlo patient simulation, comparing prepectoral versus subpectoral implants. The BREAST-Q tool was used to assess patient satisfaction by converting BREAST-Q scores into Breast Quality-Adjusted Life Years (B-QALYs). The primary model outcome was the incremental cost-effectiveness ratio (ICER), or cost per B-QALY gained for prepectoral versus subpectoral reconstruction.

Results: The model was run over a 10-year horizon. Among non-irradiated patients, prepectoral placement was associated with a 0.3 increase in B-QALYs and a $1,037 decrease in medical costs. Thus, among these patients, prepectoral reconstruction was the dominant technique, even when considering revisionary procedures. However, amongst irradiated patients, prepectoral placement was associated with a 0.2 increase in B-QALYs but a $2,556 increase in medical costs. These conclusions were robust to probabilistic and deterministic sensitivity analyses.

Conclusion: Prepectoral placement is more cost-effective than subpectoral placement in non-irradiated patients. Among radiated patients, neither technique was dominant. Such information can help guide cost-conscientious care among women undergoing implant-based breast reconstruction.

Development of a Portable Device to Quantify Hepatic Steatosis in Donated Livers using an AI Algorithm

Mac Klinkachorn, Christian Tsoi-A-Sue, Raja R. Narayan, Marc L. Melcher

Introduction: Accurate estimation of liver fat content is necessary to predict how a donor liver will function after transplantation. This can be challenging at the many hospitals that lack liver pathology expertise. Therefore, we developed a low-cost, mobile artificial intelligence (AI) platform to evaluate liver fat content on donor liver biopsy slides in real-time.

Methods: We loaded our previously described AI algorithm that labels and quantifies fat globules onto a microcomputer with a GPU. The computer was embedded into a 3D printed case and connected to a 12MP camera and display. The device is capable of acquiring an image of a liver biopsy through a microscope, labeling the fat globules, and outputting the percent steatosis. Three images were taken of each slide (Figure 1a).

Results: The assessment of steatosis on 33 slides by the device was compared to the whole slide assessment using the same algorithm on a cloud based platform previously described by our group. There was strong positive correlation (r=0.871) between the two techniques (Figure 1b).

Conclusion: This all-in-one, point-of-care device could be used on donor procurements to obtain an objective assessment of liver fat content even when a trained pathologist is not available. The correlation between the cloud and device-determined assessment of steatosis is very good and might be improved by increasing the number of images taken and assessed by the device. Hopefully, such a device could streamline appropriate matching of donors and recipients.

Figure 1a

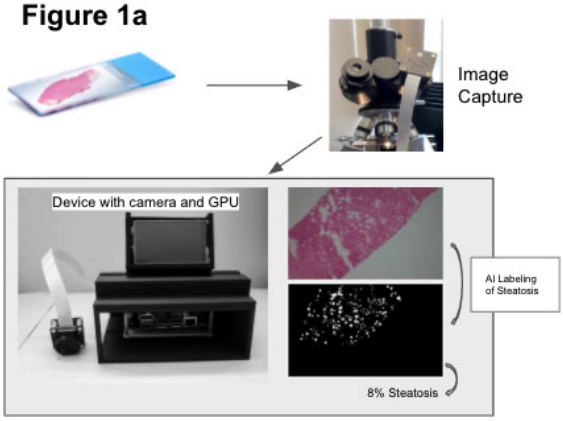

Figure 1b

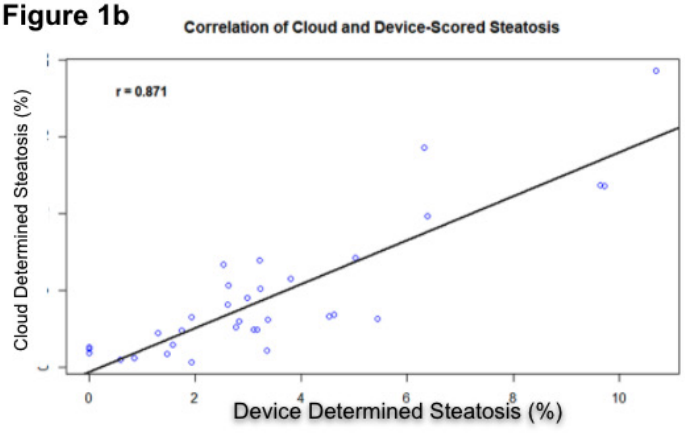

See One Online, Do One, Teach One: YouTube as a Learning Resource for Surgeons

DeLong, J; Hindin, D; Bungo, C; McCarthy, M; Dua, M; Visser, B; Gurland, B

Introduction: Seeing an operation has long been recognized as the first step towards learning a procedure. Once limited to the operating room, visual learning has become increasingly accessible to contemporary surgical trainees due to online surgical content. YouTube is the most common platform leveraged by practicing surgeons and trainees. To better assess unmet content needs, we sought to determine the number of videos available relative to the search frequency for specific general surgical operations.

Methods: We identified 28 laparoscopic and robotic general surgical procedures on YouTube. Searches were filtered by Most Views, Most Relevant, and Highest Rated. The top 5 results per category were analyzed for characteristics including views, runtime, date added, comments, and likes. Site:youtube.com Google searches determined the number of videos/procedure and vidIQ analytics determined the number of searches/month.

Results: For each operation, YouTube searches/month were plotted against YouTube videos available. For 6/28 (21.4%) procedures, videos available matched the number of searches/month. For 13/28 (46.4%) videos outweighed the number of searches and for 9/28 (32.2%) there were fewer videos available relative to searches indicating an unmet need.

Conclusion: YouTube is a highly utilized and broadly accessible learning resource for surgeons. In the majority of cases, there is an imbalance between the content availability and the need as evidenced by the number of searches per month. In the present study, we identified 9 cases where additional content may satisfy a currently unmet need. Future analysis will address video quality and satisfaction.

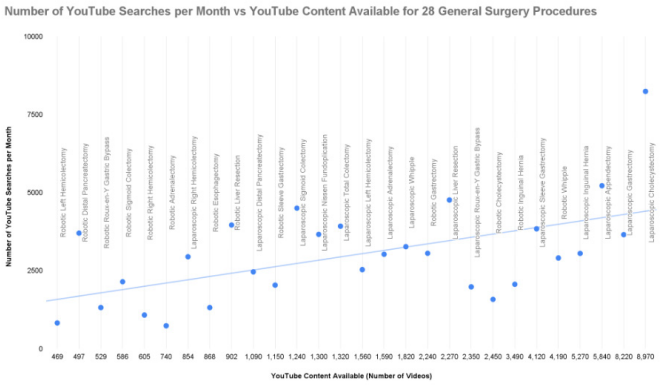

Foot Burns in Persons with Diabetes—Outcomes from the National Trauma Data Bank

David Perrault[1], Jason Cobert[2], Veda Gadiraju[2], Ayushi Sharma[1], Geoffrey Gurtner[1], Tam Pham[2,3], Clifford Sheckter[1]
[1]Department of Surgery. Stanford University
[2]Department of Surgery. University of Washington
[3]Harborview Injury Prevention and Research Center (HIPRC). University of Washington

Background: Diabetes Mellitus (DM) complicates the treatment of burn injuries. Foot burns in diabetic patients are challenging problems with unfavorable outcomes. National-scale evaluations are needed, especially with regard to limb salvage. We aim to characterize lower extremity burns in persons with DM and evaluate the likelihood of amputation.

Methods: The National Trauma Data Bank (NTDB) was queried from 2007-2015 extracting encounters with primary burn injuries of the feet using International Classification of Diseases (ICD) 9th Edition codes. Logistic regression modeled predictors of lower extremity amputation. Covariables included age, sex, race/ethnicity, comorbidities including DM, % burn total body surface area (TBSA), mechanism, and region of burn center. Poisson regression evaluated temporal incidence rate changes in DM foot burns.

Results: Of 116,796 adult burn encounters, 7,963 (7%) had foot burns. Of this group, 1,308 (16%) had DM. 5.6% of encounters with DM foot burns underwent amputation compared to 1.5% of non-DM encounters ($p<0.001$). Independent predictors of lower extremity amputation included DM (OR 3.70, 95% CI 2.98 – 4.59), alcohol use, smoking, chronic kidney disease, burn size >20%, African American/Black race, male sex, and age>40 years (all $p<0.01$). The incidence of DM foot burns increased over the study period with an incidence rate ratio (IRR) of 1.07 (95% CI 1.05 – 1.10, $p<0.001$).

Conclusion: DM was associated with nearly a 4-fold increase in amputation after adjusting for covariables. Furthermore, the incidence of DM foot burns is increasing. Strategies for optimizing care in persons with DM foot burns are need to improve limb salvage.

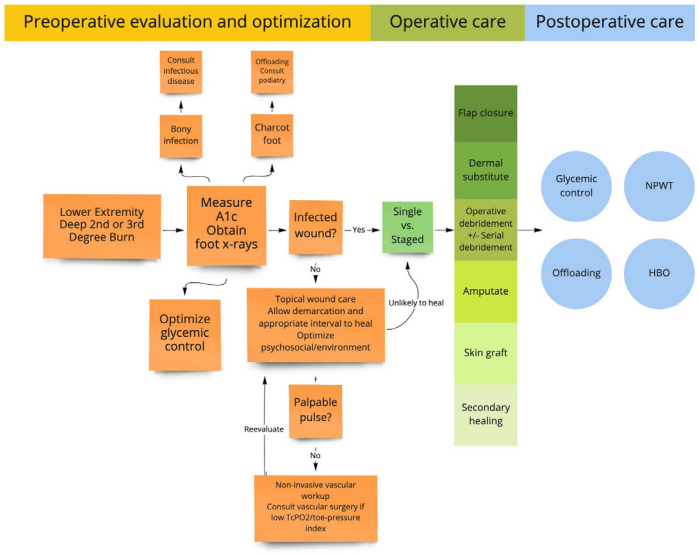

Fibroblast sub-populations are modified with fat grafting to treat radiation-induced fibrosis

Darren B. Abbas, M.D.[1]; Jason L. Guo, PhD1, Michelle Griffin, MBChB, Ph.D[1]; Hendrik Lintel, M.D.[1]; Nicholas J. Guardino, B.S.[1]; Charlotte E. Berry, BS[1]; Adrian Pu[1]; Arash Momeni, MD[1]; Michael T. Longaker, M.D., M.B.A.[1], Derrick C. Wan M.D.[1]
[1]Hagey Laboratory for Pediatric Regenerative Medicine, Division of Plastic and Reconstructive Surgery, Department of Surgery, Stanford University School of Medicine, Stanford, CA
[2]Institute for Stem Cell Biology and Regenerative Medicine, Stanford University, Stanford, CA

Introduction: One of the main deleterious side effects of radiation is fibrosis of the surrounding skin and soft tissue. Clinically, this phenomenon is seen routinely and can be ameliorated with fat grafting; however, the underlying pathophysiologic changes driving this effect are not well understood. With this study, we aim to better delineate these mechanisms driving fat grafting's regenerative effects.

Methods and Materials: 20 adult wild-type mice underwent 5 Gy of radiation every other day for 12 days, 30 Gy total, of the dorsal skin. After 4 weeks of recovery post-radiation, mice were separated into two treatment cohorts: fat grafted and non-grafted groups. Fat grafts were placed into the subcutaneous space of the dorsal skin. The grafts were maintained for 4 weeks and then the skin was harvested. Samples underwent single-cell RNA sequencing to identify transcriptionally distinct subpopulations and cross-referenced with Enrichr to identify relevant genetic pathways.

Results: Dermal thickness and collagen deposition was significantly decreased in the fat grafted cohort. (A,B). Five distinct fibroblast subpopulations were identified, including inflammatory, immunomodulatory, ECM, angiogenic, and mechano-fibrotic (C-E). Angiogenic fibroblasts expression was significantly enhanced with fat grafting, while inflammatory fibroblast expression was significantly dampened by fat grafting. Mechano-fibrotic fibroblast expression was also significantly inhibited with fat grafting. Lastly, the immunomodulatory fibroblast cluster had an almost 10-fold increase in expression with fat grafting (F).

Conclusion: Modulation of these heterogenous fibroblast sub-populations with fat grafting provide insight into the cellular changes that manifest clinically in fat grafting's ability to improve radiation-induced fibrosis.

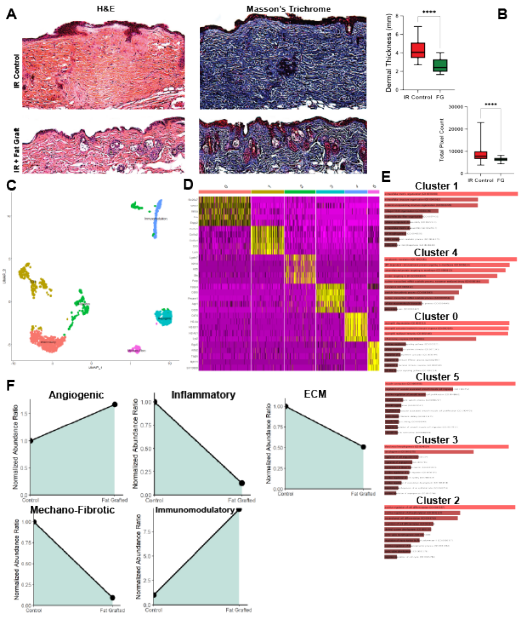

Multi-Modal Analysis of Cell Populations and Architectural States Mediating the Progression and Resolution of Pulmonary Fibrosis

Jason L. Guo, Ph.D.[1], Michelle Griffin, M.D., Ph.D.[1], Nicholas J. Guardino, B.S.[1], Darren B. Abbas, M.D.1, John M. Lu, B.S.1, Amanda F. Spielman, B.S.[1], Hendrik Lintel, B.S.[1], Asha C. Cotterell, B.S.[1], Derrick C. Wan, M.D., F.A.C.S.[1], Michael T. Longaker, M.D., M.B.A., F.A.C.S.[1]

[1]Hagey Laboratory for Pediatric Regenerative Medicine, Division of Plastic and Reconstructive Surgery, Department of Surgery, Stanford University School of Medicine, Stanford, CA

Introduction: Pulmonary fibrosis is a significant clinical burden that is often idiopathic and progressive. Nevertheless, the temporal progression of pulmonary fibrosis remains largely unexplored, and no studies to date have analyzed reparative cell populations at single-cell resolution. Thus, we performed a multi-modal analysis that combines machine learning models of fibrotic/reparative pulmonary architecture with single-cell RNA sequencing (scRNAseq) of associated cell populations.

Methods: C57BL/6 mice were intranasally instilled with 1.25mg bleomycin/mg body weight. At each timepoint, lungs were stained (Picrosirius red) and analyzed using an unsupervised machine learning algorithm for ultrastructural analysis (>2,500 images, 294 local/global fiber features), which were processed by uniform manifold approximation and projection and fitted to a minimum spanning tree-based pseudotime model. Individual lungs were imaged in situ by microcomputed tomography, quantified by standard collagen assay, and digested using collagenases and RBC lysis buffer for scRNAseq.

Results: Pulmonary matrix progressed from baseline to aberrant architecture after bleomycin administration, with peak pseudotime (fibrotic progression) at POD 21-28 and return to baseline by POD 42 (Fig. 1A-1C). Similar trends were observed in collagen concentration and lung radiological density (Fig. 1D-1E). Baseline, fibrotic, and reparative lungs (PODs 0, 14, 35) presented variable cell populations, with significant shifts in composition of fibroblast subpopulations (Fig. 1F-1H). Smooth muscle cells and matrix/ECM-modulating fibroblasts dominated the actively fibrotic state, while chemotactic and immunomodulatory fibroblasts emerged during active repair.

Conclusions: Distinct cell subpopulations mediate the progression of fibrotic pulmonary architecture, with a transition from classical matrix-modulating fibroblasts to immune-reactive fibroblasts during the evolution of active fibrosis to post-fibrotic repair.

Figure 1: Multi-modal analysis of progression and resolution of pulmonary fibrosis in a mouse model. (A) Pseudotime model/manifold of matrix architectures in pulmonary fibrosis across timepoints of 0-49 days after PBS or bleomycin instillation. (B) Progression of ultrastructural states from 0-49 days, demonstrating retention of baseline with PBS instillation and progression of fibrosis with bleomycin instillation. (C) Correlation of matrix architectural pseudotime with post-bleomycin timepoints. (D) Progression of bulk collagen concentration in lungs after bleomycin instillation. (E) Progression of lung radiological density after bleomycin instillation. (F) Manifold of cell phenotypes identified in scRNAseq of baseline, fibrotic, and reparative lungs (PODs 0, 14, 35). (G) Sub-analysis of fibroblast subpopulations in scRNAseq dataset. (H) Highest magnitude shifts in subpopulation representation during active fibrosis (smooth muscle cells, ECM modulating fibroblasts) and active repair (chemotactic fibroblasts, immunomodulatory fibroblasts).

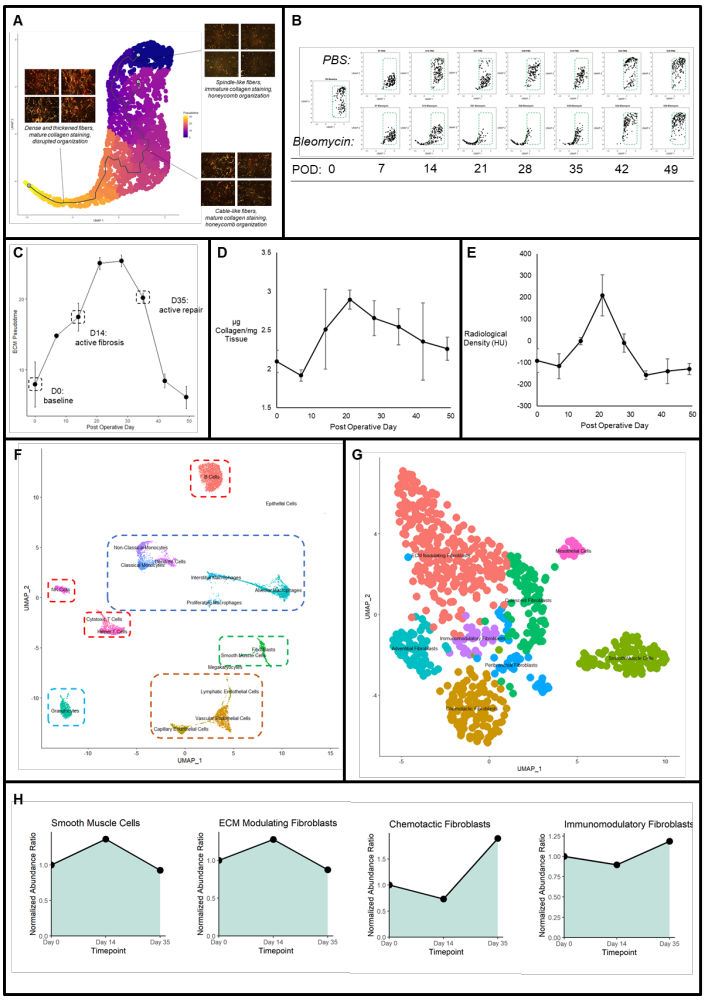

Predicting Abnormal Left Ventricular Ejection Fraction Using Echocardiograms

Vy T Ho MD, Raghav M Garg, Katelyn Bechler BS, Steven Asch MD MPH, Jonathan H Chen MD PhD, Jason T Lee MD, David Ouyang MD

Introduction: Left ventricular ejection fraction (LVEF) is an important but resource-intensive measure of cardiac function, requiring volumetric software, certified sonographers, and supervising cardiologists. Use of a machine learning model to predict abnormal LVEF at point of care can improve diagnosis and treatment in emergent and/or low-resource settings.

Methods: A corpus of 10,024 deidentified apical echocardiograms were randomly split into a 60% training, 20% validation, and 20% test set. LVEF lower than 50% and greater than 75% were labeled abnormal. Six deep learning models were developed using the training set, followed by hyperparameter tuning on the validation set. All models received two images as input: a single end-systolic frame and a single end-diastolic frame per patient. Model performance was measured by overall accuracy on the test dataset, followed by area under the receiver operating characteristic curve (auROC), sensitivity, and specificity.

Results: The VGG-16 convolutional neural network had the best performance on the held-out test set, with an accuracy of 85%, area under the receiver operating characteristic curve of 90%, sensitivity of 79%, and specificity of 88% (Figure 1). In discriminant subanalysis, the model had greatest difficulty distinguishing abnormal LVEF slightly below the 50% threshold; false-negative cases had a mean LVEF of 45.5% compared to true positive cases with a mean 37.2% (Student's t-test, p-value < 0.05)

Conclusion: Deep learning models can accurately identify abnormal LVEF using two images from an echocardiogram. This technology may improve care in emergent settings such as trauma bays or ambulances, or low-resource settings without cardiovascular laboratories.

Figure 1. Deep learning model schema and performance

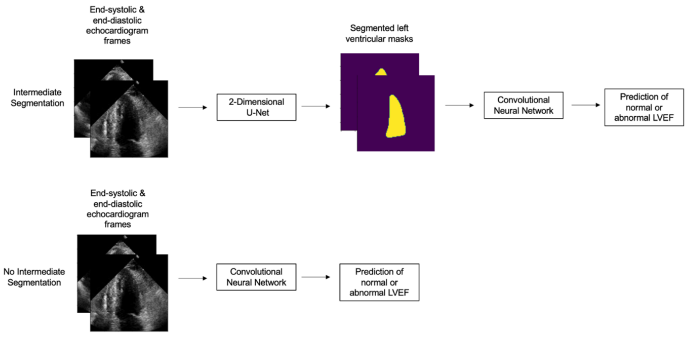

	Accuracy	auROC	Sensitivity	Specificity
Simple CNN	0.84	0.84	0.72	0.82
InceptionV3	0.84	0.84	0.74	0.77
VGG-16	0.85	0.90	0.79	0.88
2D U-Net + Simple CNN	0.77	0.51	1.0	0
2D U-Net + Inception V3	0.81	0.51	0.84	0.17
2D U-Net + VGG-16	0.77	0.51	1.0	0

EBV+ PTLD tumor microRNAs Detected in Circulating Extracellular Vesicles are Decreased in Pediatric Transplant Recipients with EBV+PTLD

A. Sen, J. Enriquez, M. Rao, M. Glass, Y. Balachandran, S. Syed, C. J. Twist, K. Weinberg, S. D. Boyd, D. Bernstein, A. Trickey, D. Gratzinger, B. Tan, M. G. Lapasaran, M. A. Robien, M. Brown, B. Armstrong, D. Desai, G. Mazariegos, C. Chin, T. Fishbein, R. S. Venick, A. Tekin, H. Zimmermann, R. U. Trappe, I. Anagnostopoulos, C.O. Esquivel, O. M. Martinez, S. M. Krams

Introduction: Epstein-Barr Virus (EBV)-associated post-transplant lymphoproliferative disorder (PTLD) is a serious complication of solid organ transplantation (SOT). Previously, we demonstrated that EBV reshapes the microRNA (miR) landscape in EBV+ B cell lines leading to increased IL-10 production.

Methods: To establish the miRNAome of PTLD tumors we analyzed FFPE shavings of tumors from SOT recipients with EBV+ PTLD (n=14) and EBV- PTLD (n=10), by miR microarray analysis and qPCR. Blood was obtained from pediatric SOT recipients enrolled at seven sites in NIAID-sponsored Clinical Trials of Organ Transplantation in Children (CTOTC)-06, a prospective study to identify viral and immune biomarkers of EBV-associated PTLD. Using qPCR, we quantitated miRs-17, 19, 106a, 155, and 194 in the plasma and extracellular vesicles (EV) of EBV+ PTLD+ SOT recipients (n=18) and matched controls (n=37).

Results: The miRNAome of EBV+ PTLD differs substantially from EBV- PTLD tumors with the levels of miRs-17, 19, 106a, and 194 reduced in the EBV+ PTLD with miR-194 ($p<0.01$) significantly reduced compared to EBV- controls. Plasma and EV levels of miRs-17 ($p=0.034$; plasma), 19 ($p=0.029$; EV), 106a ($p=0.007$; plasma and EV), and 194 were reduced in the EBV+ PTLD+ group compared to matched controls. miR-155 was unchanged between the groups. Importantly, ~90% of the cell-free miR were contained within the EV.

Conclusion: EBV+ PTLD tumor-derived miRs are detected in the circulation. These miRs in tumor-derived EVs may have the potential to regulate immune cell function. Further development of diagnostic and potential therapeutic uses of these miRs in PTLD is warranted.

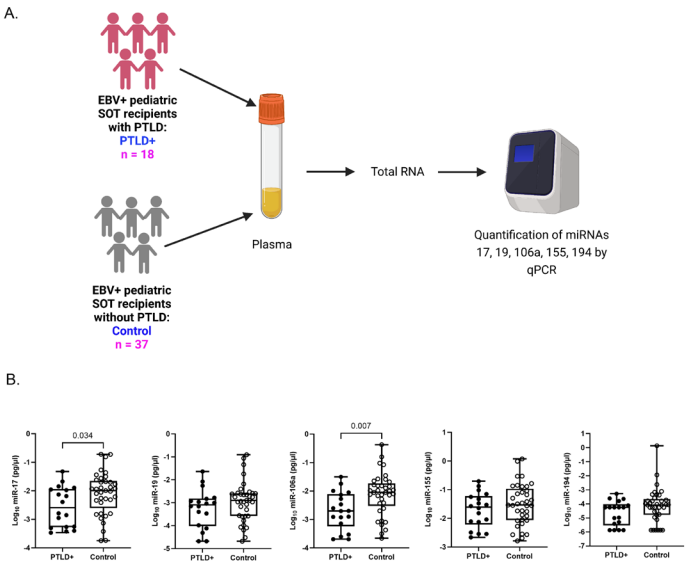

Identification of Engrailed-1 Positive Fibroblasts within Fibrotic Capsule During Foreign Body Response

Jennifer Parker, BSc[1,2]; Michelle Griffin, MBChB MRes MSc PhD MRCS[1]; Heather E. Talbot, BSc[1,2]; Shamik Mascharak, PhD[1,2]; Amanda F. Spielman, BSc[1]; Asha Cotterell, MSc[1]; Darren Abbas, MD[1]; Michael Januszyk, MD, PhD[1]; Derrick Wan, MD[1]; and Michael T. Longaker, MD, MBA[1,2]
[1]Department of Surgery, Division of Plastic and Reconstructive Surgery, Stanford University School of Medicine, Stanford, CA 94305, USA.
[2]Institute for Stem Cell Biology and Regenerative Medicine, Stanford University School of Medicine, Stanford, CA 94305, USA.

Introduction: We have recently shown that En1 positive fibroblasts (EPFs) predominate in wounds and are responsible for scar formation. Meanwhile, foreign body response (FBR) is a common surgical complication whereby a fibrotic capsule forms around an implant. Though believed to have some mechanistic overlap with normal wound healing, the specific cell populations responsible are unknown.

Methods: $En1^{Cre}$ transgenic driver mice were crossed with $R26^{mTmG}$ reporter mice, generating $En1^{Cre}$; $Rosa26^{mTmG}$ (En1+) mice. In these mice, cells that express En1 also express GFP, while all other cells express RFP. Silicone discs were surgically implanted below the subcutaneous layer of En1+ mice dorsi, and fibrotic capsules surrounding the implants were harvested at POD30. Immunohistochemistry and flow cytometry (FACS) analysis were utilized to evaluate the cellular characteristics of the En1+ cells.

Results: Using immunohistochemistry, En1+ cells were found to be more prevalent in the fibrotic capsule relative to unwounded tissue (*P<0.05, n=6). Furthermore, immunofluorescence staining and FACS revealed that GFP+ cells within the fibrotic capsules expressed pro-fibrotic markers such as Col-I, a-SMA, and Col-III. These cells were also negative for CD41 and CD45, endothelial and immune cell markers, respectively. These data indicate that En1+ cells seen within fibrotic capsules were primarily of fibroblast origin.

Conclusion: As with normal wound healing, where EPFs are prevalent within a healing scar, our findings strongly suggest that En1 plays a key role in fibrotic capsule formation. Further understanding of the mechanisms that drive En1 positive fibroblasts towards fibrosis may offer potential therapeutic targets to prevent fibrotic capsule formation.

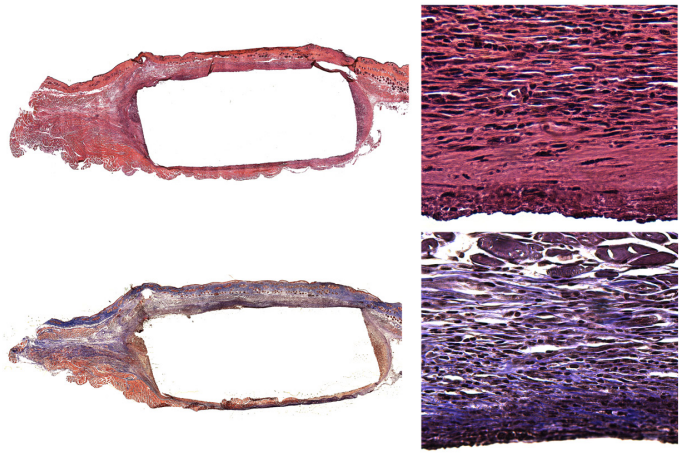

Figure 1: Sample H&E (top) and Masson's trichrome (bottom) staining illustrating the fibrotic capsule that forms around the silicone implant after 4 weeks post-transplant. Images on the left were taken at 10x, while those on the right were taken at 40x.

Adipocyte progenitor cells embedded in collagen gels accelerate bone formation in a murine calvarial critical defect model

Asha C. Cotterell[1], Amanda F. Spielman[1], Michelle Griffin[1], Evan Fahy, Nicholas Guardino, Darren Abbas[1], Hendrik Lintel, Jennifer Parker[1], Derrick Wan[1,2], and Michael T. Longaker[1,2,3]
[1]Hagey Laboratory for Pediatric Regenerative Medicine, Department of Surgery, School of Medicine, Stanford University, Stanford, CA, United States.
[2]Division of Plastic and Reconstructive Surgery, Department of Surgery, Stanford University School of Medicine, Stanford, CA, United States.
[3]Institute for Stem Cell Biology and Regenerative Medicine, Stanford University, Stanford, CA, USA.

Introduction: Adipocyte progenitor cells (APCs) defined by flow-assisted cell sorting have been identified as cells with the capacity to form vessels and adipocytes; the ability of APCs to contribute to bone healing is unknown. Our study evaluates the use of a subset of APCs to heal calvarial defects.

Methods: APCs were isolated by FACS according to a Sca1+, CD34+ and Pdgfra+ sorting strategy and seeded into collagen gels for 24 hours to allow for attachment. Adult C57Bl/6 mice (6–8-week-old) (n = 6) were then randomized into three conditions: 1. Calvarial (6mm) defect (Control group), 2. Calvarial defect with a collagen gel seeded with isolated APC (APC group), and 3. Calvarial defect with a collagen gel alone (gel group). Mice were euthanized at 12 weeks post-calvarial defect for histological and FACS analysis. MicroCT was collected at 0, 2, 4, 8, and 12 weeks to evaluate bone formation.

Results: MicroCT confirmed bone formation was significantly greater in the APC group, compared to the Control and Gel group at 12 weeks (*$p < 0.05$. Histological analysis by H&E and Pentachrome staining confirmed enhanced bone formation at 12 weeks compared to the Gel and Control group (*$p < 0.05$). FACS analysis revealed the Sca1+, CD34+, Pdgfra+ remained at the defect site in the collagen gel at 12 weeks.

Conclusions: Our results suggest that APCs represent a progenitor cell population that may enhance bone formation and vascularization. Collagen gels provide a system for APC delivery to enhance bone formation post-injury.

Transdermal Deferoxamine Improves Acute Wound Healing In Chronic Irradiated Skin In A Mouse Model

Hendrik Lintel, BS[1]; Darren B. Abbas, MD[1]; Christopher Lavin, MS[1]; Jason L. Guo, PhD[1]; Michelle Griffin, MBChB, PhD[1]; Nick Guardino, BS[1]; Andrew Churukian; Geoffrey C. Gurtner MD[1]; Michael T. Longaker, MD, MBA[1,2]; Derrick C. Wan MD[1]

[1]Hagey Laboratory for Pediatric Regenerative Medicine, Division of Plastic and Reconstructive Surgery, Department of Surgery, Stanford University School of Medicine, Stanford, CA

[2]Institute for Stem Cell Biology and Regenerative Medicine, Stanford University, Stanford, CA

Introduction: Radiation-induced skin fibrosis is a common chronic sequelae of radiation therapy which can be complicated by impaired wound healing. Transdermal deferoxamine (DFO) has been shown to improve wound healing and mitigate radiation-induced skin fibrosis in prior studies. In this study, we aim to investigate the effects of DFO on excisional wound healing in chronically irradiated skin in a mouse model.

Methods: Thirty C57BL/6 mice had their dorsal skin irradiated with 30 Gy fractionated over 6 doses of 5 Gy every other day. After waiting 4 weeks post-radiation for chronic fibrosis to develop, two 5mm excisional stented wounds were created on each mouse's dorsum. Mice were divided into 3 groups: an irradiated (IR) control, a vehicle-only patch, and a DFO patch. Another 10 nonirradiated wild-type mice were used as a normal wound comparison (A). Wound perfusion was assessed via Laser doppler and scar elasticity via suction Cutometer. Wounds were harvested at closure.

Results: DFO-treated mice grossly demonstrated faster wound closure rates than the vehicle and IR control groups but slower than nonirradiated wounds (B). Wound perfusion throughout healing and scar elasticity upon closure was similar in the DFO-treated and nonirradiated wounds (C-D). Histology also revealed increased collagen density and a more similar collagen ultrastructure to nonirradiated wounds in DFO-treated wounds when compared to vehicle and IRC wounds (E-F).

Conclusion: Transdermal DFO demonstrates potential as a treatment modality to improve acute wound healing outcomes in chronically irradiated skin.

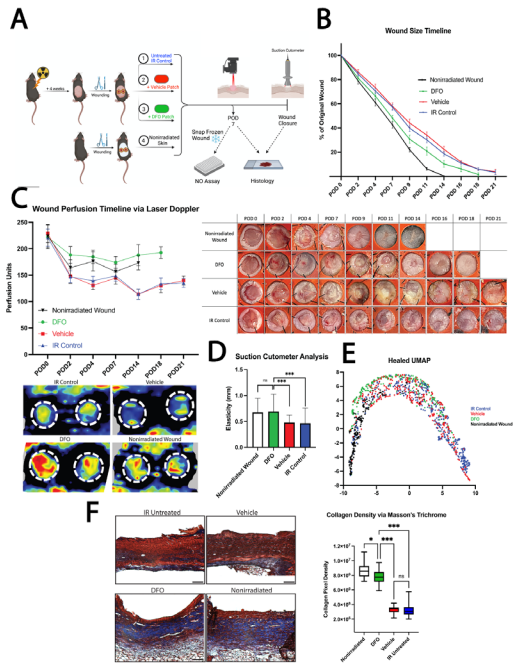

Quantitative Analysis of the Collagen Matrix Ultrastructure in Mouse Hearts after Myocardial Infarction

John M. Lu, Michelle F. Griffin, Jason L. Guo, Shamik Mascharak, Michael T. Longaker

Introduction: After acute myocardial infarction (MI), cardiac fibroblasts create a dense collagen scar that replaces the dead cardiac muscle to prevent acute cardiac rupture. Over time, however, the fibrotic scar is maladaptive and triggers hypertrophy and fibrosis in the remote myocardium, leading to ischemic cardiomyopathy and congestive heart failure. Large fibrotic scars are a poor prognostic predictor in post-MI patients. Despite the central role the MI collagen scar in the pathogenesis of ischemic cardiomyopathy, the formation and remodeling of the MI scar over time are poorly understood. To study MI scar formation, we sought to quantitatively analyze changes in the ultrastructure of the extracellular matrix after MI.

Methods: We subjected adult C57BL/6 mice to ischemic cardiac injury by permanent surgical ligation of the left anterior descending artery. We harvested hearts from ligated and sham-operated mice at 4, 7, and 14 days after ischemic injury. To examine the ultrastructure of the extracellular matrix, we developed an image-processing algorithm to profile 294 ultrastructural features (fiber length, width, etc.) from Picrosirius Red–stained histology viewed under polarized light.

Results: We demonstrate that the extracellular matrix massively expands and matures after acute MI (Fig 1a). The matrix ultrastructure is quantitatively distinct in fibrosed and control hearts (Fig 1b). We propose a model by which cardiac fibroblasts clonally proliferate to generate the MI scar.

Conclusion: The extracellular matrix ultrastructure follows a pro-fibrotic trajectory after MI. In the future, our extracellular matrix ultrastructure algorithm can be used quantify the effects of new anti-fibrotic therapies.

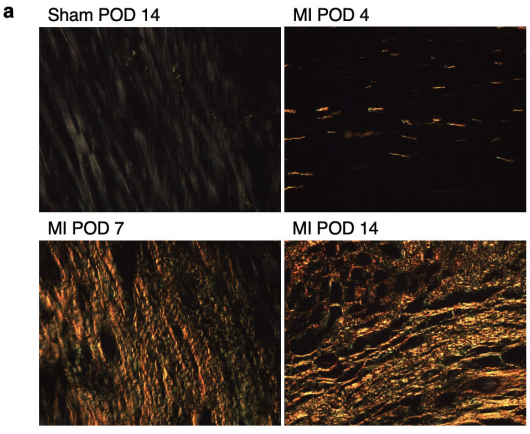

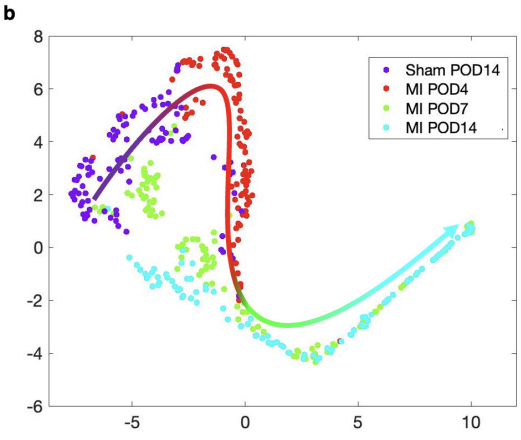

ABSTRACTS

Tackling the Bedside Artificial Intelligence Barrier: Natural Language Processing to Extract Injury ICD10 Diagnosis Codes Real-Time from Electronic Medical Records

Jeff Choi MD MSc, Yifu Chen BSc, Alexander Sivura BSc, Jenny Wang BSc, David A. Spain MD

Introduction: Despite surging interest, artificial intelligence (AI) prediction tools rarely reach the bedside. Many prediction tools require ICD10 diagnosis codes as inputs, yet these are time-consuming to extract manually. To tackle this prevalent AI adoption barrier, we aimed to build a natural language processing (NLP) algorithm that outputs injury ICD10 diagnosis codes real-time using unstructured text from the electronic medical record.

Methods: Our dataset comprised deidentified trauma tertiary survey notes from 3,472 patients (split 60-20-20 into train-validation-test sets) admitted to our trauma center between 2016 and 2020. We trained and fine-tuned a deep learning Bidirectional Encoder Representations from Transformers algorithm to automatically extract injury ICD10 codes from unstructured text. We compared algorithm-extracted ICD10 codes with manually-extracted codes (ground truths).We measured test set performance using micro-area under the curve (AUC) and compared our algorithm's performance against that of an industry benchmark (Amazon Comprehend Medical).

Results: Our NLP algorithm was trained using 1986 tertiary survey notes with 7914 injury ICD10 diagnosis codes (3957 ground truths, 3957 randomly-generated negative samples). The model automatically produced injury ICD10 diagnosis codes after users input free text describing injuries (e.g. injury list, radiology report). Compared with Amazon Comprehend Medical's micro-AUC of 0.76, our algorithm achieved validation set micro-AUC of 0.90.

Conclusion: We built a NLP algorithm that automatically extracts injury ICD10 diagnosis codes real-time from unstructured free text, with performance exceeding that of a leading industry benchmark. Automated ICD10 diagnosis code extraction could connect the missing link for many AI prediction tools to reach the bedside.

Figure. Workflow to extract injury ICD-10 diagnosis codes real-time from unstructured free text in electronic medical records

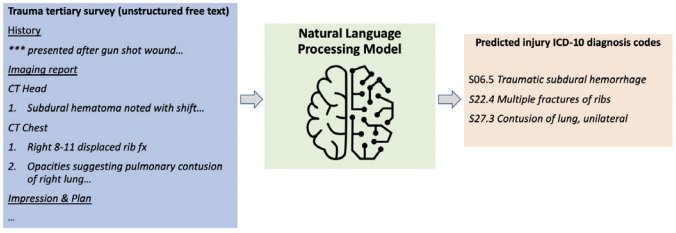

Predictive Value of Clinical Complete Response After Chemoradiation for Rectal Cancer

Charles Liu MD MS[1], Ana Carolina A. Boncompagni BA[1], Kenneth Perrone MD[1], Ank A. Agarwal BA[1], Dong G. Hur BA[1], Ivan Lopez BA[1], Vipul Sheth MD PhD[2], Arden M. Morris MD MPH[1]
[1]Department of Surgery, Stanford University School of Medicine
[2]Department of Radiology, Stanford University School of Medicine

Introduction: Previous research demonstrated that clinical complete response (cCR) after neoadjuvant therapy for rectal cancer only predicts pathologic complete response (pCR) in the surgical specimen about 25% of the time. Neoadjuvant therapy has improved, however, and assessment for cCR now includes technically advanced studies such as pelvic MRI, leading to consideration of selective non-operative management. We therefore evaluated the association between cCR and pCR in locally-advanced rectal cancer using a contemporary patient cohort.

Methods: We identified patients with rectal adenocarcinoma who underwent neoadjuvant chemoradiation followed by index proctectomy at Stanford Hospital from January 2012-December 2021. Patients without restaging imaging after neoadjuvant radiation were excluded. We defined cCR as absence of residual disease on restaging imaging. MRI was used for cCR determination if available, followed by PET and/or CT. We defined pCR as absence of residual adenocarcinoma in surgical pathology specimens.

Results: Among 523 eligible patients, 360 met inclusion criteria (57 had prior attempted resection, 71 no restaging imaging, and 35 excluded for other reasons); 36.9% were female, 51.9% were nonwhite, and mean age was 57.3 years (SD 13.4). cCR was determined in 167 patients by MRI, 115 by PET, and 78 by CT. Overall, 13.6% of patients had cCR and 12.2% had pCR. The sensitivity and positive predictive value of cCR were 34.1% and 30.6%, respectively.

Conclusion: Despite improvements in therapy and imaging technology, only 1/3 of patients with cCR after neoadjuvant chemoradiation for rectal adenocarcinoma had pCR at time of proctectomy. The limitations of cCR should be considered when contemplating non-operative management.

Table

	No cCR	**cCR**	**Total**	
No pCR	282 (78.3%)	34 (9.4%)	316 (87.8%)	Specificity: 89.2%
pCR	29 (8.1%)	15 (4.2%)	44 (12.2%)	Sensitivity: 34.1%
Total	311 (86.4%)	49 (13.6%)		
	NPV: 90.7%	PPV: 30.6%		

Out-of-Pocket Spending and Work Loss After Common Surgical Procedures Among Working-age Adults

Kathryn Taylor, Pooja Neiman, Zhaohui Fan, Andrew Ibrahim, John Scott

Introduction: Half of surgical patients report financial toxicity, which results from direct out-of-pocket (OOP) costs and indirect loss of income. This study aimed to assess the economic impact of common surgical procedures on patients' OOP spending and work loss among working-age adults.

Methods: We used the 2017-2019 MarketScan Database to identify adults ages 19-64 who underwent 1 of 20 common surgical procedures. These data were linked to the Health Productivity and Management (HPM) Database, which reports work absence and disability for a subset of employers. Outcomes included spending after index surgery, disability, and return to work. Multivariable regression models adjusted for patient demographics and clinical variables. To control for secular trends, we used 4:1 propensity score matching using patient and employment variables.

Results: We identified 135,480 patients and 541,920 matched controls. Among this cohort, 25% of patients had a non-elective presentation and 12% had an ICU admission. Spending, missed work, and disability for patients linked to the HPM database are shown in the Table. Non-elective presentation was associated with higher OOP spending and more short-term disability ($p<0.05$). Patients requiring ICU stays had higher OOP spending and more missed days of work and disability ($p<0.05$).

Conclusion: Patients recovering from surgery face high OOP payments, miss over a month of work on average, and 1 in 3 receive short-term disability benefits. These findings demonstrate the double burden of medical expenses and productivity loss, and can inform policies for improved financial risk protection after surgery.

Table: Six Month OOP Spending and Missed Work Following Common Surgical Procedures

	Surgical Patients	Matched Controls	Difference	p-value
Mean OOP Spending (Median, IQR)	$3,487 ($2,020, $749-3597)	$636 ($12, $0-422)	$2,851	<0.001
Any Missed Work	62.1%	32.5%	29.6%	<0.001
Mean Total Days Missed (Median, IQR)	23 (15,4-36)	3 (2, 0-4)	20	<0.001
Any Short-Term Disability	36.2%	2.7%	33.5%	<0.001
Mean Total Days of Short-Term Disability (Median, SD)	41 (32, 19-56)	35 (15, 0-54)	6	<0.001

Note: Surgical cohorts include common cardiac, vascular, general, and orthopedic procedures. OOP spending represents coinsurance, copays, and deductibles per patient. Missed work and short-term disability outcomes are only for those linked to the HPM database and employed at time of index admission.

Despite increasing costs, perfusion machines expand the donor pool of livers and could save lives

Thomas J. Handley, MBBS, MRCS; Katherine D. Arnow, MS; Marc L. Melcher, MD, PhD

Introduction: Liver transplantation is a highly successful treatment for liver failure and disease. However, demand continues to outstrip our ability to provide transplantation as a treatment. Many livers initially considered for transplantation are not used because of concerns about their viability or logistical issues. Recent clinical trials have shown discarded livers may be viable if they undergo machine perfusion, which allows a more objective assessment of liver quality.

Methods: Using the Scientific Registry of Transplant Recipients dataset, we examined discarded and un-retrieved organs to determine their eligibility for perfusion. We then used a Markov decision-analytic model to perform a cost-effectiveness analysis of two competing transplant strategies: Static Cold Storage (SCS) alone vs. Static Cold Storage and Normothermic Machine Perfusion (NMP) of discarded organs

Results: The average number of predicted successful transplants after perfusion was 383, representing a 5.6% increase in the annual yield of liver transplants. Our cost-effectiveness analysis found that the SCS strategy generated 4.64 QALYs and cost $479,226. The combined SCS + NMP strategy generated 4.72 QALYs and cost $481,885. Our model was sensitive to retransplantation rate (above 11.6% for NMP), cost of NMP transplant ($231,949) and waitlist cost ($69,842 per year). The combined SCS + NMP strategy had an incremental cost-effectiveness ratio of $33,575 per additional QALY over the 10-year study horizon.

Conclusion: Machine perfusion of livers currently not considered viable for transplant could increase the number of transplantable grafts by approximately 5% per year and is cost-effective compared to Static Cold Storage alone.

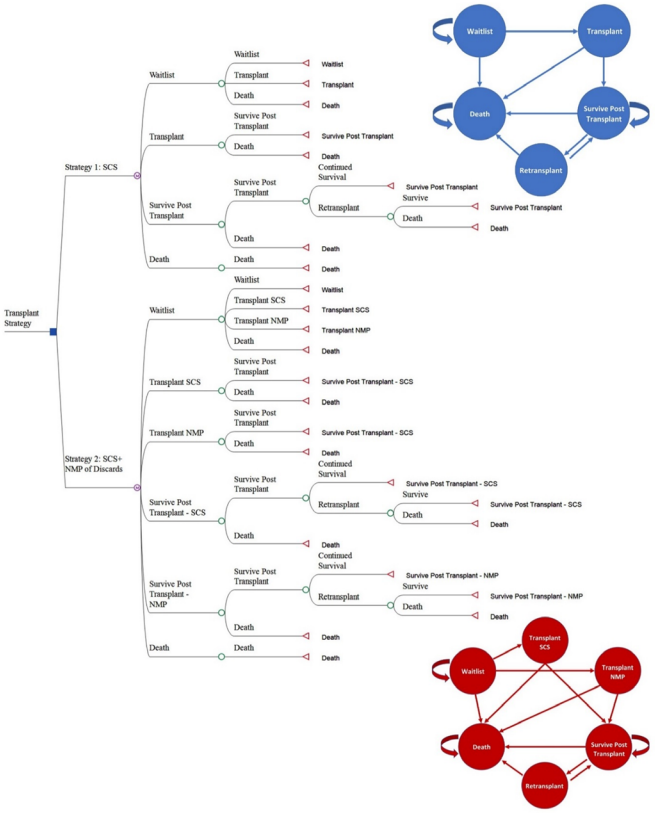

Figure 1 | Markov Model with State Transition Diagrams.

Technical Variant Liver Grafts Show Equal Graft Survival to Whole Liver Grafts in Pediatric Liver Transplantation at High Volume Transplant Centers

Dan Stoltz, MD; Amy Gallo, MD; Grant Lum, MS; Julianne Mendoza, MD; Carlos Esquivel, MD, PhD; Andrew Bonham, MD

Introduction: In the United States, 1 in 10 infants and 1 in 20 children die on the liver transplant waitlist. Technical variant liver transplantation (TVLT) is one strategy to mitigate this issue by utilizing deceased donor split or reduced grafts and live donors. Because donor recipient size mismatch remains a top reason for refusal of liver offers to pediatric candidates and living donation is not widely available, we examined if TVLT is a comparable option to whole liver transplant (WLT).

Methods: 5208 pediatric liver transplant recipients from 2010 through 2020 were identified using the Scientific Registry of Transplant Recipients database. Transplant centers were designated as high volume (HV) or low volume (LV) based on the average number of pediatric liver transplants performed per year: HV ≥5 and LV <5. Graft survival rates for WLT and TVLT up to 3 years post-transplant were compared using Kaplan-Meier curves and log-rank tests. Cox proportional hazards models were used to identify predictors of graft failure.

Results: When comparing WLT and TVLT at HV centers, there was no difference in graft survival (p=.057). TVLT at HV centers demonstrated significantly improved graft survival compared to TVLT at LV centers (p<0.001). Transplantation at a LV center was the only predictor significantly associated with graft failure: aHR 1.6 (95% CI 1.14-2.24, p=0.007) in patients <12 years of age, and aHR 1.8 (95% CI 1.13-2.87, p=0.01) in patients ≥12 years of age.

Conclusion: HV transplant centers demonstrate equivalent WLT and TVLT graft survival, suggesting there is an opportunity to transplant children in a timelier manner with increased TVLT utilization. Further training in TVLT techniques is needed to facilitate broader use and better outcomes at LV centers.

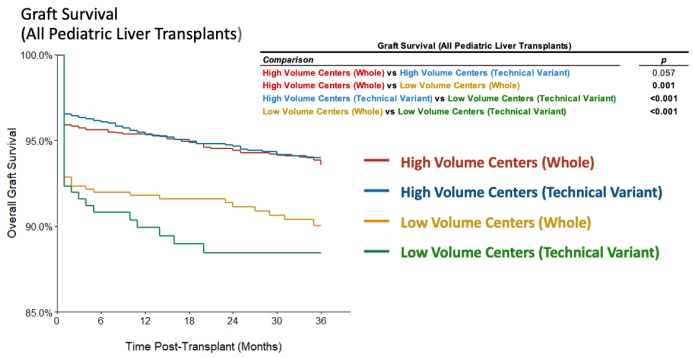

Remote Access to Electronic Medical Record Reduces Overall EMR Time for Vascular Surgery Residents

Vy T Ho MD, Mike Sgroi MD, Venita Chandra MD, Steven M Asch MD MPH, Jonathan H Chen MD PhD, Jason T Lee MD

Introduction: Surveys suggest surgical residents spend 30-40% of training on the electronic medical record (EMR), raising concerns about burnout and insufficient operative experience. We characterize resident EMR activity on a vascular surgery service to identify modifiable factors associated with high EMR use.

Methods: Resident EMR activity was queried for time spent, post-graduate year (PGY), remote access via mobile device or personal computer, and patient census including operative caseload. A linear mixed-effects model was developed with normalized daily EMR time as the outcome variable, random slopes for resident and patient census, and fixed effects of PGY level, academic year, and remote access.

Results: 53 residents from July 2015 to June 2019 were included. Mean daily usage was 1.6 hours. The most time-consuming activities were chart review (43.0-46.6%) and notes review (22.4-27.0%, Figure 1). In the linear mixed-effects model, resident seniority (Coefficient = -1.2, p-value < 0.001) and increased remote access (Coefficient = -0.44, p-value < 0.001) were associated with reduced daily EMR usage. Total EMR usage decreased significantly from the 2015-2016 academic year to 2018-2019 (mean difference 2.4 hours vs 1.78, p-value <0.001).

Conclusion: On a vascular surgery service, mean EMR time was lower than survey estimates. Resident seniority and remote access utilization were associated with reduced EMR time, independent of patient census. While EMR access via personal devices has been hypothesized to encourage poor work-life balance, our study suggests a time-saving effect by enabling expedient data review. Further work in other specialties is needed to explore implications for resident wellness initiatives.

Figure 1. Distribution of electronic medical record activities by resident level

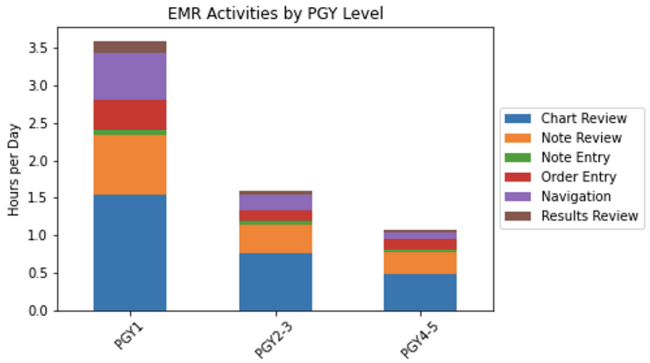

	PGY1	PGY2/3	PGY4/5
Mean Daily EMR Usage (Hours, SD)	3.6 (2.5)	1.6 (1.5)	1.1 (1.1)
Mean Time Spent per EMR Action Category (Hours, % Daily)			
Order Entry	0.40 (11.4)	0.14 (8.8)	0.13 (12.0)
Navigation	0.62 (17.5)	0.21 (12.8)	0.08 (7.5)
Results Review	0.17 (4.7)	0.05 (3.1)	0.03 (3.2)
Chart Review	1.55 (43.8)	0.76 (46.6)	0.47 (43.0)
Note Review	0.79 (22.4)	0.38 (23.8)	0.30 (27.0)
Remote Time Spent (Hours, SD) {split }	0.24 (0.6)	0.40 (0.4)	0.36 (0.4)
Patient Census	19 (11)	19 (14)	14 (13)

Machine Learning Can Predict Recurrence Patterns after Liver Transplantation in Hepatocellular Carcinoma Patients: Analysis from the US Multicenter HCC Transplant Consortium

Raja R Narayan MD MPH[1], Lida Safarnejad PhD[1], Saeed Amal PhD[1], Benjamin V Tran MD[2], Mindie H Nguyen MD MAS[3], Elsie G Ross MD MSc[1], Vatsche G Agopian[2], Marc L Melcher MD PhD[1]
[1]Department of Surgery, Stanford University School of Medicine, Stanford, CA
[2]Department of Surgery, David Geffen School of Medicine at University of California Los Angeles, Los Angeles, CA
[3]Department of Medicine, Stanford University School of Medicine, Stanford, CA

Introduction: Hepatocellular carcinoma (HCC) is a rapidly growing cause of cancer death in the US. Despite strict transplantation criteria, some develop liver (LR) and extrahepatic recurrences (ER). The goal of this study is to use machine learning to predict recurrence patterns after transplantation for HCC.

Methods: Consecutive HCC patients transplanted at 20 US centers from 2002-2013 were studied for clinicopathologic features associated with recurrence. A Random Forest classification model (an ensemble machine learning method using decision trees) was constructed. This model uses a 10-fold cross-validation strategy trained on 90% of the cohort and validated on the remaining 10%.

Results: Of 4980 patients, 594 (11.9%) recurred with a median follow up of 47 months. Only LR occurred in 137 (23.1%), only ER in 372 (62.6%), and 63 (10.6%) had ER + LR. Patients with LR more commonly had hemachromatosis (2.5% vs 0.4%, p=0.030) whereas use of any locoregional therapy was associated with any (77.6% vs 71.2%, p=0.001) and ER (78.2% vs 71.3%, p=0.003) but uniquely not LR (77.5% vs 71.7%, p=0.086). On averaging the area under the curve (AUC) for the ten strategies, mean AUC=0.68 and 0.74 were obtained for LR and ER, respectively (Figure 1A-1B). Shapley plots for recurrence revealed similar pre-transplant features associated with LR and ER (Figure 1C-1D).

Conclusion: Recurrence after liver transplantation for HCC was uncommon but usually extrahepatic. Without information on donor livers, similar pre-transplant features predicted LR and ER. More information on the donor liver is needed to predict the risk for recurrence by location.

Figure 1: Receiver operator curves are shown for A: LR and B: ER after 10-fold Random Forest classification. Shapley plots are shown for C: LR and D: ER with most predictive features for recurrence listed at the top and features with greater Shapley (SHAP) values portending greater risk of recurrence.

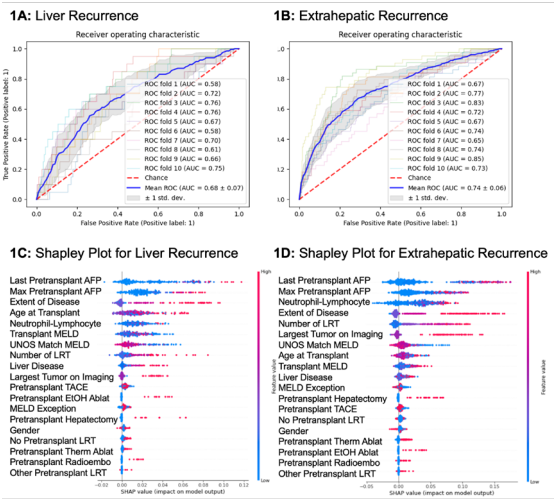

Health Equity Ratings of US Burn Centers—Does For-Profit Status Matter?

Nada Rizk, MS; Clifford C Sheckter, MD

Introduction: Achieving health equity is forefront in national discussions on health care delivery. Burn injuries transcend racial and socioeconomic boundaries. Burn center funding ranges from safety-net to for-profit without an understanding of how funding mechanisms translate into equity outcomes. We hypothesized that health equity would be highest at non-profit centers and safety-net centers.

Methods: All American Burn Association verified and non-verified burn centers in 2022 were collated. Safety-net status, for-profit status, and health equity rating were extracted from datasets furnished by the Lown Institute. Equity ratings were compared across national burn centers and significance was determined with comparative statistics and ordinal logistic regression.

Results: On an equity grade of A to D (A is the best), 27.6% of centers were rated A, 27.6% rated B, 41.5% rated C, and 3.3% rated D. 17.1% of all burn centers were designated as for-profit compared to 21.1% of centers that were safety-net. 73.1% of safety-net centers scored an A rating, and 14.3% of for-profit centers scored an A rating. Safety-net centers were 21.8 times more likely (p<0.001) to have the highest equity score compared to non-safety-net centers. There was an 80% decrease in the odds of having a rating of A for for-profit centers compared to non-profit centers (p=0.04).

Conclusion: Safety-net centers had the highest equity ratings while for-profit burn centers scored the lowest. For-profit funding mechanisms may lead to the delivery of less equitable burn care. Burn centers should focus on health equity in the triage and management of their patients.

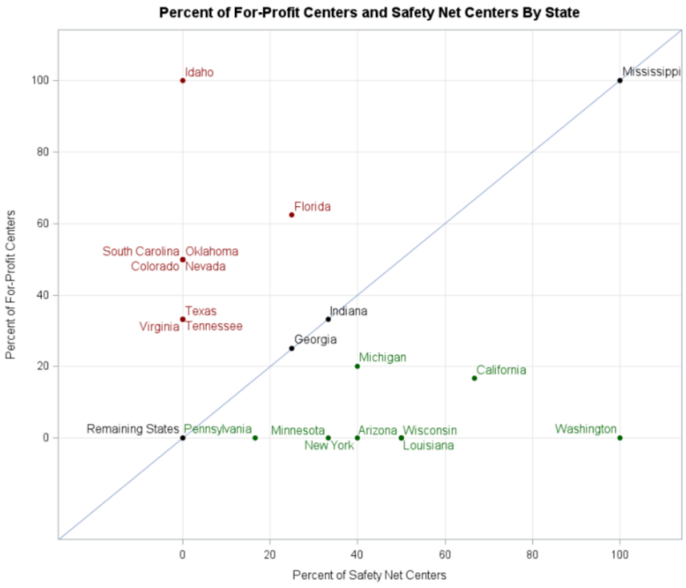

Figure 1: Percent of For-Profit and Safety-Net Centers shown by state. The x-axis of this figure shows the percentage of burn centers classified as safety-net centers and the y-axis is the percentage of burn centers classified as for-profit centers. Each dot represents a state or multiple states, if they share the same proportion of safety-net and for-profit burn centers. States that appear in green have a higher proportion of safety-net to for-profit burn centers, states in red have a higher proportion of for-profit to safety-net burn centers, and states in black on the y=x slope line have equal proportions of safety-net and for-profit centers.

Development Of A Dynamic Map Of Peripheral Myeloid Cells Associated With Acute Rejection Of Vascularized Composite Tissue Allografts

James T. Harden, Samuel Fuentes, Xi Wang, Jeanna Enriquez, Andrea Reitsma, Carlos O. Esquivel, Olivia M. Martinez, Sheri M. Krams

Introduction: Myeloid cells are involved in early alloactivation in response to organ allografts and can initiate acute rejection. The heterogeneity of myeloid populations and the modulation of surface markers during the immune response make it difficult to delineate between subsets using traditional myeloid lineage markers and pairwise gating. We therefore performed high-dimensional unsupervised analysis using single cell mass cytometry (Cytometry by Time-Of-Flight; CyTOF) to characterize myeloid cells in acute rejection using a panel of 46 metal-conjugated antibodies.

Methods: We developed a fully MHC mismatched (BALB/c onto C57Bl/6) murine vascularized composite allotransplant (VCA) model with heterotopic transplantation of donor limb onto recipient mice to investigate how composite tissue allografts impact myeloid immunity. In this VCA model, rejection is characterized by scarring and color change of the graft by day 3-5 post-transplant, and rejection is complete by day 8-10. We collected splenocytes on days 3, 5, and 7 from groups (n=4) of syngeneic and allogeneic graft recipients. All samples (n=24) were barcoded and stained with an antibody panel against 46 surface antigens and analyzed by CyTOF.

Results: The antibody panel was designed to identify macrophages, classical and non-classical monocytes, granulocytes, type 1 and type 2 conventional dendritic cells (cDC1 and cDC2), plasmacytoid dendritic cells, and monocyte-derived dendritic cells. By day 3 of alloimmunity, classical monocytes have 10-fold elevated expression of CCR2, a chemokine receptor that enables monocyte trafficking. By day 5, the proportion of CCR2+ classical monocytes was increased significantly ($p < 0.05$) in allograft recipients. In addition, a subset of CCR2+ monocytes upregulated MHCII and PDL1 was upregulated on a subset of Ly6G+/Ly6C- neutrophils. By day 7 post-transplant we observed a sustained, increased proportion of CCR2+ monocytes along with elevated CLEC10a on both cDC2 and MHCII+ monocytes.

Conclusion: In summary, we developed a dynamic myeloid map of early VCA acute rejection representing multiple myeloid populations, protein markers, and time-points. Our systems level high-dimensional analysis is the groundwork for characterizing pathways critical for acute rejection, identifying biomarkers that distinguish rejecting from non-rejecting grafts, and developing therapeutic strategies that specifically target alloreactive myeloid cells.

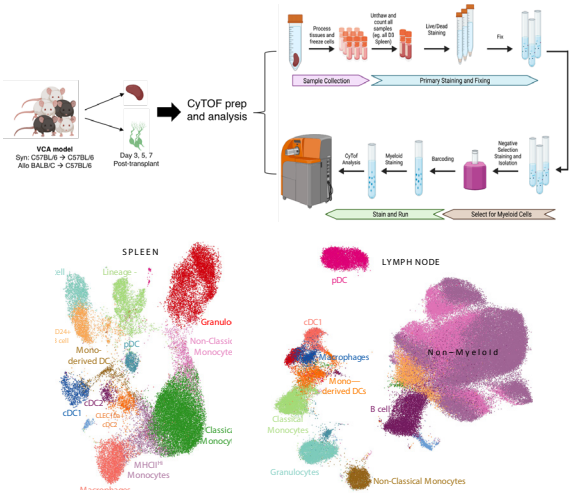

Inhibiting Yes-associated protein prevents scarring and promotes regeneration in a large animal model of wound repair

Heather E. Talbott, AB; Michelle F. Griffin, MD, PhD; Shamik Mascharak, BS; Nicholas J. Guardino, BS; Darren Abbas, MD; Christopher Lavin, MS; Jason L. Guo, PhD; Amanda F. Spielman, BS; Asha Cotterell, MS; Jennifer B.L. Parker, BS; Michael Januszyk, MD, PhD; H. Peter Lorenz, MD; Derrick C. Wan, MD; Michael T. Longaker, MD, MBA

Introduction: We recently showed that inhibiting mechanotransduction (Yes-associated protein [YAP]) in mouse wounds yields regeneration without scarring. However, rodents are loose-skinned and fail to recapitulate key aspects of human wound repair. We sought to elucidate the effects of YAP inhibition in red Duroc pig wounds, the most human-like model of scarring.

Methods: Full-thickness excisional wounds (2x5cm hexagons) were produced on the dorsum of adult pigs. Wounds received intradermal verteporfin (YAP inhibitor; 2mg/mL) or vehicle control (PBS) followed by primary repair with 3-0 Vicryl deep dermal and 3-0 Monocryl running subcuticular sutures. Cutometer measurements were obtained to assess tissue stiffness every two weeks. Wounds and unwounded skin were harvested after 16 weeks for histologic (hematoxylin and eosin staining), mechanical (Instron strength testing), and scRNA-seq (10X Chromium) analyses.

Results: Grossly and histologically, verteporfin treatment significantly reduced scarring and promoted skin regeneration, including recovery of hair follicles/glands (Figure 1A-B). Verteporfin-treated wounds were both significantly less stiff (Figure 1C) and stronger (Figure 1D) than PBS-treated wounds, with mechanical properties similar to those of unwounded skin. scRNA-seq identified two novel fibroblast subpopulations, one enriched in regenerating (verteporfin) wounds and unwounded skin, the other enriched in scarring (PBS) wounds (Figure 1E-F; clusters 1 and 4, respectively). Pseudotime trajectory constructs demonstrated putative state transitions between these two populations, which were supported by prospective FACS isolation and force manipulation in a 3D culture system.

Conclusion: One-time local administration of verteporfin following injury significantly reduces scarring and induces regenerative healing in a large animal model.

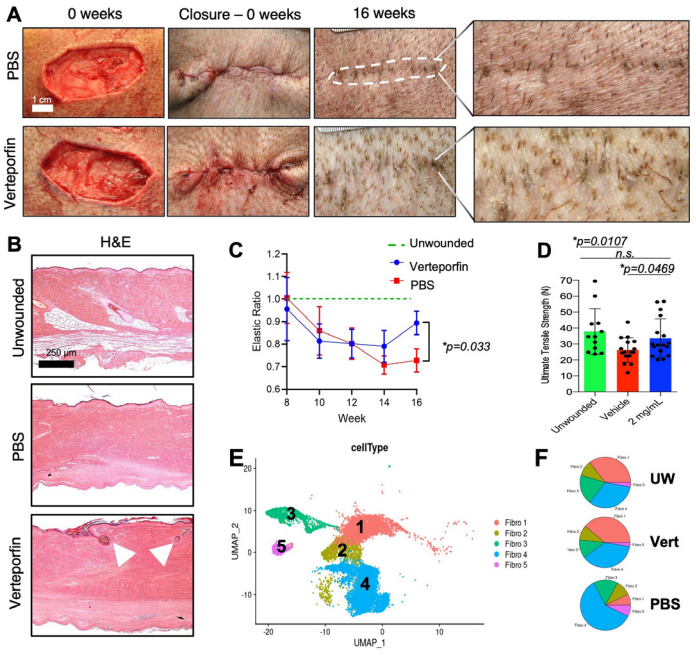

Single-cell CyTOF profiling of pediatric immune responses to organ transplantation demonstrates that allograft type determines post-transplant immune makeup

Mahil Rao, Meelad Amouzgar, James T. Harden, M. Gay Lapasaran, Amber Trickey, Brian Armstrong, Jonah Odim, Tracia Debnam, Carlos O. Esquivel, Sean C. Bendall, Olivia M. Martinez, and Sheri M. Krams

Introduction: Solid organ transplant is lifesaving for children with end-stage heart, liver, or kidney disease. To date, there has been no comprehensive analysis of the peripheral blood immune response to a solid organ allograft in children.

Methods: Blood was obtained from 52 pediatric recipients of liver, heart, kidney, or intestinal grafts enrolled at seven sites in the NIAID-sponsored Clinical Trials of Organ Transplantation in Children (CTOTC)-06. Patients were varied with respect to age, time from transplantation, and allograft health status. Peripheral blood mononuclear cells from patients were stained with 37 immune-cell markers and analyzed by single-cell mass cytometry. The abundance of 32 populations of immune cells was determined by manual gating.

Results: Principal component analysis revealed that allograft type is an important driver of differences in post-transplant immune composition. Liver and kidney recipients were more like each other and distinct from heart recipients. Heart recipients had higher proportions of CD4 EM, CD4 effector T cells, plasmablasts, and naïve B cells compared to liver or kidney recipients. We observed the same phenomenon using linear discriminant analysis, an independent method of analyzing differences between cohorts. When controlling for differences in allograft type, we also observed a decreased proportion of a novel T cell population ($CD45^+CD3^+CD19^-CD4^+CD8^-CD25^{lo}CD5^+CD38^-FoxP3loCD45RA$) in patients with graft rejection.

Conclusion: We identified distinct differences in immune response based on allograft status and identified a population whose abundance is associated with decreased graft stability. Additional studies will determine if this T cell population can be harnessed to predict or prevent allograft rejection.

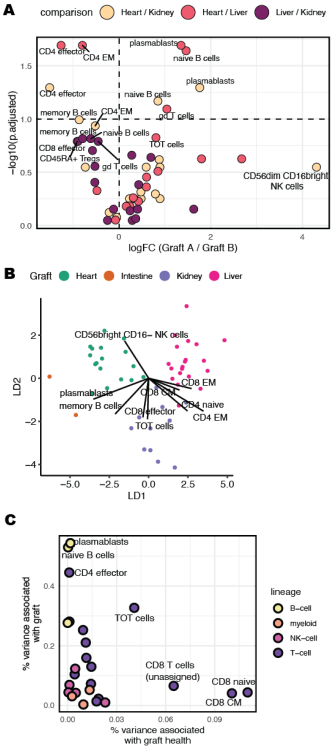

Adipocytes the forgotten cell in skin fibrosis; exploring the mechanism of fat driven skin fibrosis

Michelle Griffin, Heather E. desJardins-Park, Nicholas Guardino, Amanda F. Spielman, Kellen Chen, Kristian E. Bauer-Rowe, Jason Guo, Michael Januzyk, Derrick Wan, and Michael T. Longaker

Introduction: Adipocytes have previously been implicated in skin wound healing in both metabolic and non-metabolic roles. We hypothesized that mature adipocytes directly participate in wound repair via conversion into fibroblasts, and that adipocyte-derived fibroblasts contribute to skin scarring.

Methods: $AdipoqCre^{ERT}$ transgenic driver mice were crossed to R26mTmG reporter mice to generate $AdipoqCre^{ER}T$;ROSA26mTmG mice to perform lineage tracing of mature adipocytes. To achieve local adipocyte ablation AdipoqCre;ROSA26mTmG;R26tm1(HBEGF) Awai mice were generated and wounded, and diphtheria toxin (DT) was injected into the wound base. DT- and vehicle control-treated wounds underwent histologic analysis. Lastly, we performed scRNAseq on wounded and unwounded tissue to identify fibrotic fibroblast subpopulations.

Results: Using our AdipoqCre;ROSA26mTmG adipocyte lineage-tracing model(Fig.1A), we identified significantly greater number of adiponectin lineage-positive cells (GFP+) within wounds at post-operative day-14 (POD-14) compared to unwounded skin (*P<0.05, n=6)(Fig.1B). FACS further confirmed that the GFP+ cells were fibroblasts and increased to 10% at POD-14(Fig.1C). Compared to typical subcutaneous adipocytes, the GFP+ cells exhibited upregulation of fibroblast markers and downregulation of adipocyte markers(Fig.1D). DT-induced ablation of Adipoq lineage-positive cells(Fig.1E) exhibited reduced scar thickness(Fig.1F) and collagen deposition at POD-14 compared to control wounds (*P<0.05, n=6) (Fig.1G). scRNAseq analysis revealed novel markers for distinct mechanosensitive fibroblast subpopulations responsible for scar formation(Fig.1H).

Conclusion: Our findings strongly suggest that mature adipocytes in the skin undergo conversion to pro-fibrotic fibroblasts in response to injury. Local adipocyte ablation resulted in reduced scarring, suggesting that adipocyte-derived fibroblasts are important contributors to wound fibrosis. These findings together suggest that adipocyte mechanosensitive fibroblast subpopulations drive dermal scar formation.

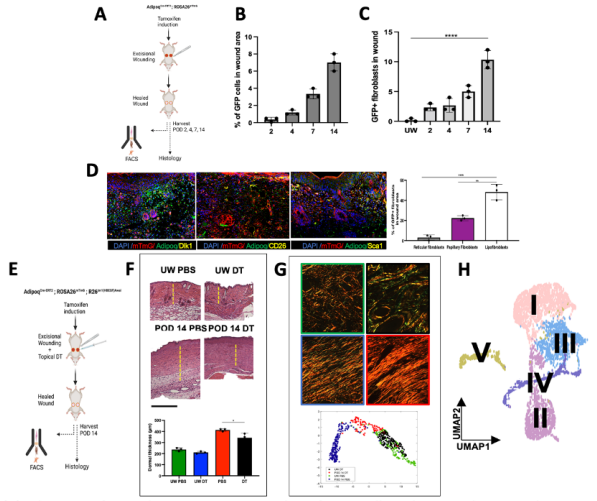

(A) Schematic of wounding experiment. Number of GFP+ cells in the wound increased at POD-14 by histology (B) and FACS (C). (D) GFP+ cells lost adipocyte markers and gained fibroblast markers in the wounds. (E) DTR adipocyte ablation following wounding decreased dermal thickness (F) and collagen deposition (G). (H) scRNAseq UMAP analysis identified distinct fibroblast populations in the skin following wounding.

Appendiceal mucinous neoplasms and pseudomyxoma peritonei tumors are defined by distinct cellular states and a goblet cell identity.

Ayala CI[1], Sathe A[3], Grimes S[4], Shen J[2], Bai X[3], Poultsides G[1], Lee B[1] and Ji HP[3,4]

[1]Division of Surgical Oncology, Department of Surgery, Stanford University School of Medicine, Stanford, CA, United States
[2]Department of Pathology, Stanford University School of Medicine, Stanford, CA, United States
[3]Division of Oncology, Department of Medicine, Stanford University School of Medicine, Stanford, CA, United States
[4]Stanford Genome Technology Center, Stanford University, Palo Alto, CA, United States

Introduction: Pseudomyxoma peritonei (PMP) develops after perforation of the appendix in the presence of an appendiceal mucinous neoplasm (AMN). This results in tumor cell dissemination. Current mainstem therapy consists of cytoreductive surgery and heated intraperitoneal chemotherapy using mitomycinC (MMC). However, the origins of this tumors remain elusive.

Methods: Patients were consented using IRB protocols. Surgically collected specimens were dissociated into single cells suspensions used to generate cDNA libraries that were sequenced followed by bioinformatic analysis. The ex-vivo treatments were conducted with saline or MMC for 2 hours at 37 degree C.

Results: Using single cell transcriptomic analysis of AMN (n=5) and PMP (n=9) patient tumors we show the tumor cells have a goblet cell identity. Our trajectory analysis shows both cohorts have progenitor states of goblet cells differentiating and the co-existence of multiple cellular states. Meanwhile, PMP tumor cells have a differentiated metastatic state. Our bioinformatic analysis, discovers dysregulation in tetraspanin, kallikrein, MYC, mTOR and RAS pathways. Interestingly, the AMN and PMP tumor microenvironment (TME) contained CD4 T follicular helper-like cells and cytotoxic CD8 T cells with features of immune exhaustion. Last, we show that ex-vivo treatment of dissociated tumor (n=1) using MMC results in cytotoxicity for lymphocytes and goblet cells.

Conclusion: We have discovered AMN and PMP tumors contain distinct cellular states of differentiating goblet cells. We show tumors of both cohorts are heterogenous with a TME that contains characteristics amenable to checkpoint inhibition therapy. Last, we show that current mainstem therapy, MMC, is cytotoxic for tumoral cells.

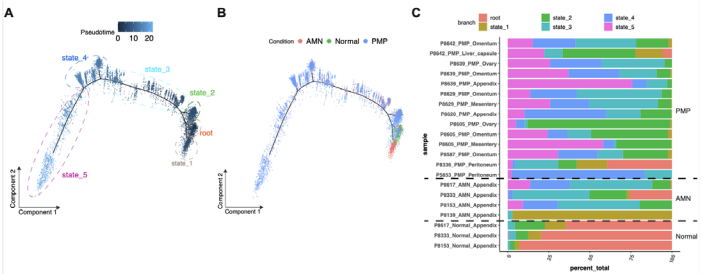

Neoadjuvant Intratumoral Immunotherapy with TLR9 Activation and Anti-OX40 Antibody Eradicates Metastatic Cancer

Wan Xing Hong, Idit Sagiv-Barfi, Debra K. Czerwinski, Adrienne Sallets, Ronald Levy

Introduction: The combination of the synthetic TLR9 ligand CpG and agnostic OX40 antibody can trigger systemic anti-tumor immune responses upon co-injection into the tumor microenvironment, eradicating simultaneous untreated sites of metastatic disease. Here we explore the application of this in situ immunotherapy to the neoadjuvant setting.

Methods: CT26 tumor cells were injected into the tail vein and a day later subcutaneously at the right side of the abdomen. 4T1 tumor cells were injected orthotopically into the right abdominal mammary fat pad under direct visualization. When tumors size reached 0.7 cm in the largest diameter, mice were randomized to the experimental groups except in T cell depletion studies, in which animals were randomized prior to tumor cell inoculation. In groups receiving local treatments, either PBS or CpG and anti-OX40 were injected into the tumor in a volume of 50μL. In groups undergoing resection, the primary tumor is surgically resected 4 days after the last intratumoral treatment.

Results: We demonstrated that local administration of neoadjuvant immunotherapy improves survival and systemic disease control and decreases local recurrence in two separate preclinical solid tumor models. The importance of CD8+ T cells was consistently underscored in our depletion experiments, in which the anti-tumor effect and survival benefit of neoadjuvant immunotherapy was abrogated in both tumor models.

We also established baseline parameters around timing for neoadjuvant treatment. We found that with neoadjuvant local immunotherapy an interval, albeit short, was needed between immunotherapy and surgical resection. When the neoadjuvant immunotherapy was given too close to resection the efficacy of neoadjuvant immunotherapy was lost. No animals treated with this single delivery of high dose intratumoral immunotherapy were lost to systemic toxicity or had resection of their primary tumor delayed due to ill effects, attesting to safety of the local treatment modality.

Lastly, the lungs of tumor bearing mice treated with intratumoral CpG and aOX40 had significant upregulation of PD-1 on macrophages, T cells and CD11b+ c dendritic cells. When mice bearing 4T1 tumor were treated as above with neoadjuvant immunotherapy with or without the addition of anti PD-1 antibody, the group that received systemic aPD-1 in addition to local CpG/aOX40 demonstrated improved local and systemic disease control.

Conclusion: By extending the use of local immune modulating treatment with a TLR9 agonist and an anti OX40 antibody to the neoadjuvant setting, we demonstrated effectiveness in eliminating distant pulmonary metastases and overall survival. and in conferring lasting tumor immunity. The two different preclinical solid tumor models utilized demonstrated the broad applicability of this neoadjuvant therapeutic modality to a diverse array of tumor types and its additional efficacy when combined regimen with systemic PD1 blockade. These results provide a strong rationale for translating this neoadjuvant intratumoral immunotherapy to the clinical setting, especially in conjunction with established checkpoint inhibitors.

Decoding and modulation of spiking activity of the sciatic nerve in an awake and moving rodent

Eric T. Zhao[1], Zeshaan N. Maan[2]*, Katharina S. Fischer[2]*, Janos Barrera[2], Allyson K. Davis[3], Nofar Hemed[4], Dominic Henn[2], Kellen Chen[2], Chikage Noishiki[2], Michael Januszyk[2], Geoffrey G. Gurtner[2], Nicholas A. Melosh[4]*

** These authors contributed equally towards this work.*
[1] Department of Chemical Engineering, Stanford University, Stanford, CA
[2] Department of Surgery, Stanford University, Stanford, CA
[3] Department of Comparative Medicine, Stanford University, Stanford CA
[4] Department of Materials Science and Engineering, Stanford University, Stanford CA

Introduction: Conventional prostheses do not interface directly with neural signals but use either body motion or muscle activity as a proxy. Consequently, these prostheses are difficult to use, tiring, have limited function, and provide no sensory feedback. For the development of an advanced anthropomorphic prosthetic arm that can recapitulate the degrees of freedom and sensory feedback of the human hand, it is critical to design a low damage, high fidelity, and stable peripheral nerve interface (PNI). The key innovation of our microfabricated device, is that our electrodes are orders of magnitudes more compliant than existing PNIs, approximately 1500 and 40,000,000 times more compliant than the Transverse Intrafascicular Multichannel Electrode (TIME) and Utah Slanted Electrode Array (USEA) respectively.

Methods: The device consists arrays of individual 1 µm thick, and 4 µm wide electrodes, each with a 15 µm diameter recording/stimulation pad, mimicking the dimensions, compliance, and spatial distribution of axon bundles in the peripheral nerve. An electrochemically etched, 80 µm tungsten microwire was threaded through a hole on the device and drawn through the sciatic nerve of a C57BL/6J mouse. A custom designed circuit board was mounted on a 3D-printed backpack to facilitate chronic recording and stimulation.

Results: Mice ran voluntarily on a cylindrical treadmill in a head strained condition, while we recorded the neural activity with our device. Spiking activity was readily observed in our electrodes, where we isolated 6 single units across our 16 electrodes. Using markerless pose estimation, we extracted the joint angles innervated by the sciatic nerve and found a robust correlation between spiking activity and gait. The ultra-small size of the electrodes and their proximity to individual axons permitted extremely local stimulation – down to eliciting movement in a single toe.

Discussion: To our knowledge, we are the first to record single neuron spiking activity in the peripheral nervous system of an awake and moving rodent. This represents a substantial advance, in that we overcame a series of challenges involving: (1) Microfabrication of ultra-thin electrodes to mirror the surrounding biomechanical environment to minimize the foreign body response, (2) Device robustness under substantial movement and strain, (3) Microsurgical device implantation to minimize acute insertion damage. Future work will involve electrical modulation to augment movement in peripheral nerve neuropathies and translation into larger animal models with increased channel counts for movement decoding.

Treating lymphedema with a propeller lymphatic tissue flap combined with nanofibrillar collagen scaffolds.

Peter Deptula, MD; Dimitrios Dionyssiou, MD; Anastasios Topalis, MD; Michael Paukshto, PhD; Tatiana Zaitseva, PhD; Efterpi Demiri, MD, PhD; Stanley Rockson, MD; Dung Nguyen, MD, PharmD.

Introduction: The aim of our study was to evaluate a new propeller vascularized lymphatic tissue flap (pLNT) combined with aligned nanofibrillar collagen scaffolds (CS) (BioBridge™) in reducing established lymphedema in the rat lymphedema model.

Methods: Unilateral hindlimb lymphedema was created in 15 female Sprague–Dawley rats following inguinal and popliteal lymph node resection and radiation. An inguinal pLNT was elevated from the contralateral groin and transferred through a skin tunnel to the affected groin. Four collagen threads were attached to the flap and subcutaneously inserted to the hind limb. The three study groups consisted of Group A (control), Group B (pLNT), and Group C (pLNT + CS). Volumetric analysis of both hind limbs was performed using micro-CT imaging at 1 and 4 months postoperatively. Lymphatic drainage was assessed with ICG fluoroscopy for number and morphology of new collectors and ICG transit time.

Results: An increased limb volume remained in group A (5,321% ± 4,74), while there was a significant mean limb volume reduction in group B (-13,395% ± 8,545) and an even greater reduction in group C (-14,560% ± 5,042). ICG fluoroscopy proved the functional restoration of lymphatic vessels through the CS and viability of pLNT in group C (p=0.043).

Conclusions: The pedicled lymphatic tissue flap combined with collagen scaffolds is an effective procedure for the treatment of lymphedema in rats. It can be translated into treatment of humans' lower and upper limb lymphedema; further clinical studies are required prior to recommend the above method.

Figure 1: Representative photographs of three study groups during ICG evaluation.

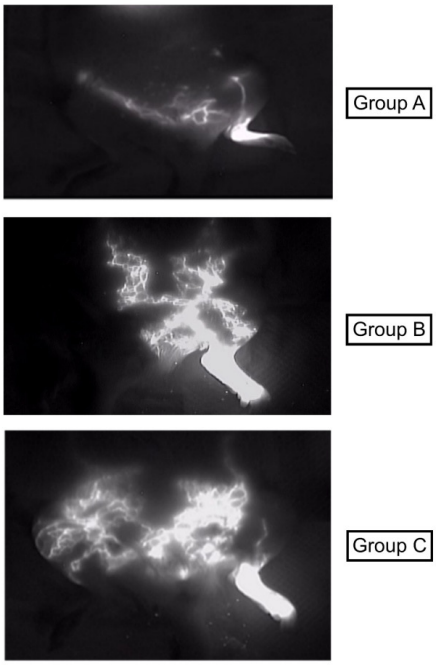

Improved lymphatic drainage and an increase in the number of new lymphatic collectors is demonstrated in treatment groups B and C. Group C (pLNT + CS) demonstrates statistically significant increase in number of collectors compared to control.

VIRTUAL POSTER SESSION

In addition to the top eight posters featured today on the CAM Courtyard the following 37 abstracts can be viewed online at https://surgery.stanford.edu/holman/2021.html

Resident Research Day

Virtual Poster Session – Basic

Title of Presentation	Presenter
Gastrointestinal Myoelectric Measurements via Simultaneous External and Internal Electrodes in Pigs	Fereshteh Salimi Jazi, MD
High-resolution natural killer cell phenotyping by mass cytometry in EBV+ and EBV- individuals	Wenming Zhang, PhD
Lineage tracing reveals adipocytes are responsible for muscle fibrosis following nerve injury	Amanda Spielman, MD
Changes in gut muscularis immune cell composition correlated with aging and fecal incontinence	Madison McCarthy
Investigating the Role of Natural Killer Cells in the Control of Latent Epstein-Barr Virus Infection	Josselyn Pena

Title of Presentation	Presenter
Craniofacial dysmorphology and impaired suture patterning in a mouse model of Frank-ter-Haar syndrome	Julika Huber, MD
Eradication of Bacterial Growth with Topical Antibiotic Treatment in Human Collagen Hydrogel Carrier	Evan Jarman
The Safety of Elution of Multiple Antibiotics from Collagen-Rich Hydrogel for Topical Treatment of Chronic Polymicrobial Wounds	Ayushi Sharma
Leveraging Technology-Based Interventions to Identify Barriers to Breast Health Awareness and Engagement in Preventative Practices Among Diverse Communities	Cassidi Goll

Resident Research Day

Virtual Poster Session – Clinical

Title of Presentation	Presenter
Radiographic, Biochemical or Pathologic Response to Neoadjuvant Chemotherapy in Resected Pancreatic Cancer: Which is Best?	M. Usman Ahmad, MD
Evaluating the Impact of the COVID-19 Pandemic on Emergency Medicaid Programs: Have Insurance Rates Improved Among Trauma Patients?	Ana Carolina Boncompagni
Complications associated with subsequent vascular access in pediatric ECMO patients	Katelyn Chan
Two Stage Nipple Sparing Mastectomy Does Not Compromise Oncologic Safety	Julia Chandler, MD. MS
Where to Next? Geographical Impact of Plastic Surgery Residency to Fellowship Placement	Gina Eggert
Association of parathyroidectomy vs. observation with the development of worsening chronic kidney disease (CKD) in adults with primary hyperparathyroidism - consider poster presentation	Adam Furst, MS, JD
Warming of Donor Kidneys During Recipient Transplantation	Keith Hanse, MD
Use of Antibiotic-Impregnated Polymethylmethacrylate (PMMA) Plates for Prevention of Periprosthetic Infection in Breast Reconstruction	Thomas Johnstone
Effect of Climate on Development of Surgical Site Infections	Raymond Liou, MD
Laser treatment of breast reduction scars: A patient reported outcomes study	Kelsey Lipman, MD
Location Matters: The Geographical Impact of Plastic Surgery Residency to First Job Placement	Bhagvat Maheta
Machine Learning to Elucidate National Trends in Crowdfunding for Surgical Care	Advait Patil
AI-Based Video Segmentation: Procedural Steps or Basic Maneuvers?	Calvin Perumalla, PhD
Avoiding the Emergency Department After Ambulatory Surgery: Can We Do Better?	Charlotte Rajasingh, MD
Leveraging Embedded Haptic Sensor Technology for Force Mapping in Orthoses for Adolescent Idiopathic Scoliosis	Brett Wise
Generating Rare Surgical Events Using CycleGAN: Addressing Lack of Data for AI Event Recognition	Su Yang
Hybrid Breast Reconstruction with Adjustable Saline Implants: A Five Year Review	Anna Zhou, MD
Adoption of a standardized treatment protocol for pilonidal disease leads to low recurrence	Talha Rafeeqi, MBBS
Where there is fat there is fibrosis: Elucidating the mechanisms of creeping fat-driven stricture formation.	Khristian E. Bauer-Rowe

Gastrointestinal Myoelectric Measurements via Simultaneous External and Internal Electrodes in Pigs

Fereshteh Salimi-Jazi, MD, Anne-Laure Thomas, MS, Talha Rafeeqi, MD, Modupeola Diyaolu, MD, Lauren S.Y. Wood, MD, Steve Axelrod, PhD, Anand Navalgund, PhD, Lindsay Axelrod, MS, James C.Y. Dunn, MD, PhD

Background: Currently, there is no accurate noninvasive measurement system to diagnose GI motility disorders. Wireless skin patches have been introduced to provide an accurate noninvasive measurement of GI myoelectric activity which is essential for developing neuro-stimulation devices to treat GI motility disorders. The aim of this study is to compare the external and internal electrical signal measurements in ambulatory pigs.

Methods: Yucatan pigs underwent placement of internal electrodes on the stomach, small intestine, and colon. Wires were brought through the abdominal wall. Signals were collected by a wireless receptor. Four external patches were placed on the abdominal skin to record the signals simultaneously. Pigs were kept for 6 days while the sensors were continuously recording the data from both systems.

Results: Internal sensors detected rich signals from each organ. The stomach had a dominant frequency that ranged from 4 to 4.5 cpm, with occasional higher frequencies at 2, 3 and 4 times that. Small intestine signals had their primary energy in the 12-15 cpm range. Colon signals primarily displayed a dominant broad peak in the 4-6 cpm region. External skin patches detected a substantial fraction of the activities measured by the internal electrodes. A clear congruence in the frequency spectrum was observed between the internal and external readings.

Conclusion: Internally measured myoelectrical signals confirmed different patterns of rhythmic activity of the stomach, small intestine, and colon. Skin patches provided GI myoelectric measurement with a range of frequencies that could be useful in the diagnosis and treatment of motility disorders.

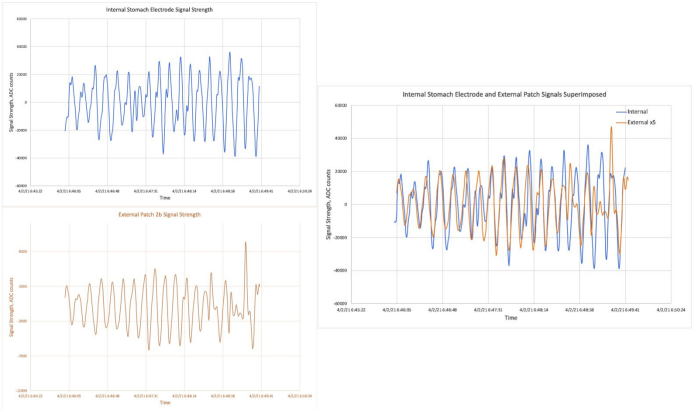

Figure 2: portion of raw data of a spectrum from stomach shown in figure 3; A: Signals detected from internal electrode, B: Signals detected from external patch, and C: overlapped signals detected from internal electrode and x5 strength signal detected by external patch.

High-resolution natural killer cell phenotyping by mass cytometry in EBV+ and EBV- individuals

*Wenming Zhang[1], Josselyn K. Pena[1,2], Potchara Boonrat[1,2], James T. Harden[1,2], Olivia M. Martinez[1,2], *, Sheri M. Krams[1,2],**

[1] Department of Surgery, Stanford University School of Medicine, Stanford, CA, USA

[2] Stanford Immunology, Stanford University School of Medicine, Stanford, CA, USA

** equal contributions*

Introduction: While it is known that natural killer (NK) cells are important in control of Epstein Barr virus (EBV) infection, the specific populations involved remain to be determined. Previous work in our laboratory has shown that NKG2A+ NK cells are enriched in the NK cell population that can recognize and respond to B cells latently infected with EBV. The purpose of this study was to: 1) determine whether EBV alters the proportion of NKG2A+ NK cells in vivo and 2) achieve high-dimensional phenotyping of the NKG2A population associated with EBV, including activation receptor expression.

Methods: Using mass cytometry, we analyzed the phenotype and function of NK cell subsets in a cohort of pediatric transplant patients enrolled in a perspective, multicenter, observational trial (CTOT-C-06). We established a 48-marker panel and analyzed peripheral blood NK cells (3-5x10^6 PBMCs) obtained 6-9 months post-transplant from 32 participants who were either EBV naïve (n=18) or EBV seropositive (n=14).

Results: There was a significant increase in the proportion of CD3-NKG2A+CD56+ NK cells in individuals who were EBV+ compared to those who were EBV- (median: 3.86%, 2.1%, respectively, p = 0.0143). High dimensional analysis of the NKG2A+ NK cells revealed unique populations.

Conclusion: Our findings indicate: 1) EBV infection is associated with increased proportions of NKG2A+ NK cells in vivo and 2) NKG2A+ NK cells include subsets that are phenotypically and functionally diverse and express NK cell activation receptors including CD94, NKG2D, NKp46, DNAM-1. Understanding the NK cell subsets that control EBV infection will lead to improved therapies for transplant recipients.

Lineage tracing reveals adipocytes are responsible for muscle fibrosis following nerve injury

Amanda F. Spielman[1], Michelle Griffin[1], Asha C. Cotterell[1], Kristian E. Bauer-Rowe[1], Jason Guo[1], Jennifer Parker[1], Darren Abbas[1], Hendrick Lintel[1], Derrick Wan[1,2], and Michael T. Longaker[1,2,3]
[1]Hagey Laboratory for Pediatric Regenerative Medicine, Department of Surgery, School of Medicine, Stanford University, Stanford, CA, United States.
[2]Institute for Stem Cell Biology and Regenerative Medicine, Stanford University, Stanford, CA, USA.

Introduction: The culprits of muscle fibrosis in aging, muscular dystrophies, and following muscle injury are unknown. Adipocytes have been shown to participate in organ fibrosis but their role in muscle scarring is yet to be determined. We compared the behavior of adipocytes in murine muscle fibrosis models caused by both chemical and nerve injuries.

Methods: *Adipoq*^{Cre} transgenic driver mice were crossed to *R26*^{mTmG} reporter mice to generate *Adipoq*^{Cre}*;ROSA26*^{mTmG} mice, in which mature adipocytes (*Adipoq*/adiponectin-expressing cells) express green fluorescent protein (GFP), and all other cells express a red fluorescent protein (RFP). *Adipoq*^{Cre}*;ROSA26*^{mTmG} mice underwent sciatic nerve injury or barium chloride injections. Injured tibialis anterior muscles were harvested at postoperative day-14 (POD14) and underwent immunofluorescent staining for fibroblast (collagen type IV/col-IV, alpha-smooth muscle actin/α-SMA) and adipocyte (perilipin) cell markers.

Results: We identified a significantly greater number of adiponectin-lineage-positive cells (GFP+) within injured muscle caused by both chemical and nerve injuries compared to uninjured muscle at POD14 (*$P<0.05$, $n=5$). The GFP+ cells that infiltrated the muscle injury exhibited upregulation of fibrotic markers including col-IV and α-SMA, and downregulation of adipocyte markers including perilipin, indicating conversion of adipocytes into pro-fibrotic fibroblasts.

Conclusion: Our findings show that adipocytes undergo conversion to pro-fibrotic fibroblasts in muscle fibrosis in response to both chemical and nerve injuries. Further study into the interaction between nerves and adipocytes warrants further investigation to overcome muscle fibrosis.

Changes in gut muscularis immune cell composition correlated with aging and fecal incontinence

Madison S McCarthy[a], Hong Namkoong[b], Leila Neshatian[b], Laren Becker[b], Brooke Gurland[a]
[a] Department of Surgery, Stanford University School of Medicine
[b] Department of Gastroenterology and Hepatology, Stanford University School of Medicine

Introduction: Little is known about the immune composition of the muscularis layer in human intestine, but inflammation has been speculated as an etiology for declining gut function. The goal of this study was to assess the relationship between immune cell composition, aging, and fecal incontinence (FI)

Methods: Distal colon tissue was obtained under an IRB-approved study in patients undergoing surgery for indications including: cancer, prolapse, diverticulitis, constipation, and volvulus. Muscularis was dissected from colon specimen and analyzed using flow cytometry to identify macrophages (CD14+), lymphocytes (CD3+CD19+), and DCs (CD14-CD11c+). FI was measured using a validated CCF ("Wexner") Incontinence Score. Pearson correlation was used for statistical analysis.

Results: Tissue was taken from 26 patients, 21 female (80.8%), ranging from 25-95 years of age. 14/26 patients (53.8%) completed the CCF Incontinence Score. Using Pearson correlation, age was associated with rising macrophages (R2=0.05, p=0.28) and declining lymphocytes (R2=0.05, p=0.27), measured as a percent of CD45+ cells (Figure 1). Higher incontinence scores were significantly correlated with increasing macrophages (R2=0.33,p=0.02) and declining lymphocytes (R2=0.61,p=0.0006) (Figure 2). Levels of DCs did not correlate with age or incontinence score.

Conclusion: Our findings suggest a shift in the immune composition that favors muscularis macrophages might contribute to age-dependent underlying GI disease pathogenesis. Future studies are necessary to determine whether immunotherapies may be effective treatments for these disorders.

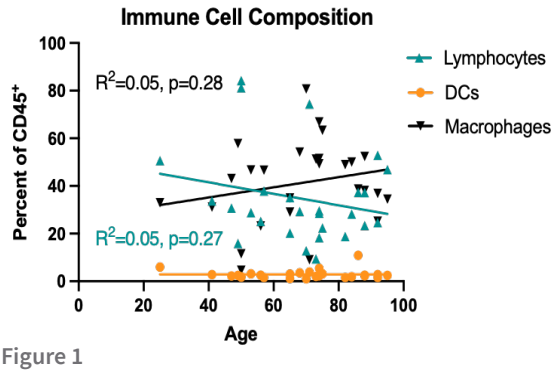

Figure 1

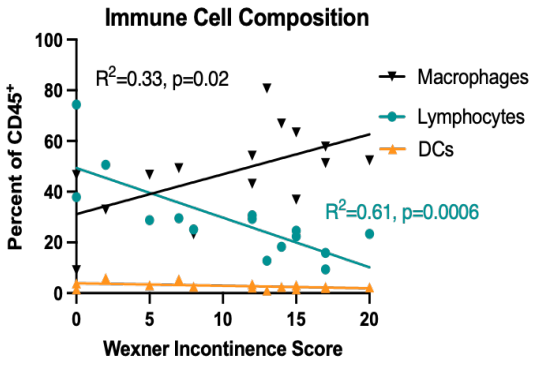

Figure 2

Investigating the Role of Natural Killer Cells in the Control of Latent Epstein-Barr Virus Infection

Josselyn K. Peña, Jiaying Toh, Hong Zheng, Wenming Zhang, Purvesh Khatri, Carlos O. Esquivel, Olivia M. Martinez and Sheri M. Krams

Introduction: Epstein–Barr virus (EBV) is a ubiquitous gamma-herpesvirus that persists as a chronic, asymptomatic infection in over 90% of the adult human population. EBV infections are mainly asymptomatic and subside due to a vigorous host T cell response with the virus transitioning to latency in a subset of memory B cells. Failure to control latent EBV infection can result in a variety of EBV-associated malignancies, including lymphoproliferative diseases in immunocompromised people. Studies in both experimental models and humans suggest that NK cells are critical in the host defense against EBV. In previous work, we demonstrated that NK cells expressing the inhibitory receptor NKG2A were specifically able to recognize and kill autologous B cell lines latently infected with EBV. We also demonstrated that HLA-E-presented peptides derived from EBV latent cycle proteins can impair NKG2A recognition and its downstream inhibitory signaling, potentially leading to NK cell activation.

Methods: To better understand the phenotype of NK cells that respond to EBV-infected B cells, we generated a panel of EBV-lymphoblastoid cell lines (EBV-LCL) and performed co-culture experiments with primary NK cells and either autologous EBV-LCL or autologous B cells. Responsive (CD107a+) NK cells were FACS-sorted and sequenced via 10X Genomics single-cell RNA sequencing. Subsequent analyses were completed in R using the Seurat v3 package.

Results: Confirming what we and others had previously observed, NKG2A is upregulated in EBV-LCL-responsive NK cells and increased IFNg and IL2RA upregulation distinguish EBV-LCL-responsive NK cells from other CD107a+ cells. ISG15 and CCL3 are also upregulated by EBV-LCL-responsive NK cells. ISG15 has been implicated as a central player in the antiviral response and CCL3 is important in inflammatory responses.

Conclusion: Additional experiments are underway using a novel mass cytometry panel of over 40 NK functional and phenotypic markers to provide insights into the mechanism whereby NKG2A+ NK cells can recognize and kill EBV-LCL.

Craniofacial dysmorphology and impaired suture patterning in a mouse model of Frank-ter-Haar syndrome

Huber J, Dr. med., Menon S, BS, Lopez M, BS, Wu J, PhD, Longaker, Michael T, MD, PhD, Quarto, Natalina, PhD

Introduction: Podosomes, actin-rich organelles on the cell membrane, contribute to embryo development by facilitating cell migration, extracellular matrix degradation and cell adhesion. Multiple genetic syndromes have been associated with mutations of podosomal proteins encoded on the *SH3PXD2B* gene. In our study, we aimed to analyze the impact of a non-functioning podosomal apparatus on craniofacial development using a *Sh3Pxd2b*$^{nee\ -/-}$ mouse, a model of human Frank-ter-Haar syndrome.

Methods: Micro-CT imaging, Alizarin Red and calcein whole mount staining was performed to characterize craniofacial deformities. Histological analysis and immunofluorescent staining was conducted to characterize differences in suture patterning. Proliferation, migration and osteogenic potential was assessed *in-vitro* and *in-vivo*. Transcriptomic profile was performed by bulk RNA sequencing analysis.

Results: *Sh3Pxd2b*$^{nee\ -/-}$ mice displayed severe craniofacial dysmorphology with shortened noses, domed skulls, generally smaller skeletons and abnormal suture patterns (Fig.1A,B). Histological analysis (Fig. 1C) and immunofluorescence (Fig.1D) revealed lack of endochondral ossification in the posterofrontal suture preventing physiological closure and dysmorphic suture pattern with ectopic bone formation and hypomineralization in the sagittal suture (Fig.1E) in mutant mice. Neural crest-derived dura mater cells from *Sh3Pxd2b*$^{nee\ -/-}$ mice demonstrated decreased proliferative, migratory and osteogenic potential (Fig.1F-I) compared to the Wild-Type (WT) *in-vitro* and *in-vivo*. Bulk-RNA sequencing specified differences in gene expression between the mutant and the WT mice.

Conclusion: Taken together, these findings highlight the important role of functional podosome complex in craniofacial development and suture patterning.

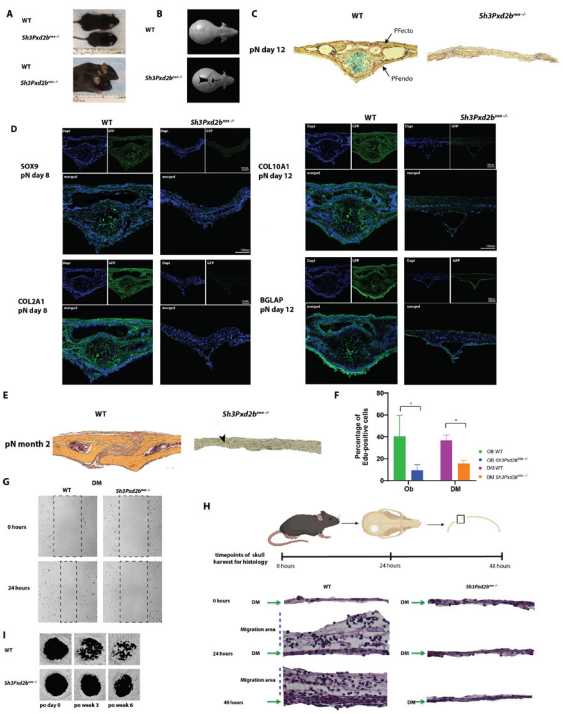

Figure 1
(A) Photos of a WT (top) and a mutant Sh3Pxd2b$^{nee\ -/-}$ mouse (bottom). The mutant mouse showing craniofacial and skeletal dysmorphology. (B) Micro-CT image of a WT (top) and mutant (bottom) skull 30 days postnatally. The images show enlarged and patent PF and Sag sutures and a non-mineralized area in the centre of the PF and Sag sutures. (C) Pentachrome staining of the PF suture on postnatal (pN) day 12, showing the WT suture undergoing endochondral ossification, while the mutant PF displays a lack of endochondral ossification (D) Immunofluorescence staining for chondrogenic markers in WT and mutant PF sutures present in endochondral ossification during the time of physiological PF suture fusion. No signal is present in the mutant PF sutures emphasizing lack of endochondral ossification. (E) Pentachrome staining of the WT and mutant Sag sutures in pN month 2 ,showing disrupted suture patterning in the mutant Sag compared to the WT. (F) EdU-proliferation assay of dura mater (DM) cells and osteoblasts (Ob) derived from WT and mutant mice showing decreased proliferation in mutant DM cells. (G) Scratch assay of mutant and WT DM cells revealing significantly decreased migration in mutant cells after 24 hours. (H) Schematic depicting the creation of calvarial defects in the parietal bone of WT and mutant mice. H&E staining of histological sections of the defect area demonstrating lack of upward migration of cells in mutant mice (bottom panels). (I) Micro-CT analysis of the calvarial defect area in mutant and WT mice showing decreased bone regeneration in mutant mice.

Eradication of Bacterial Growth with Topical Antibiotic Treatment in Human Collagen Hydrogel Carrier

Evan Harris Jarman[1,2], Ayushi Sharma[1,2], James Chang MD[1,2], Paige Fox MD PhD[1,2]
[1] Division of Plastic & Reconstructive Surgery, Department of Surgery, Stanford University School of Medicine, Stanford, California, USA
[2] Division of Plastic & Reconstructive Surgery, Veterans Affairs Palo Alto Health Care System, Palo Alto, California, USA

Purpose: Bacterial infections in chronic wounds can be clinically devastating, leading to prolonged and complicated care. Current treatment of infected chronic wounds consists of high-dose oral and intravenous antibiotics; however, this treatment causes systemic side-effects and is often ineffective at eliminating bacterial biofilms. Our lab has developed a novel human collagen hydrogel (cHG) embedded with antibiotic (cHG-abx) for topical treatment of infected wounds. We hypothesize that topical administration of our novel cHG-abx will effectively inhibit growth of multiple clinically significant bacteria over time.

Methods: Prepared 2.5% cHG was mixed with 100X minimum inhibitory concentration of clindamycin (100 µg/ml) or gentamycin (500 µg/ml) to treat *C. perfringens* and MRSA, respectively. Fibroblasts and ADSCs from humans and mice were topically treated for up to 72 hours to test physiologic cytotoxicity of treatment. To determine the elution of antibiotics over time, cHG-abx combinations were pre-eluted in PBS at multiple timepoints between 0 -72 hours. Modified Kirby-Bauer and crystal violet assays were used to assess the effectiveness of cHG-abx inhibition of bacterial growth over time.

Results: No significant mammalian cell death was found at any time point. Both Kirby-Bauer and crystal violet assays demonstrated significant bacterial inhibition for 48 hours compared to no treatment for *C. perfringens* and MRSA (Figures A&B). Furthermore, significant differences in bacterial elimination over elution time indicate sustained release of antibiotics.

Conclusion: Human collagen hydrogel embedded with antibiotics is capable of sustained low-dose antibiotic release to successfully inhibit growth of various clinically relevant bacterial strains while maintaining mammalian cell viability.

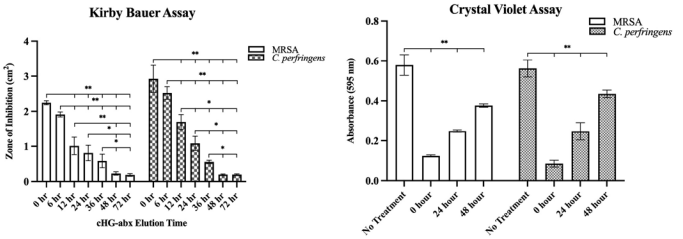

Figures: A) Quantification of zone of Inhibition from cHG-abx eluted over 72 hours. B) Quantification of bacterial viability post-treatment with various eluted cHG-abx by crystal violet absorbance (595 nm). * indicates p<0.05, ** indicates p<0.001

The Safety of Elution of Multiple Antibiotics from Collagen-Rich Hydrogel for Topical Treatment of Chronic Polymicrobial Wounds

Ayushi Sharma BS[1,2], Evan Harris Jarman BS[1,2], Amar Singh PhD[1,2], Paige Fox MD PhD[1,2]
[1] Division of Plastic & Reconstructive Surgery, Department of Surgery, Stanford University School of Medicine, Stanford, California, USA
[2] Division of Plastic & Reconstructive Surgery, Veterans Affairs Palo Alto Health Care System, Palo Alto, California, USA

Introduction: Chronic non-healing wounds significantly strain modern healthcare systems, affecting 1-2% of the population in developed countries with costs ranging between $28.1 and $96.8 billion annually[1]. Additionally, it has been established that chronic wounds complicated by comorbidities, such as peripheral vascular disease and diabetes mellitus, tend to be polymicrobial in nature.[2] Treatment of polymicrobial chronic wounds with oral and IV antibiotics can result in antimicrobial resistance, leading to more difficult-to-treat wounds. Ideally, chronic ulcers would be topically treated with antibiotic combinations tailored to the microbiome of a patient's wound. We have previously shown that a topical collagen-rich hydrogel (cHG) can elute single antibiotics to inhibit bacterial growth in a manner that is nontoxic to mammalian cells.

Methods: We analyzed the microbiology of cultures taken from human patients diagnosed with diabetes mellitus suffering from wounds present for more than 6 weeks. We then examined the safety of the elution of multiple antibiotics from cHG in differentiated and undifferentiated mammalian cells in vitro.

Results: The majority of human chronic wounds in our study were polymicrobial in nature. (Figure 1) Additionally, the elution of multiple antibiotics from cHG designed to treat these polymicrobial wounds was well-tolerated in mammalian cells.

Conclusion: This study demonstrates that the application of a topical drug-eluting hydrogel with a combination of antibiotics in the hydrogel is safe for use in mammalian cells. This could transform the treatment of chronic diabetic wounds, which are often polymicrobial with unique resistance patterns requiring multiple antibiotics.

Figure 1. The microbiology of ten adult patients diagnosed with diabetes mellitus and a chronic wound defined as a wound present for more than 6 weeks.

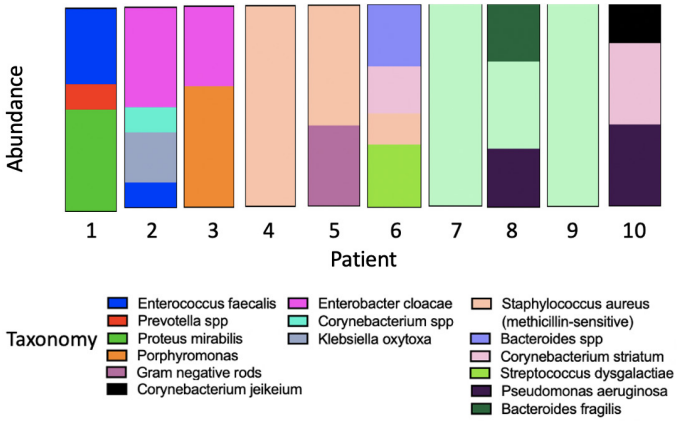

[1] Nussbaum SR, Carter MJ, Fife CE, et al. An Economic Evaluation of the Impact, Cost, and Medicare Policy Implications of Chronic Nonhealing Wounds. *Value Heal*. Published online 2018. doi:10.1016/j.jval.2017.07.007
[2] Dalton T, Dowd SE, Wolcott RD, et al. An In Vivo Polymicrobial Biofilm Wound Infection Model to Study Interspecies Interactions. *PLoS One*. 2011;6(11):27317. doi:10.1371/JOURNAL.PONE.0027317

Leveraging Technology-Based Interventions to Identify Barriers to Breast Health Awareness and Engagement in Preventative Practices Among Diverse Communities

Cassidi Goll, Pamela Ratliff, Rina Bello, Colleen Carvalho, Michelle Earley, Dr. Alyce Adams, Dr. Carla Pugh

Introduction: Black women are 42% more likely to die from breast cancer in part due to delayed diagnosis and inadequate treatment.[1] Early detection is critical to addressing inequities in breast cancer outcomes. Focusing on Black women, this research seeks to identify barriers to breast health awareness and assess acceptance of a technology-based intervention to promote engagement in early detection.

Methods: This is a bi-directional community engagement research project using cross-sectional survey methods to assess breast health knowledge and perceptions and their relationship to the use of evidence-based preventive services (e.g., mammogram) among a diverse cohort of women attending community breast health events (Breast Cancer and African Americans, Bay Area Cancer Connections).

Results: Among 306 survey respondents, women not trained on how to perform breast self-exams (BSEs) are more likely to never have received a mammogram (31% vs. 10%), are more likely to receive a mammogram only when there is a suspected mass (25% vs. 13%), and are more likely to receive zero clinical breast exams per year (50% vs. 11%). Black women were least likely to report having been trained to do a BSE compared to non-Black women (84% of Black women, 92% of non-Black women trained).

Conclusion: Among this diverse group of women from community settings, women who had not been trained in BSEs were less likely to receive early detection services. Additional research evidence is needed to understand the links between breast self-exam training and use of evidence-based, life-saving preventive services to inform public policy.

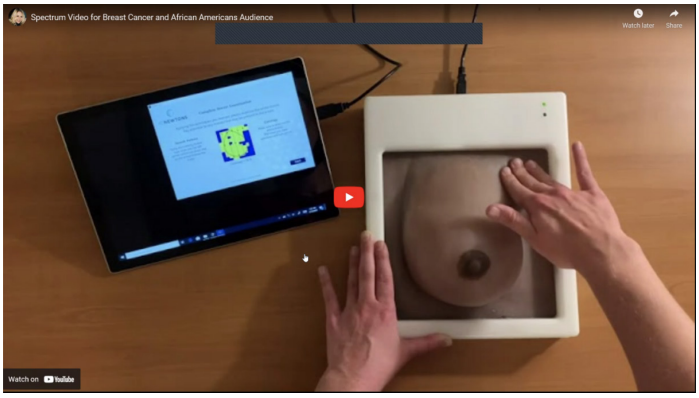

We developed and piloted a multi-pronged educational experience, including immersive community engagement at two levels: (A) an educational video featuring a digital breast exam simulator to facilitate breast health knowledge and engagement in preventive care (pictured above); (B) a culturally competent survey to assess breast health experience, knowledge, and training and its relationship to use of evidence-based preventive services (e.g., mammogram) among a diverse cohort of women. Dissemination was conducted in partnership with two community breast health events: Breast Cancer and African Americans; Bay Area Cancer Connections.

[1]Wilson J, Sule A. Disparity In Early Detection Of Breast Cancer. StatPearls Internet. Published online January 2022.

Radiographic, Biochemical or Pathologic Response to Neoadjuvant Chemotherapy in Resected Pancreatic Cancer: Which is Best?

Ahmad MU, Javadi C, Chang JD, Forgo E, Fisher GA, Chang DT, Delitto DJ, Dua MM, Lee B, Visser BC, Norton JA, Poultsides GA

Introduction: Disease response to neoadjuvant chemotherapy (NAC) for pancreatic ductal adenocarcinoma (PDAC) may be assessed by change in tumor size, change in CA 19-9, and tumor regression grade (TRG). The relative prognostic significance of each type remains unclear. We analyzed the predictive ability of individual and collective disease responses in survival.

Methods: Patients with NAC and PDAC resection were retrospectively analyzed from 2011 to 2021 at a single institution. Radiographic, CA19-9 and pathologic response were analyzed. Overall survival (OS) was calculated with the Kaplan–Meier method and compared with log rank and Cox proportional hazard methods.

Results: 146 patients met criteria and received NAC (FOLFIRINOX, n=101; Gem-Abraxane, n=30; other, n=15). 21% (n=30) received radiation and 51% (n=75) required porto-mesenteric venous reconstruction. Median OS was 53 months. OS improved with: CA19-9 decrease > 25% (NR vs 23 months, p< 0.0001), TRG score of ≤ 2 (53 vs 28 months, p< 0.001) and decrease in radiographic tumor size > 50% (NR vs. 35 months, p=0.034). Response Evaluation Criteria in Solid Tumors (RECIST 1.1) was not predictive of OS. In multivariate analysis, CA 19-9 decrease > 25% was associated with OS (HR=0.36, p=0.026), whereas pathologic (p=0.074) and radiographic response (p=0.16) were not. OS was optimal in the presence of all 3 types of response compared to CA19-9 alone.

Conclusion: PDAC patients with radiographic, biochemical, and pathologic response to NAC have improved prognosis. In the absence of concordance between the three types of response, biochemical response (CA19-9 decrease by > 25%) best predicts long-term survival.

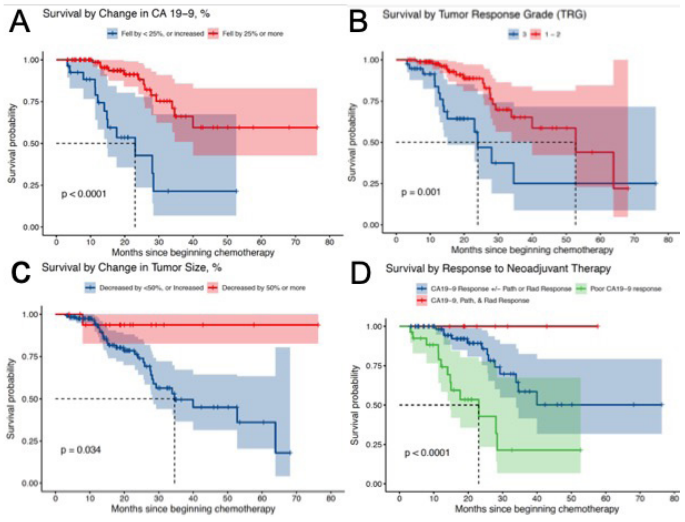

Evaluating the Impact of the COVID-19 Pandemic on Emergency Medicaid Programs: Have Insurance Rates Improved Among Trauma Patients?

Ana C. Boncompagni, BA, Thomas J. Handley, MD, Katherine Arnow, MS, Marzena Sasnal, PhD, Amber W. Trickey, PhD, MS, CPH, Arden M. Morris, MD, MPH, Lisa M. Knowlton, MD, MPH

Introduction: Trauma patients are twice as likely to be uninsured as the general population, leading to limited access to post-injury resources and higher mortality. The Hospital Presumptive Eligibility (HPE) program offers a route to insurance for eligible patients by enrolling them in Medicaid at the time of hospitalization. As HPE eligibility criteria changed during the COVID-19 pandemic, we sought to quantify the success of the HPE program during this time.

Methods: An explanatory sequential mixed-methods study was performed, including retrospective unadjusted and multivariable analysis of trauma registry data from a Level I trauma center comparing HPE approvals from 2015-2019 (pre-COVID) to 2020-2021 (post-COVID) and thematic analysis of semi-structured interviews with key stakeholders (social workers, financial counselors, and contractors).

Results: Among 221 trauma patients who were uninsured at the time of hospitalization 2020-2021, 199(90.0%) were screened for HPE and 120(60.3%) were approved for HPE, compared to 812(85.8%) screened and 386(47.5%) approved among 946 uninsured patients pre-COVID (Figure 1). After adjusting for demographic and clinical characteristics, the post-COVID period was associated with an increased likelihood of HPE approval (vs. pre-COVID: aOR 1.69; 95% CI 1.19-2.41; p=0.003). Stakeholder interviewees indicated two explanatory mechanisms: an improvement in remote approval (via telephone/video conferencing) and state-based expansion in HPE approval eligibility.

Conclusion: Trauma patients experienced improved screening for and approval of HPE during the pandemic, partly due to adaptations in remote approvals and expanded eligibility criteria. Ensuring these changes remain a part of health policy is key to improving ongoing access to care for patients.

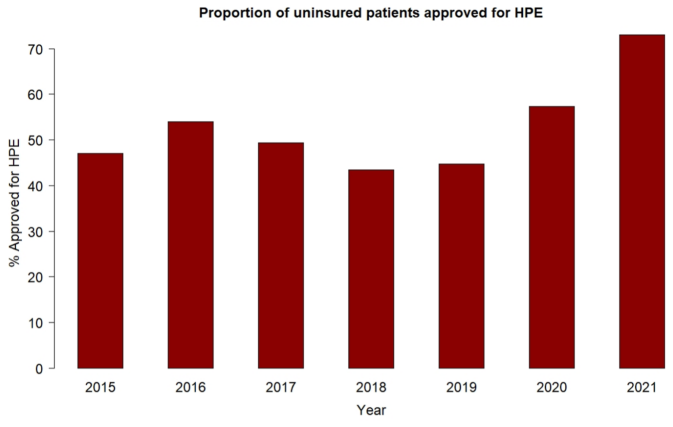

Figure 1. Proportion of Uninsured Patients Approved for HPE

Complications associated with subsequent vascular access in pediatric ECMO patients

Katelyn Chan, Nolan Martin, Talha Rafeeqi, Fereshteh Salimi-Jazi, Stephanie Chao

Introduction: Achieving central venous access in children can be challenging. Following ECMO decannulation, the need for central venous access often persists in this critically ill population. Intensivists and surgeons must consider whether to reuse the cannulation site for subsequent central venous catheters (CVC), or seek access at a remote location. This study investigates the risk of infectious complication associated with the reuse of peripheral ECMO cannulation sites for subsequent central access.

Methods: A retrospective review was conducted for patients aged 0-18 years, who underwent peripheral ECMO cannulation between 2009 and 2021 at a single children's hospital. We hypothesized there would be increased rate of central line-associated bloodstream infections (CLABSIs) among patients who underwent contemporaneous CVC placement at the time of ECMO decannulation using the same access site.

Results: Of the 227 charts reviewed, after ECMO decannulation, 53 patients received a CVC at the same location, 25 received a CVC at a different location, 63 received a peripherally inserted central catheter (PICC), and 87 had no subsequent vascular access placed within 30 days of decannulation. Among the patients with secondary access placed at the same site, there were 2 CLABSIs or 1.87 CLABSIs per 1000 line days. Patients with PICC lines after ECMO decannulation had 0.43 CLABSIs per 1000 line days. In comparison, the institution's hospital-wide CLABSI rate was 1.46 per 1000 line days during this same period. The rate of CLABSI among patients with secondary access at the site of decannulation was higher than the rate among patients with PICC lines and the institutional rate. However, this did not rise to the level of statistical significance (p=0.91 and p=0.79 respectively). There were no CLABSIs reported among those with secondary access at a different site or those with no subsequent vascular access.

Conclusion: CVC placement at the time of ECMO decannulation had no significant difference in CLABSI development compared with institutional CLABSI rates. Compared with ECMO patients with subsequent CVCs placed at an alternative access site or via PICC after decannulation, patients with contemporaneous CVC placement at the site of decannulation trended towards slightly higher rates of CLABSIs, but this did not reach statistical significance.

Two Stage Nipple-sparing Mastectomy Does Not Compromise Oncologic Safety

Candice Thompson MD, Julia Chandler MD MS*, Tammy Ju MD, Irene Wapnir MD*

Introduction: Two Stage nipple-sparing mastectomy (2S NSM) is used to improve collateral blood flow to the nipple-areolar complex (NAC) prior to mastectomy in order to decrease complications. The first stage consists of devascularization of the NAC and central skin envelope, followed weeks later by completion NSM. Here we analyze the oncologic safety of 2S NSM by comparing pathology at first stage devascularization to that after completion NSM.

Methods: Patients who underwent 2S NSM from 2015-2021 were identified. All patients underwent sub-nipple biopsy at first stage devascularization, and those with known cancer underwent lumpectomy and nodal staging. The histology at devascularization was compared to the histology after completion NSM. Patients were excluded if they underwent chemotherapy and/or radiation after devascularization or if they delayed treatment.

Results: One hundred fifty-three breasts underwent 2S NSM; 55 were for invasive cancer, 16 were for DCIS, and the remainder were prophylactic. The median time between operations was 28 days for invasive cancer and 36 days for DCIS. After completion NSM, 2 patients were upstaged from DCIS to IDC due to the presence of microinvasive disease, and 3 in the prophylactic group were upstaged DCIS.

Conclusions: The median time interval between stages was relatively short and a minority of patients with invasive disease had residual disease at the time of completion mastectomy, suggesting that 2S NSM does not compromise oncologic safety.

Table 1: Histology at first stage devascularization vs final pathology

Histology at Devascularization	Final Pathology at NSM	# Cases (%)	Median # of Days	Range of Days
Invasive n=55	Benign	21 (38.2%)	28	11-97
	Invasive	15 (27.3%)	30	21-84
	DCIS	19 (34.5%)	28	12-84
DCIS n=16	Benign	6 (37.5%)	34	21-49
	Invasive	2 (12.5%)	36	31-42
	DCIS	8 (50%)	38	21-82
Prophylactic N=82	Benign	79 (96.3%)	32	11-139
	DCIS	3 (3.7%)	29	22-30

Where to Next? Geographical Impact of Plastic Surgery Residency to Fellowship Placement

Gina Eggert, BS; Ashraf Patel MD; Bhagvat Maheta, BS; Kometh Thawanyarat, BA; Rahim Nazerali, MD, MHS, FACS

Introduction: The relationship of residency location to fellowship placement informs decisions for current and future trainees, as well as program directors and faculty members. This study explores geographical trends of where trainees complete residency and where they pursue fellowship training.

Methods: A retrospective study identified graduates from integrated plastic surgery residency programs in the United States (2015-2021). The data was categorized on whether the proximity of the graduate's fellowship location to residency was within 100 miles, within the same state, within the same geographic region, within the United States, or international. A Chi-Squared value was calculated to determine if the geographic location of the fellowship was due to chance.

Results: 365 residency graduates from 51 programs that attended a plastic surgery fellowship were included in the sample. The sample size included 41 graduates in 2015, 57 in 2016, 67 in 2017, 63 in 2018, 59 in 2019, 64 in 2020, and 10 in 2021 (5 did not have a graduating year). 18.08% (n=66) stayed within a 100-mile radius, 47.67% (n=174) stayed within the same geographic region, and 3.56% (n=13) pursued training internationally. These findings were statistically significant ($p = 0.001$).

Conclusion: Graduates who completed their integrated residency in a certain geographic location are more likely to stay in that area for their fellowship. This may be explained by graduates continuing training with their original program and personal factors such as family and friends. Further research with personal interviews may highlight additional details regarding residency to fellowship matching.

Association of parathyroidectomy vs. observation with the development of worsening chronic kidney disease (CKD) in adults with primary hyperparathyroidism

Adam Furst MS; Calyani Ganesan MD MS; Alan C. Pao MD; Glenn M. Chertow MD MPH; John T. Leppert MD MS; Amber W. Trickey PhD MS CPH; Electron Kebebew MD; Manjula Kurella Tamura MD MPH; Carolyn D. Seib MD MAS

Introduction: Multidisciplinary guidelines recommend parathyroidectomy to mitigate the risk of worsening chronic kidney disease (CKD) among patients with primary hyperparathyroidism (PHPT) who have an estimated glomerular filtration rate (eGFR) <60 mL/min/1.73 m2. However, there are limited data documenting the association of parathyroidectomy with long-term kidney function. Our objective was to compare the time-to-progression to stage 4 or worse (4+) CKD in patients with PHPT treated with parathyroidectomy versus non-operative management.

Methods: We performed a longitudinal cohort study of patients diagnosed with PHPT within the Veterans Health Administration from 2000 to 2019. Stratified analyses were conducted to separately analyze patients with 'high' pre-treatment eGFR≥60 and 'low' pre-treatment eGFR<60. We calculated inverse-probability weighted multivariate Cox proportional hazards regression models.

Results: Among 41,083 patients with PHPT, 2831 (6.9%) developed stage 4+ CKD over a median follow-up of 4.5 years; 5-year event rate was 3.2% in parathyroidectomy and 6.7% in the nonoperative group, 10-year event rate was 7.3% (parathyroidectomy) and 13.0% (nonoperative). Among the high eGFR group, parathyroidectomy was associated with a lower adjusted hazard of developing stage 4+ CKD than non-operative management (hazard ratio [HR] 0.60, 95%CI 0.46-0.77). See Key Figure. There was no difference in time-to-CKD progression among the low eGFR group (HR 0.95, 95%CI 0.72-1.27).

Conclusion: Treatment of PHPT with parathyroidectomy is associated with an adjusted decreased rate of progression to stage 4+ CKD among patients with normal baseline kidney function compared to non-operative management. Parathyroidectomy should be considered in patients with PHPT and normal kidney function to mitigate the risk of progressive renal insufficiency.

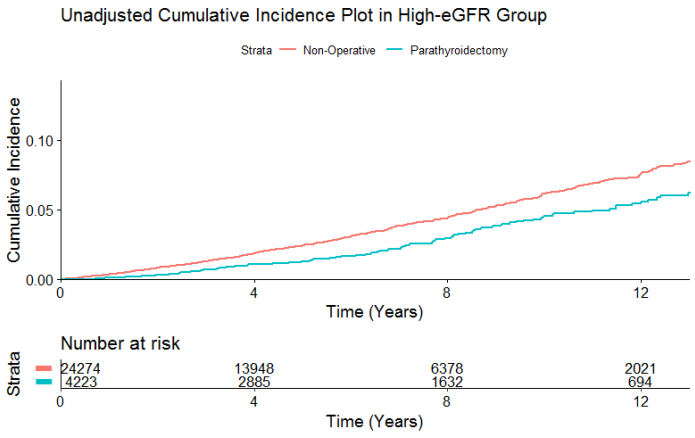

Warming of Donor Kidneys During Recipient Transplantation

Keith S. Hansen, MD, Victoria Wu and Marc Melcher, MD, PhD

Introduction: Warming of a donor kidney during the vascular anastomosis of a transplant i.e., second warm-ischemia time (SWIT), is independently associated with higher rates of delayed graft function, premature graft failure, and the discard of high-risk kidneys. SWIT is protracted in patients with complex anatomy, obesity, and in minimally invasive transplantation. The objective of this study was to outline donor kidney temperature variations during transplantation.

Method: Following IRB approval and patient consent, recipient body temperature, donor kidney volume and weight, and the temperature of flushing solutions were recorded during deceased donor kidney transplantations. Patient anatomy and donor kidney (allograft) anatomy were recorded to assess their influence on kidney temperatures during anastomosis. Kidneys were covered in ice and gauze during the anastomosis. Temperature measurements were recorded using a FLIR ONE Gen 3 - iOS - Thermal Camera at 5-minute intervals during the vascular anastomosis and validated with a secondary temperature gun.

Results: Average SWIT was 30.1 ± 1.4 min. Kidney temperatures reached the ischemic threshold of necrosis of 15oC (59oF) at 17±1.8 minutes (n=6). Final kidney temperatures were associated with prolonged anastomosis time and higher starting temperatures.

Conclusion: The relationship between kidney temperature and warming was outlined and found to be higher than anticipated. An elevated initial temperature of the donor organ resulted in higher final kidney temperatures and an earlier crossing of the threshold of necrosis. While a trend towards earlier crossing of the necrotic threshold due to kidney volume and anastomosis time was found, additional datapoints are required to determine statistical significance.

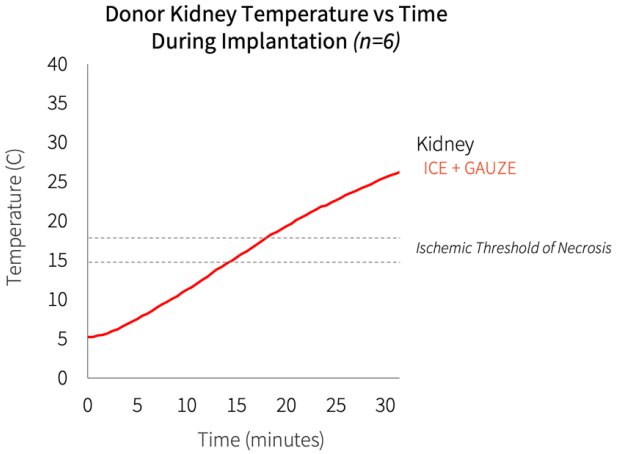

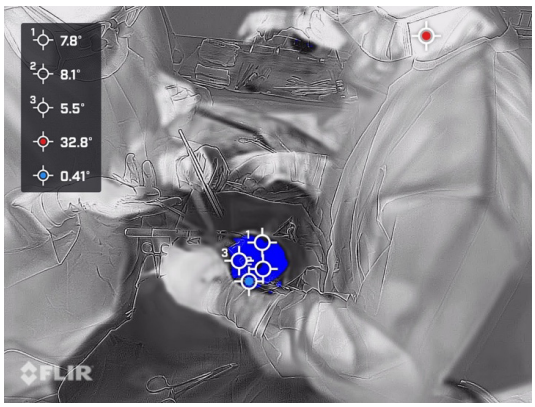

Use of Antibiotic-Impregnated Polymethylmethacrylate (PMMA) Plates for Prevention of Periprosthetic Infection in Breast Reconstruction

Thomas Johnstone BA; Kelsey Lipman MD; Nathan Makarewicz BA; Jennifer Shah BA; Elizabeth Turner PA-C; Victoria Posternak MS, RN; Daniel Chang MD; Brian Thornton MD; Rahim Nazerali MD

Introduction: Periprosthetic infections remain a major challenge for breast reconstruction. Local antibiotic delivery systems such as antibiotic beads and spacers have been widely used within other surgical fields, but their use within plastic surgery remains scarce. In this study, we demonstrate the use of antibiotic impregnated plates for infection prophylaxis in tissue expander (TE)-based breast reconstruction.

Methods: A retrospective review of patients who underwent immediate breast reconstruction with pre-pectoral (P1) TE and antibiotic plate placement over a 13-month period was performed. Antibiotic plates were created using a PMMA base (Stryker, Kalamazoo, Michigan) impregnated with 2.2 grams of tobramycin and 3 grams of vancomycin, divided in half for each breast. Data pertaining to patient demographics, operative details, and post-operative outcomes were recorded. Antibiotic plates were removed at TE to implant exchange.

Results: Fifty patients (83 breasts) were identified during the study period, average age 50.2 years and BMI 27.1 kg/m2. Average intraoperative fill and final fill volumes were 354 cc and 469 cc, respectively. No patients reported chest wall discomfort from the antibiotic plate. There were 6 nonoperative complications including 2 seromas (4%) that improved with bedside aspiration and 2 cases of wound dehiscence (4%) that resolved with local wound care. One patient with a history of diabetes and significant obesity experienced recurrent dehiscence ultimately resulting in TE/antibiotic plate explantation. Notably, no cases of infection were identified. Average follow up was 4.3 months. Local antibiotic delivery using antibiotic-impregnated PMMA plates can be safely and effectively used for infection prevention with tissue expander-based breast reconstruction.

Table 1: Patient Demographics	
Sample Size	50
Average Age	50.28 (9.49)
Average BMI (Standard Deviation)	27.05 (4.75)
Number of Patients that Actively Smoke (% of Cohort)	6 (12.0)
Number of Patients with Type II Diabetes Mellitus (% of Cohort)	3 (6.0)
Number of Patients with Hypertension (% of Cohort)	11 (22.0)
Other Comorbidities (% of Cohort)	
Crohn's Disease	1 (2.0)
Hyperlipidemia	1 (2.0)
Osteoporosis	1 (2.0)
Pulmonary Embolism	1 (2.0)
Rheumatoid Arthritis	1 (2.0)
Thrombocytopenia	1 (2.0)
Number of Patients with Prior Irradiation of the Breast (% of Cohort)	4 (8.0)
Number of Patients Receiving Neoadjuvant Chemotherapy (% of Cohort)	13 (26.0)
Table 2: Operative Characteristics	
Number of Immediate Reconstructions (% of Cohort)	49 (98.0)
Average Intraoperative Air Fill Volume in mL (Standard Deviation)	354.90 (146.09)
Number of Patients Undergoing Unilateral Reconstruction (% of Cohort)	19 (38.0)
Mastectomy Incision Pattern (% of Cohort)	
Circum-lateral	8 (16.0)
Inframammary fold	7 (14.0)
Nipple-sparing	24 (48.0)
Non-nipple-sparing	3 (6.0)
Skin-sparing	4 (8.0)
Transverse	1 (2.0)
Trapezoid	1 (2.0)
Vertical	2 (4.0)
Accompany Lymph Node Procedure (% of Cohort)	
Axillary Lymph Node Dissection	6 (12.0)
Sentinel Lymph Node Biopsy	31 (62.0)
Sentinel Lymph Node Dissection	3 (6.0)
Average Resected Breast Weight in Grams (Standard Deviation)	532.59 (232.20)
Table 3: Postoperative and Complication Data	
Average Length of Postoperative Stay in Hours (Standard Deviation)	11.78 (12.65)
Average Duration of Postoperative Antibiotic Regimen in Days (Standard Deviation)	18.58 (4.55)
Number of Patients Receiving Adjuvant Radiation (% of Cohort)	13 (26.0)
Number of Patients Receiving Adjuvant Radiation (% of Cohort)	9 (18.0)
Average Days Between Reconstruction and Wound Drain Removal (Standard Deviation)	18.11 (9.83)

Effect of Climate on Development of Surgical Site Infection

Raymond Liou BS, Michelle Earley MS, Joseph D. Forrester MD MSc

Introduction: Meteorological variables may represent a neglected group of risk factors for surgical site infections (SSI). We investigate whether increases in temperature, humidity, and precipitation increases SSI rate.

Methods: Records of surgical encounters and follow-ups within National Healthcare Safety Network-designated surveillance windows (30 or 90 days) were extracted from MarketScan® databases from 2007-2014. Data extracted included age, sex, admission date, ICD-9 codes, and metropolitan statistical area (MSA) where procedures occurred. Daily minimum temperature, specific humidity, and precipitation in associated MSAs were extracted from the Gridded Surface Meteorological dataset and standardized. SSI risk was analyzed with a multinomial model including environmental and previously identified risk factors with outcomes being 1) no SSI 2) SSI during admission and 3) SSI diagnosed follow-up. Adjusted p-values were derived using Holm's method.

Results: A total of 7,702,846 patient records were extracted from 393 MSAs. Every 10cm increase of maximum daily precipitation resulted in a 1.09 odds increase in SSI after discharge, while every g/kg unit increase in specific humidity resulted in a 1.03 odds increase in SSI risk after discharge (Table 1). Minimum temperature was negatively correlated with SSI rates after discharge (OR: .995, p<.001). When running an identical model with specific humidity omitted, minimum daily minimum temperature was positively correlated with SSI after discharge (OR: = 1.004, p<.001).

Conclusion: Development of SSIs may be influenced by meteorological variables, with the effect of temperature likely driven by increases in specific humidity. Further investigations into relationships between climate and SSI may help inform future SSI prevention strategies.

	SSI during admission				SSI after discharge			
	B (SE)	OR (95% CI)	p	Adjusted p	B (SE)	OR (95% CI)	p	Adjusted p
Sex (1 = female)	-0.14 (.14)	0.87 (0.84-0.90)	<.001	<.001	0.032 (.008)	1.03 (1.01-1.05)	<.001	<.001
Medicare	-0.4 (.018)	0.67 (0.64-0.69)	<.001	<.001	-0.31 (.01)	0.73 (0.72-0.75)	<.001	<.001
Inpatient	2.98 (.031)	19.7 (18.5-20.9)	<.001	<.001	0.54 (.009)	1.72 (1.68-1.75)	<.001	<.001
Charlson Comorbidity Index	0.054 (.002)	1.06 (1.05-1.06)	<.001	<.001	0.068 (.001)	1.07 (1.07-1.07)	<.001	<.001
Length of Stay	0.028 (.0004)	1.03(1.03-1.03)	<.001	<.001	0.015 (.0004)	1.02 (1.01-1.02)	<.001	<.001
Years	-0.039 (.003)	0.96 (0.96-0.97)	<.001	<.001	-0.029 (.002)	0.97 (0.97-0.97)	<.001	<.001
Maximum daily precipitation (cm/day)	0.002 (.004)	1.002 (0.99-1.01)	0.65	0.065	0.009 (.002)	1.009 (1.006-1.013)	<.001	<.001
Maximum daily specific humidity (g/kg)	-0.008 (.004)	0.99 (0.99-1.0)	0.037	0.07	0.026 (0.002)	1.03 (1.02-1.03)	<.001	<.001
Minimum daily minimum temperature (°C)	0.0042 (.0015)	1.004 (1.001-1.007)	0.004	0.01	-0.005 (.0007)	0.995 (0.99-1.00)	<.001	<.001

Table 1: Multivariate multinomial analysis coefficients and odds ratios for predictors of surgical site infection. Procedure categories (n=15) and MSA (n=393) were included in analysis but omitted from the table. Years are measured from 2007 up to 2014

Laser treatment of breast reduction scars: A patient reported outcomes study

Kelsey Lipman MD; Peter Deptula MD; Dung Nguyen PharmD, MD

Introduction: Surgical scars after reduction mammaplasty are a leading cause of patient dissatisfaction. Laser therapy is commonly used to treat hypertrophic and keloid scar pain, itching, and improve on scar appearance. However, literature on its use in the breast reduction population remains scarce.

Methods: Female patients interested in scar treatment after breast reduction > 1 month postoperatively were identified at a single institution. Study participants were treated with the Aerolase Neo Elite 1064 nm Nd:YAG laser (Aerolase Corp., Tarrytown, NY). Patients underwent three total treatments spaced four weeks apart with three passes per treatment session. The Breast-Q Reduction/Mastopexy module was administered before and at the conclusion of treatment. Formal clinical assessment of scars using a 3-point scale (-1 (worse), 0 (no change), 1 (better)) was performed at each time point by a plastic surgeon. T-testing and multivariate regression analyses were performed when appropriate, $p < 0.05$ was considered statistically significant.

Results: Sixteen patients with an average age of 49.3 years and BMI 28.5 kg/m2 were included. Patients ranged from Fitzpatrick type II to V. After completion of treatment, average Breast-Q scores improved overall (139.3±15.0 versus 144.9±11.9, $p<0.001$) and individually within each subsection. Patients noted an improvement in scar visibility (3.2±0.7 versus 3.9 ±0.7, $p < 0.001$). This subjective improvement was supported by improvement in rating of overall scar appearance by the plastic surgeon post-treatment ($p<0.001$).

Conclusion: The Nd:YAG laser is both safe and effective for scar treatment after breast reduction. Utilizing this laser technique postoperatively results in higher patient satisfaction and improved scar appearance.

Figure 1: Pre and Post Laser Treatment Scar Appearance

Figure 1: 1A demonstrates pre-treatment baseline scarring. 1B demonstrates scar appearance after completion of three sessions of Aerolase Neo Elite Nd:YAG laser, highlighting improvement in erythema and overall appearance.

Location Matters: The Geographical Impact of Plastic Surgery Residency to First Job Placement

Bhagvat Maheta BS, Ashraf Patel MD, Gina Eggert BS, Kometh Thawanyarat BA, Rahim Nazerali, MD, MHS, FACS

Introduction: Residency location may indicate where a resident begins their practice, the type of practice, or attending fellowship. Identifying the impact location has on a resident's future will be a confounding factor in the integrated plastic surgery match.

Methods: Graduates' first job location after integrated plastic surgery residency programs in the United States (2015-2021) were retrospectively collected. This data was categorized based on whether the proximity of the graduate's first job location to residency was within 100 miles, within the same state, within the same geographic region, within the United States, or international. To calculate if the relative geographic location of the first job was due to chance, a Chi-squared analysis was conducted.

Results: The sample size consisted of 279 residency graduates from 41 programs, of which 48 graduated in 2015, 56 in 2016, 54 in 2017, 48 in 2018, 45 in 2019, 26 in 2020, and 6 in 2021. 36.92% (n=103) stayed within a 100 mile radius of their residency, 68.46% (n=191) stayed within the same geographic region, and 1.08% (n=3) went internationally. These findings were statistically significant ($p = 0.001$).

Conclusion: The results show that if a graduate completed their integrated plastic surgery residency in a certain geographic location, they are more likely to stay in that area for their first job. The implications of this can be attributed to their established network in the area after years of residency, a shift to focus on family life, and increased opportunities to join the private practice industry.

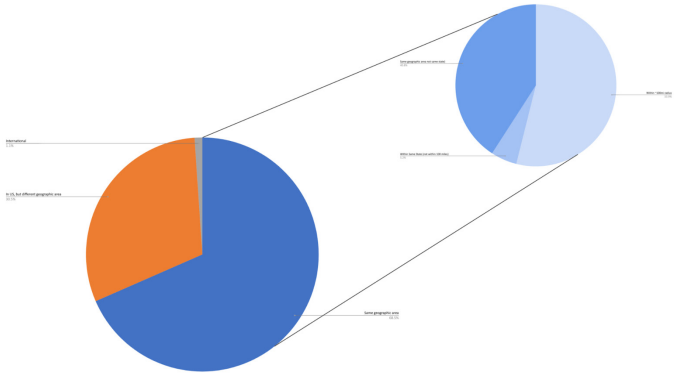

Machine Learning to Elucidate National Trends in Crowdfunding for Surgical Care

Advait Patil; Jeff Choi MD, MSc

Introduction: Online crowdfunding platforms have been increasingly used to cover healthcare costs and are associated with gaps in social safety-net systems. However, nationwide trends in prevalence and financial volume of crowdfunding campaigns for surgical care has yet to be explored. We aimed to characterize the funds raised, success rate, national trends, and most frequent conditions for surgery-related crowdfunding campaigns.

Methods: The dataset comprised a webscraper-generated extraction of all GoFundMe campaigns between May 2010 to December 2020. We included campaigns associated with surgical care using text matching to keywords. We leveraged scispaCy's natural language processing models for named entity recognition in medical text (trained on 5818 diseases from 1500 PubMed papers). We applied this model to extract clinical disease descriptors including cancer subtypes from campaign stories.

Results: During our study period, 66,514 GoFundMe campaigns associated with surgical care raised $355.6 million of $1.1 billion sought (32.3%). California, Texas, Florida, and New York had the greatest funds raised, while Alaska, Vermont, Colorado, and Maine had the most campaigns per capita (Figure 1a, b). Cancer comprised the most common reason for campaigns (18.8%), followed by trauma (9.2%). The most common cancer funds were sought for cancers of the breast, brain, colon, and blood (Figure 1c). We found a disproportionately high number of brain cancer surgery campaigns compared to national prevalence.Our results shed light into the size of crowdfunding for surgical care and provide insight into the chief reasons for fundraising.

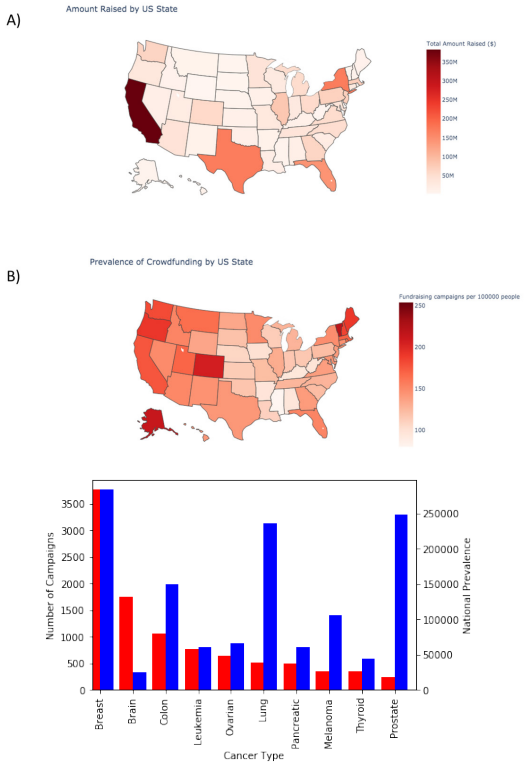

Figure 1: State-level geographic distribution of a) funds raised through surgical crowdfunding campaigns, and b) campaigns per capita. c) Distribution of cancer types (as identified by our machine learning model) in our dataset compared with national prevalence.

AI-Based Video Segmentation: Procedural Steps or Basic Maneuvers?

Calvin Perumalla, LaDonna Kearse, Michael Peven, Shlomi Laufer, Cassidi Goll, Brett Wise, Su Yang, Carla Pugh

Introduction: Video-based review of surgical procedures has proven to be useful in training by enabling efficiency in qualitative assessment of surgical skill and intraoperative decision-making. Current video segmentation protocols focus largely on procedural steps. While some operations are more complex than others, many of the steps in any given procedure involve an intricate choreography of basic maneuvers such as suturing, knot-tying and cutting. Use of these maneuvers at certain procedural steps can convey information that aids in assessment of complexity of the procedure, surgical preference and skill. Our study aims to develop and evaluate an algorithm to identify these maneuvers.

Methods: A standard deep-learning architecture was used to differentiate between suture throws, knot-ties, and suture cutting on a dataset comprised of videos from practicing clinicians (N=52) who participated in a simulated enterotomy repair. Perception of the added value to traditional AI segmentation was explored by qualitatively examining the utility of identifying maneuvers in a subset of steps for an open colon resection.

Results: An accuracy of 84% was reached in differentiating maneuvers. The precision in detecting the basic maneuvers was 87.9%, 60% and 90.9% for suture throws, knot ties, and suture cutting, respectively. The qualitative concept mapping confirmed realistic scenarios that could benefit from basic maneuver identification.

Conclusion: Basic maneuvers can indicate error management activity or safety measures and allow for assessment of skill. Our deep-learning algorithm identified basic maneuvers with reasonable accuracy. Such models can aid in AI-assisted video review by providing additional information that can complement traditional video segmentation protocols.

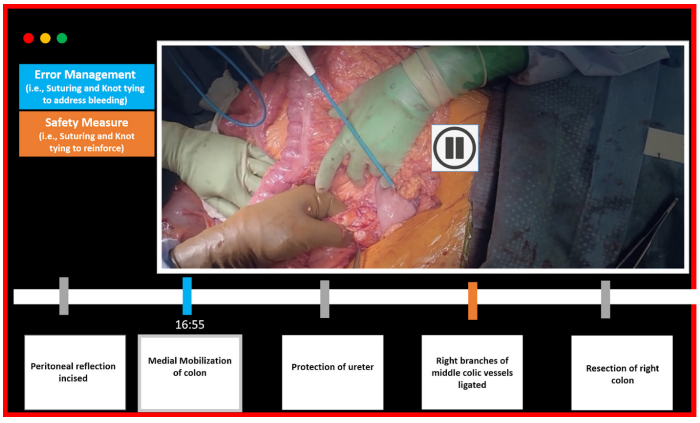

Figure 3: Figure shows a concept diagram of a video segmentation tool that is incorporated with our algorithm. The algorithm is able to identify basic maneuvers and based on the procedure step is able to provide information about any error management or safety measures undertaken from the surgeon.

Avoiding the Emergency Department After Ambulatory Surgery: Can We Do Better?

Charlotte M Rajasingh, Sherry M Wren

Introduction: Post-operative emergency department visits are potentially preventable. We investigated the rate of post-operative ED visits after ambulatory surgery at freestanding and hospital-owned surgery centers.

Methods: Florida, New York, and Wisconsin patients undergoing elective, same-day discharge cholecystectomy, laminectomy, or transurethral prostate resection were extracted from the SASD. Procedures were considered separately. Analysis was stratified by facility type: freestanding (F) or hospital-owned (HO). Outcome was postoperative ED visit within 30-days. For risk-adjusted models, a sensitivity analysis examined patients with and without a prior admission within 1-year of surgery separately; in patients with prior admissions, adjusted models accounted for calculated Elixhauser scores.

Results: Of 147,641 patients, 17,145 underwent surgery at freestanding centers and 130,496 at hospital-owned facilities. Cholecystectomy was the most frequent procedure (116,090), followed by laminectomy (17,791) and TURPS (13,760). 10.1% of the cohort had a prior admission. For all procedures, 30-day ED visits rates were lower for freestanding centers (F: 3.7-10.3%) than hospital owned (HO: 6.3-12.0%), including in subgroup analysis of patients with prior admissions (Figure 1A). Freestanding centers had a significantly lower aOR of 30-day ED visit in patients without prior admissions for all operation groups. For patients with a prior admission, the association was not statistically significant after adjusting for comorbidities; point estimates were similar (Figure 1B).

Conclusion: Underlying patient factors may account for some but likely not all the differences observed in 30-day ED visit rate after surgery at hospital-owned ambulatory centers. Factors that account for this gap including process of care measures should be a focus of future work.

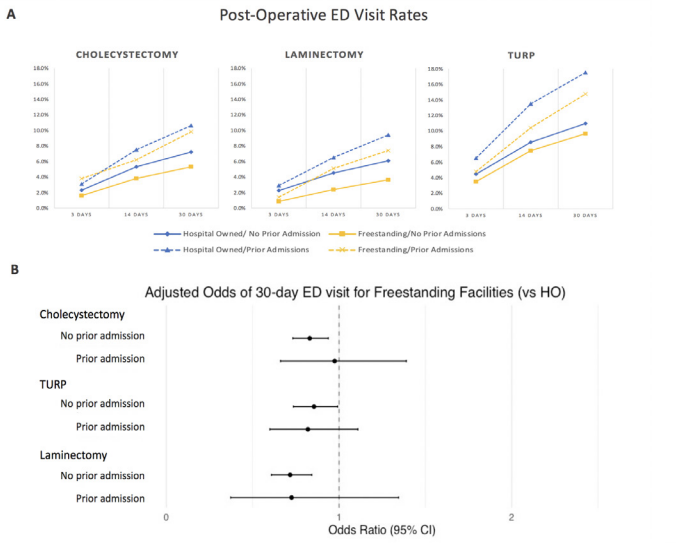

Figure 1. (A) Unadjusted rates of ED visits stratified by facility type and whether patients had a prior admission. (B) Adjusted odds ratios for 30-day ED visit associated with surgery at a freestanding center (vs. a hospital-owned center). Separate models were run for patients with a prior admission and those without for each operative group.

Leveraging Haptic Sensor Technology for Force Mapping in Orthoses for Adolescent Idiopathic Scoliosis

Brett Wise, BS, Su Yang, BS, Calvin Perumalla, MS PhD Cassidi Goll, BA, Audrey Bowler, AA, John Vorhies, MD, Carla Pugh, MD, PhD

Introduction: The gold standard of non-operative management of Adolescent Idiopathic Scoliosis (AIS) is the prevention of progression by means of a custom-fitted rigid orthosis/brace. However, the effectiveness of orthoses is limited by the predominantly qualitative methodologies of brace fitting and adjustment. Developing novel technology that uses flexible force sensors to longitudinally measure the force profile of a scoliosis orthotic may result in better outcomes and fewer operations.

Methods: Three new technologies were introduced to the clinic. The first force sensor developed was a fabric matrix, another was a customizable fabric sensel which was designed and fabricated in-house. Commercially available sensors were also explored, and the company BodiTrak provided a pressure mapping sensor to test.

Results: The sensors were tested in the clinic, force data plus qualitative user experience data was gathered. The fabric matrix design had multiple engineering issues and was uncomfortable for patients. The BodiTrak senor was able to provide hotspot information but was unable to capture high enough force values. The custom fabric sensel design performed best and was tested on one patient. The three sensels showed feasibility in collecting force data from specific hotspots identified by physicians.

Conclusion: By combining orthotics with force sensels, there is huge potential to improve the efficacy of bracing through quantitative force mapping and providing aid in clinical decision-making related to brace adjustments with personalized data. Over the long run, this solution can improve orthotic treatment of AIS, resulting in the prevention of invasive, costly, and potentially morbid surgical interventions.

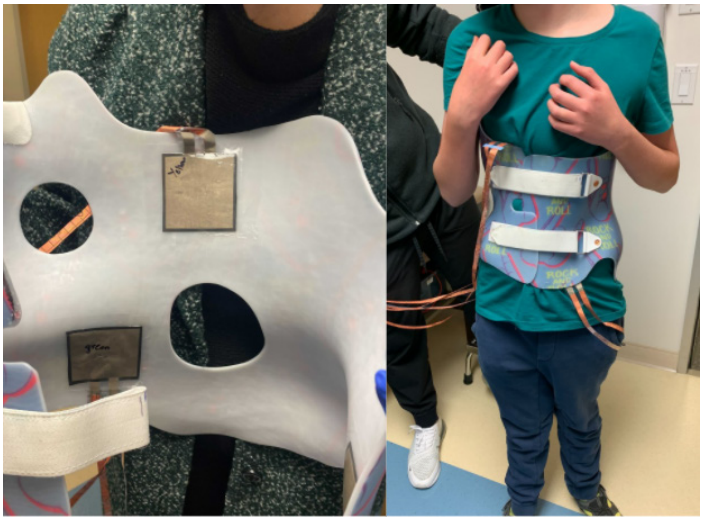

This picture shows the sensels developed in-house placed in specific locations inside of the brace, followed by the patient wearing the brace in the standing position and collecting force readings.

Generating Rare Surgical Events Using CycleGAN: Addressing Lack of Data for AI Event Recognition

Su Yang, BSa, Hossein Mohamadipanah, PhDa, LaDonna Kearse, MDa, Brett Wise, BSa, Leah Backhus, MD, MPHb,c, Carla Pugh, MD, PhD, FACSa

Introduction: Artificial Intelligence (AI) has shown promise in facilitating surgical video review through automatic recognition of surgical activities/events. There are few public video data sources that demonstrate critical yet rare events which are insufficient to train AI for reliable video event recognition. We hypothesize that a generative AI algorithm can create artificial massive bleeding images for minimally invasive lobectomy that can be used to augment the current lack of data in this field.

Methods: A generative adversarial network algorithm was used (CycleGAN) to generate artificial massive bleeding event images. To train CycleGAN, six videos of minimally invasive lobectomies were utilized from which 1819 frames of non-bleeding instances and 3178 frames of massive bleeding instances were used.

Results: The performance of the CycleGAN algorithm was tested on a new video that was not used during the training process. The trained CycleGAN was able to alter the laparoscopic lobectomy images according to their corresponding massive bleeding images, where the contents of the original images were preserved (e.g., location of tools in the scene) and the style of each image is changed to massive bleeding (i.e., blood automatically added to appropriate locations on the images).

Conclusions: The result indicates a promising approach to supplement the lack of data for the rare massive bleeding event that can occur during minimally invasive lobectomy. Future work could be dedicated to developing AI algorithms to identify surgical strategies and actions that potentially lead to massive bleeding and warn surgeons prior to this event occurrence.

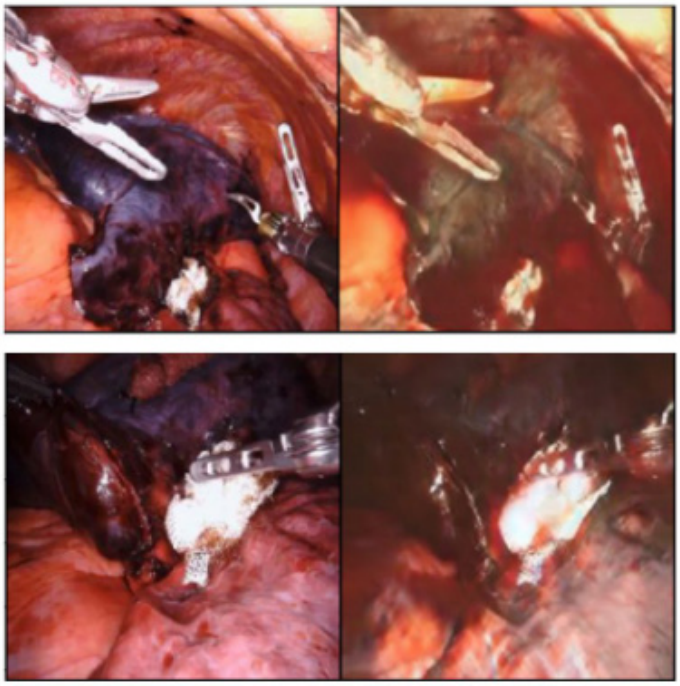

Hybrid Breast Reconstruction with Adjustable Saline Implants: A Five Year Review

Anna Zhou, MD; Victoria Posternak, AOCNS; Dung Nguyen, MD, PharmD

Introduction: Autologous reconstruction can be augmented with implants to help patients achieve their goal breast volume. Delayed implant placement is time consuming. Here, we review our experience of two stage hybrid breast reconstruction compared to immediate adjustable saline implant placement, a customizable single stage breast reconstruction strategy.

Methods: A retrospective review of hybrid breast reconstruction with immediate adjustable saline implants or delayed implants was performed. Demographics, operative details, complications, time to final breast volume, additional implant revisions, and patient satisfaction were compared using student t test and chi square test.

Results: From 2012-2022, 24 patients (44 breasts) underwent hybrid reconstruction with immediate adjustable saline implants. Seventeen patients (30 breasts) underwent delayed implant placement. There was no significant difference in age, BMI, smoking status, and diabetes between the two groups. More delayed implant patients had a history of radiation, non nipple sparing mastectomy, and higher mastectomy specimen weights. DIEP and msTRAM were most commonly performed. Complications were rare (immediate: 2 threatened anastomoses, 1 infected hematoma vs delayed: 1 hematoma). Final implant sizes were similar (immediate 197±105cc, delayed 235±76cc, p=0.09), but the immediate cohort had a larger range (25-450cc vs delayed 158-457cc). Goal breast volume was achieved more quickly in the immediate cohort (12.8±15.4 vs 49.8±42 weeks, p=0.002). Need for implant upsizing/downsizing was more common with delayed placement (40% vs 18.1%, p=0.03). There was a slightly higher proportion of very satisfied patients in the immediate implant group (figure) at final follow up (immediate 14±10 months, delayed 39±26 months, p=0.001).

Conclusion: Hybrid breast reconstruction with immediate adjustable saline implants is safe, achieves goal volume more quickly and has a lower rate of size related implant revision than delayed implant placement.

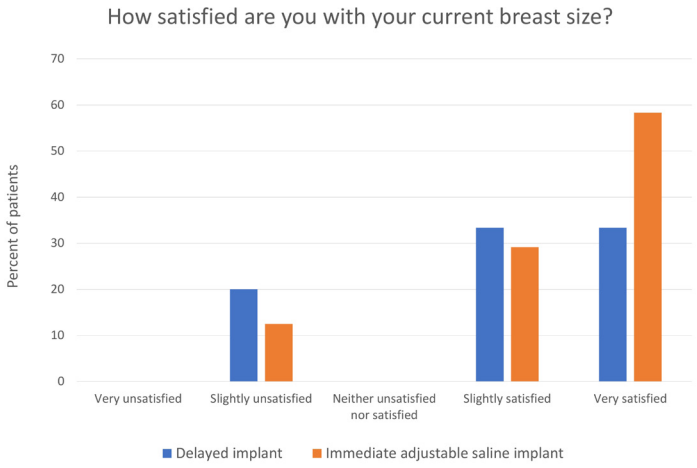

Adoption of a standardized treatment protocol for pilonidal disease leads to low recurrence

Talha Rafeeqi, MBBS, Claire Abrajano, Fereshteh Salimi-Jazi, MD, Deanna Garza, Emi Hartman, Kira Hah, Melissa Wilcox, Modupeola Diyaolu, MD, Stephanie Chao, MD, Wendy Su, MD, Thomas Hui, MD, Claudia Mueller, MD, Julie Fuchs, MD, Bill Chiu, MD

Introduction: Pilonidal disease may present as acute abscesses or chronic draining sinuses. There is no standardized treatment and recurrence rates can be as high as 30%. Within our 5-hospital network we have established a standardized treatment protocol including minimally invasive surgical trephination and aggressive epilation. We hypothesize that such a treatment protocol can be established across different hospital settings and lead to low overall recurrence.

Methods: Patients with pilonidal disease were enrolled in the study on presentation to our hospital network. Those that underwent initial surgery outside our hospital system or were noncompliant with our treatment protocol were excluded. Patients were grouped based on surgeon and treating facility. Frequency of recurrence per surgeon and per hospital was calculated and analyzed using ANOVA. P <0.05 was considered statistically significant.

Results: Out of 132 patients, 80 patients were included (45 female, 35 male) while 52 were excluded due to initial surgery at a non-network hospital or for protocol noncompliance. Mean age was 17.8±3.2 years and mean follow-up was 345±186 days. There were 6 patients who experienced at least one recurrence. There was an overall 8% recurrence rate with no significant difference noted between surgeons or hospitals (p=0.15, p=0.64 respectively).

Conclusion: We have successfully implemented a standardized treatment protocol for pilonidal disease across different hospital settings and by different surgeons, with an overall low recurrence rate. Our findings suggest that adoption of a standardized protocol for treatment of pilonidal disease can lead to low recurrence.

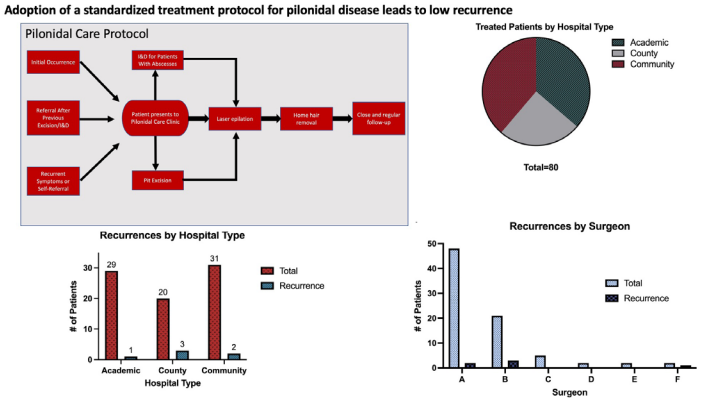

Where there is fat there is fibrosis: Elucidating the mechanisms of creeping fat-driven stricture formation.

Khristian E. Bauer-Rowe BS, Alexia Kim BS, Michelle Griffin MD, PhD, Deshka S. Foster MD, PhD, Jason Guo PhD, Shamik Mascharak BS, Heather desJardins-Park BS, Jeffrey A. Norton MD, FACS, Jeong H. Hyun MD, Michael T. Longaker MD, MBA, FACS.

Introduction: Crohn's disease (CD) is a subtype of inflammatory bowel disease (IBD) characterized by transmural inflammation and creeping fat formation. Thirty percent of CD patients develop strictures, eighty percent of which will require surgery. Creeping fat (CF) forms adjacent to strictures, but whether it promotes stricture formation is unclear. Here, we show that CF-derived fibroblasts may promote fibrosis and stricture formation.

Methods: We created anti-mesenteric colotomies in Adipoq-Cre; mTmG mice and performed lineage tracing of mature adipocytes. We selectively ablated CF adipocytes and histologically assessed stricture formation. Finally, we performed scRNA-seq separately on wounded bowel and adjacent CF to identify fibroblast and stromal progenitor subpopulations.

Results: Our surgical model phenocopies clinical features of human strictures (Figure 1A-F). Lineage tracing of mature adipocytes in Adipoq-Cre; mTmG mice revealed adipocyte-derived cells that lose adipocyte markers and acquire fibroblast markers at the colotomy site (Figure 1G, H). Selective ablation of CF adipocytes rescuedthe stricture phenotype compared to unablated controls (Figure 1I-K). scRNAseq of wounded bowel and adjacent CF revealed novel markers for mechanosensitive fibroblast and stromal progenitor subpopulations (Figure 1L-P).

Conclusions: Our surgical model in combination with lineage tracing demonstrates the presence of CF-derived fibroblasts that infiltrate the bowel wall. CF ablation is sufficient to ameliorate stricture formation. Finally, both wounded bowel and CF contain mechanosensitive fibroblast and stromal progenitor subpopulations that may drive intestinal fibrosis. Taken together, these findings suggest that CF may drive intestinal fibrosis in part through the contribution of CF-derived fibroblasts (Figure 1Q).

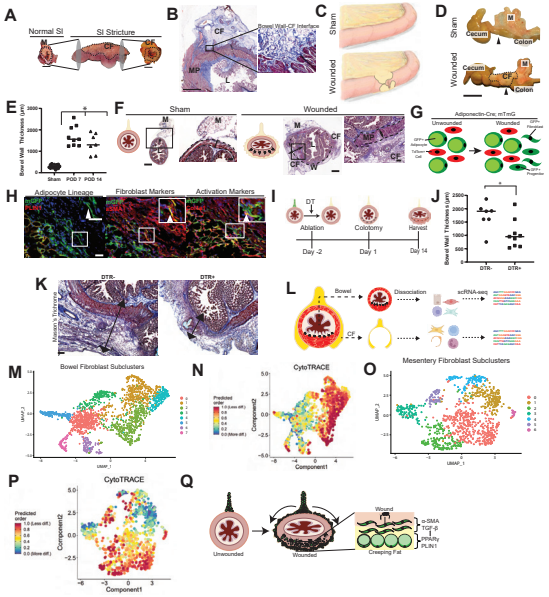

Creeping fat drives stricture formation partly through the conversion of adipocytes to fibroblasts. (**A**) Gross histology of uninvolved (left) and strictured (right) human small intestine showing increased bowel wall thickness (outlines) in stricture. (**B**) Masson's trichrome stain of human stricture showing CF, increased MP thickness, and collagen deposition (blue). (**C**) Schematic of anti-mesenteric surgical model. Arrowheads indicate colotomy site in wounded and an anatomically similar location in sham colon. (**D**) Gross histology of sham and wounded colon showing presence of CF. Arrows indicate colotomy sites. (**E**) Increased bowel wall thickness (serosa to mucosa) after colotomy creation. (**F**) Masson's trichrome of sham (left) and wounded (right) colon on POD 14 showing increased collagen deposition, MP hypertrophy, and CF formation. Dotted line indicates colotomy site. (**G**) Adipoq-Cre; mTmG system. (**H**) Immunostain for adipocyte marker PLIN1 (left), fibroblast marker ACTA2 (middle), and COL1A1 (right) in Adipoq-Cre; mTmG mice on POD 14 showing overlap with GFP+ cells. (**I**) Mesenteric adipocyte ablation studies in Adipoq-Cre; mTmG; DTR mice. (**J**) Decreased bowel wall thickness after administration of diphtheria toxin on POD 14. (**K**) Masson's trichrome after administration of diphtheria toxin to Adipoq-Cre; DTR- (left) and Adipoq-Cre; DTR+ (right) mice on POD 14 showing decreased bowel wall thickness. (**L**) Schematic showing the isolation of bowel and CF for scRNAseq on POD 14. (**M**) Fibroblast subpopulations from wounded bowel. (**N**) CytoTRACE showing stromal progenitors (less differentiated) in bowel. (**O**) Fibroblast subpopulations from wounded CF. (**P**) CytoTRACE showing stromal progenitors (less differentiated) in CF. (**Q**) Schematic showing that CF-derived fibroblasts infiltrate the wound site and participate in fibrosis.

Abbreviations: Mes = mesentery, CF = creeping fat, MP = muscularis propria, L = lumen. Muc = mucosa, Mus = muscularis, W = wound. Scale bars: 1cm (A, D), 0.3 cm (B), 300 μm (F (far left, middle right)), 75 μm (F (middle left, far right), K), 50 μm (H), 25 μm (H, insets) *P < 0.05 , **P < 0.01.

PREVIOUS VISITING PROFESSORS

Previous Emile F. Holman Lecturers

Holman Lecture	Visiting Professor	Date	Division
23rd Annual Lecture	Daniela Ladner, MD	May 13, 2022	Transplant Surgery
22nd Annual Lecture	John Alverdy, MD	May 7, 2021	General Surgery
No lecture in 2020 due to COVID-19			
21st Annual Lecture	Melina Kibbe, MD	May 3rd, 2019	Vascular Surgery
20th Annual Lecture	Paul Cederna, MD	June 1, 2018	Plastic Surgery
19th Annual Lecture	Gerard Doherty, MD	June 9, 2017	Surgery
18th Annual Lecture	Selwyn M. Vickers, MD	June 3, 2016	Surgery
17th Annual Lecture	Thomas M. Krummel, MD	June 12, 2015	Surgery
16th Annual Lecture	Douglas Fraker. MD	June 6, 2014	General Surgery
15th Annual Lecture	Allan D. Kirk, MD	June 7, 2013	Transplant Surgery
14th Annual Lecture	Chris Breuer, MD	June 8, 2012	Pediatric Surgery
13th Annual Lecture	Eliot Chaikof, MD	June 7, 2011	Vascular Surgery
12th Annual Lecture	Monica Bertagnolli, MD	June 8, 2010	Surgery
11th Annual Lecture	Carlos Pelligrini, MD	June 9, 2009	Surgery
10th Annual Lecture	Michael Mullholland, MD	June 3, 2008	Surgery
9th Annual Lecture	Ron Maier, MD	June 5, 2007	Surgery
8th Annual Lecture	Barbara L. Bass, MD	June 6, 2006	Surgery
7th Annual Lecture	William Blaisdell, MD	March 7, 2006	Surgery
6th Annual Lecture	John Connelly, MD	March 4 2005	Surgery
5th Annual Lecture	Julie Freischlag, MD	March 5, 2004	Surgery
4th Annual Lecture	Norman Rich, MD	March 7, 2003	Surgery
3rd Annual Lecture	Thomas Russell, MD	March 8, 2002	Surgery
2nd Annual Lecture	John L. Cameron, MD	March 9, 2001	Surgery
Inaugural Lecture	Halsted Holman, MD	March 17, 2000	Surgery

Stanford MEDICINE | Department of Surgery